SYNTHESIS AND CHARACTERIZATION OF STRONTIUM (Sr), BARIUM (Ba) AND CALCIUM (Ca) ALUMINATE PHOSPHORS DOPED WITH RARE EARTH IONS

by

Bakang Moses Mothudi

A thesis submitted in fulfillment of the requirements for the degree

PHILOSOPHIAE DOCTOR

in the

Faculty of Natural and Agricultural Sciences

Department of Physics

at the

University of the Free State

Republic of South Africa

Promoter: Prof H.C. Swart

Co-Promoter: Dr O. M Ntwaeaborwa

August 2009

ACKNOWLEDGEMENTS

With an immense sense of humility, I express my sincere thanks and enormous gratitude to my supervisor Professor H.C. Swart for his esteemed guidance, invaluable help and fruitful suggestions throughout the course of my work. My studies would have not been possible without his proper supervision.

I would particularly like to express my indebtedness to my co -supervisor Dr O.M Ntwaeaborwa for his guidance and encouragement during the entire course of my studies. Most importantly, I thank him for his suggestions during my experimental work and in organization of Chapters.

It is my pleasure to express hearty gratitude to Prof Kee – Sohn and his students (Sunchon National University) for introducing me to Solid State reaction Method during my research visit to South Korea.

I especially thank my fellow researchers (Patrick Nsimama, Liza Coetsee, Mart-Mari Biggs, Jafta Dolo, Pontsho Mbule, D.B Bem, and Joel Motloung) for their assistance and support.

I thank all the academic (Prof B. F Dejene, Prof Mentjies, Dr Ted Kroon, Mr JJ Dolo, Dr O.R Ocaya) and non academic (Mrs. E Pretorius) staff members of the Department of Physics for their support especially when I was on research leave.

It's a pleasure to express my gratitude to Dr MS Dlamini and Ms G. Mhlongo for their assistance with the XRD and TEM measurements.

I am thankful thank Prof J.R Botha and his students (Roro and Julien) (Nelson Mandela Metro University, Department of Physics) for the training and technical support offered during Photoluminescence measurements using a He-Cd laser.

I express my thanks to the technical staff (B Janecke and Prof PWJ Van Wyk) of Centre of Microscopy for their support and advice during SEM measurements.

I thank Prof N Revraprasadu and his student (Dr Tobi) for the training and the technical advice on the XRD system.

I would like to thank the staff members of the Department of Geology (Ms Lombard and Ms Huibrie (HCF) Joubert) for their assistance with XRD measurements.

I would like to thank Dr R E Kroon, for the help and the guidance offered when fitting the exponential decay curves of the phosphors using origin software.

I am grateful for the financial support from the South African National Research Foundation (Thuthuka Programme) and the University of the Free State.

I am greatly indebted to my fiancé (Kgomotso) and my daughter (Remofiloe), my Parents, brothers (Lucky and Ronny), sisters (Lesego, Oreeditse and Amogelang) and other family members for their encouragements and prayers which enabled me to complete this work.

I bow before the blessings of God Almighty.

ABSTRACT

The luminescent and structural properties of the alkaline earth aluminate phosphors prepared by solid state reaction, combustion and sol-gel methods are discussed. The Solid state and Sol-gel methods required much longer time (3-9 hours) for preparation of the phosphors. The annealing processes in both methods are performed at very high temperatures (1000 - 1300 ^{0}C). Furthermore in order to reduce Eu^{3+} to Eu^{2+} toxic gases such as N_2 and H_2 were introduced during the annealing process.

The combustion method is more efficient because the phosphors of high efficiency were obtained at low temperatures (500 – 600 ^{0}C) in a very short period of time (5 min). The Eu^{2+} was obtained by adding a small amount of urea to the mixture during synthesis.

$SrAl_2O_4:Eu^{2+},Dy^{3+}$ phosphors prepared by a solid state reaction method at different annealing temperatures (1000 - 1200 ^{0}C), in a reducing atmosphere of N_2 and 25%H_2, were irradiated with an excitation wavelength of 365 nm. The optimum PL intensity was shown by a sample prepared at 1100 ^{0}C. The broad emission spectra symmetric at 497 nm can be attributed to the $4f^65d^1$- $4f^7$ transition of the Eu^{2+}.

Eu^{2+} and Dy^{3+} co– doped calcium aluminate, barium aluminate and strontium aluminate phosphors were synthesized at an initiating combustion temperature of 500 ^{0}C using urea as an organic fuel. The crystallinity of the phosphors was investigated by using X- ray diffraction (XRD) and the morphology was determined by a scanning electron microscope (SEM). The low temperature monoclinic structure for both $CaAl_2O_4$ and $SrAl_2O_4$ and the hexagonal structure of $BaAl_2O_4$ were observed. Photoluminescent (PL) and phosphorescent properties were investigated by using a 325 nm He-Cd Laser and a Cary Eclipse fluorescence spectrophotometer, respectively. The broad band emission spectra with maxima at 449 nm for $CaAl_2O_4:Eu^{2+},Dy^{3+}$, 450 nm (with a shoulder at 500 nm) for $BaAl_2O_4:Eu^{2+},Dy^{3+}$ and 528nm for $SrAl_2O_4:Eu^{2+},Dy^{3+}$ were observed.

$Ca_{0.97}Al_2O_4:Eu^{2+}_{0.01},Dy^{3+}_{0.02}$ phosphors prepared at different initiating combustion temperatures were characterized by XRD), SEM and PL systems (He-Cd Laser and Cary Eclipse Fluorescence spectrophotometer). The PL emission spectra symmetric at 450 nm, in all the phosphors, confirms that only one emitting center, is present (Eu^{2+}). The optimum PL intensity and Phosphorescence was observed from the sample prepared at an initiating combustion temperature of 600 ^{0}C.

$Ba_{0.97}Al_2O_4:Eu^{2+}_{0.01},Dy^{3+}_{0.02}$ powder phosphors were prepared at different initiating temperatures ranging from 500 - 800 ^{0}C by the combustion method using urea as a comburent. The most crystalline hexagonal structure of $BaAl_2O_4$ was observed from samples prepared at the initiating combustion temperature of 500 - 600 ^{0}C. Blue-green persistent/long afterglow emission was observed from all the samples.

Red photoluminescence was observed from a nanocrystalline $SrAl_2O_4:Eu^{3+}$ powder phosphor prepared by a sol-gel process. The preparation process was carried out using $Sr(CH_3CO_2)_2.\frac{1}{2}H_2O$, Al (i-$OC_3H_7)_3$ and Eu_2O_3 as starting materials. The white foamy gel of $SrAl_2O_4:Eu^{3+}$ was dried at 60 – 200^{o}C and calcined at 1000 ^{0}C. Nanocrystals of $SrAl_2O_4$ exhibited an agglomeration of nano-rodlike particles with an edge thickness of ~27 nm on average. Based on the X-ray diffraction and photoluminescence data, $SrAl_2O_4$ was found to crystallize as metastable monoclinic rather than hexagonal phase. The crystalline structure and photoluminescent properties of $SrAl_2O_4:Eu^{3+}$ were reported.

KEYWORDS

Combustion method,

Sol- gel Method

Solid State Reaction method

Phosphorescence

Long-Afterglow

Photoluminescence

Rare earth ions

Alkaline Earth Aluminates

ACRONYMS

PL – Photoluminescence

SEM- Scanning Electron Microcopy

TEM – Transmission Electron Microcopy

He- Cd – Helium Cadmium Laser

EDS – Energy dispersive spectroscopy

XRD – X-ray Diffraction

Table of Contents

CHAPTER 1

INTRODUCTION

1.1. OVERVIEW

Luminescence is a phenomenon of emission of electromagnetic radiation by a physical system in excess of energy following excitation by electrons/photons [1]. An example of such a physical system is a phosphor (luminescent materials) which essentially emits light by converting one type of energy into another. They can be crystalline or non-crystalline [2]. A phosphor is composed of a host lattice and one or more activators in amounts from parts per million to a few mole percent. Either the host or activator can determine the luminescent properties of a phosphor. For example in zinc sulphide/cadmium sulphide: silver (ZnS:Ag/CdS:Ag) the emitted colors range from blue at zero cadmium through green, to yellow and into red as the Cd content is increased. The phosphors are generally powders having average particle sizes ranging from micro to nano-scale [3].

Due to the defects and irregularities in the crystal lattice structure, these materials have the ability to absorb incident energy and convert it into light in other regions of the electromagnetic spectrum. This process involves energy transfer from the UV source to the electrons in the phosphor crystals. The phosphor electrons are thereby raised to levels higher than the ground state and light will be emitted when electrons return to the ground state [3]. The emission of light when the electrons return to the ground state can be classified in terms of fluorescence and phosphorescence (long persistent), and the mechanisms involved will be discussed in chapter 2.

It has been discovered in the past that some of these luminescent materials show a very long lived afterglow (phosphorescence), arising from thermal emission of charge carriers from deep

traps, followed by electron hole recombination at or near a luminescent ion. They are referred to as long persistent phosphors [4]. ZnS:Cu phosphors have been well known as long persistent phosphors and used in a variety of applications since the beginning of the last century. ZnS has a long history (Leverenz 1950, Shionoya 1966), it dates back to 1866 when a French chemist Sidot found phosphorescence from ZnS crystals he grew. The afterglow of specially prepared ZnS:Cu can be used as a light indicator in clocks and watches. The afterglow arises from thermal release of electrons captured by traps [1]. However, ZnS:Cu is not bright enough for many applications and does not maintain its phosphorescence (afterglow) for more than a few hours. Furthermore, it has shown low chemical stability, low efficiency, as well as being hazardous due to radioactive materials used as a continuous excitation source [5]. In the past, various researchers tried to enhance the phosphorescence of these phosphors by adding radioisotopes such as tritium (^3H) and promethium (Pm 147), but this could not materialize due to safety and environmental concerns since these isotopes are radioactive [6]. Therefore there has been great demand of the radioactive free phosphors which are more reliable in terms of stability, brightness as well as long phosphorescence.

Alkaline earth aluminates (MAl_2O_4 (M= Ca, Sr, Ba)) co-doped with Eu^{2+} and Re^{3+} (RE = Ln, excluding Pm and Eu) ions are known to exhibit a bright and long lasting afterglow after irradiating with fluorescent light or sunlight [5]. In these types of phosphors (MAl_2O_4), Eu^{2+} activator serves as a luminescent centre which results from the $4f^65d^1$ - $4f^7$ transitions. The Eu^{2+} ions were shown to substitute Ca^{2+}, Ba^{2+} or Sr^{2+}cations in the distorted stuffed tridymite structure of MAl_2O_4 [7]. The RE ion (Dy^{3+}) has been proposed to be a hole trapping center. The incorporation of Re^{3+} ions results in many trap centers with appropriate depth in these phosphors and consequently prolonging the afterglow time at room temperature [7]. Compared to the sulphide phosphors the $MAl_2O_4:Eu^{2+},RE^{3+}$ (M= Ca, Sr, Ba) phosphors are safer, chemically stable, with no radiation, which resulted in an unexpectedly large field of applications such as luminous paints in highways, airports, buildings and ceramics products, as well as in textile, dial plates of glow watches, warning signs and escape routes [5]. In addition, some of the alkaline earth aluminates such as $SrAl_2O_4:Eu^{2+},Dy^{3+}$ composites encapsulated in silica can be used as

water temperature sensors. The water temperature can be evaluated by the variation of the phosphorescence intensity of the composite which is optically excited with a laser diode with an excitation wavelength of 405 nm as illustrated in figure 1. The phosphorescence intensity increases linearly with an increasing water temperature (0 -100 ^{0}C) [8].

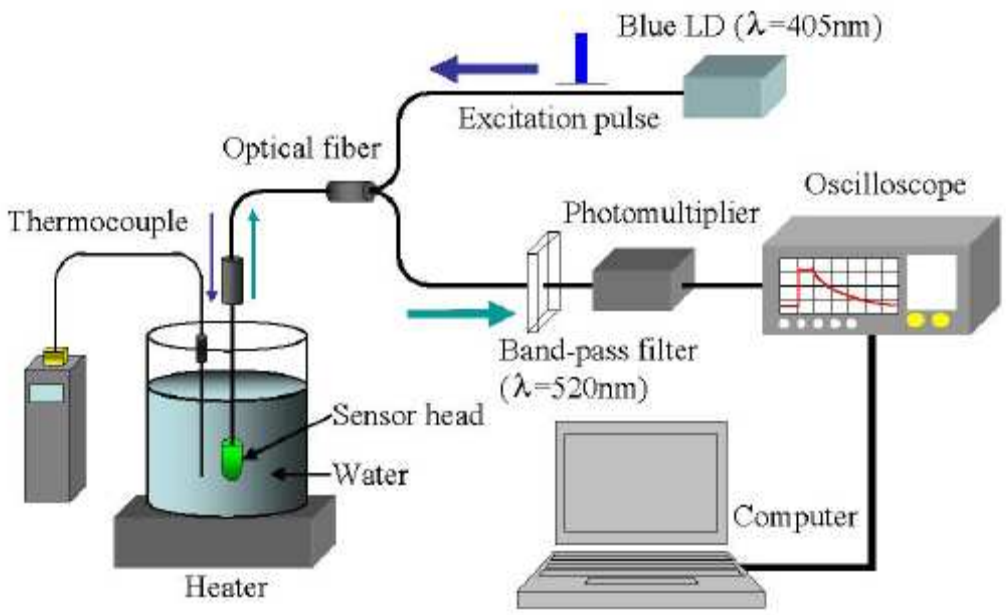

Figure 1.1: Experimental setup for water temperature measurements using the phosphorescent $SrAl_2O_4:Eu^{2+},Dy^{3+}$ composite sensor head [8].

With the development of current scientific technologies on materials, several chemical synthesis techniques have been applied to prepare phosphors and the shape and size of the particles may depend on the crystal type and particle size of the starting materials as well as the method of preparation [5]. In this study the sol-gel, combustion and solid state reaction methods were used to synthesize alkaline earth aluminate phosphors.

1.2. STATEMENT OF THE PROBLEM

ZnS doped with Cu has been known as one of the long phosphorescent phosphors which have applications in a wide range of industries. There remains, however practically important problems in ZnS phosphors. One of them is, that sulphide phosphors becomes more unstable and non luminescent in the presence of residual gases such as oxygen. Furthermore, the efficiency of ZnS phosphors decreases with an increase in an excitation density; this is called brightness saturation [1].

In the past decade long persistent phosphors, which overcame the shortcoming of the above mentioned sulphide phosphors were invented. These phosphors are Eu^{2+} activated aluminates, such as $SrAl_2O_4:Eu^{2+},Dy^{3+}$, $CaAl_2O_4:Eu^{2+},Dy^{3+}$, $Sr_4Al_{14}O_{25}:Eu^{2+},Dy^{3+}$ etc. These phosphors exhibit high brightness and long lasting afterglow without radioactivity and are therefore regarded as promising materials in the field luminescent materials [9]. The optical properties of the phosphors doped with different concentrations of the rare earth ions, as well as different preparation temperatures will be investigated.

1.3. RESEARCH OBJECTIVES

To investigate

(i) The luminescent properties of rare earths activated alkaline earth aluminate phosphor materials prepared by solid state reaction, combustion and sol-gel methods.

(ii) The effect of crystal field splitting and the distortion of different host lattices ($MAl_2O_4:Eu^{2+},Dy^{3+}$ (M= Ca, Ba,Sr)

(iii) The effects of the initiating combustion temperatures on the structural and optical properties of the long persistent phosphors ($CaAl_2O_4:Eu^{2+}$, Dy^{3+}, $BaAl_2O_4:Eu^{2+}$, Dy^{3+} and $SrAl_2O_4:Eu^{2+},Dy^{3+}$).

(iv) The influence of the stoichiometry (Sr : Al) on the luminescent and structural properties of a phosphor ($Sr_{0.97}Al_2O_4:Eu^{2+}{}_{0.01},Dy^{3+}{}_{0.02}$ and $Sr_{0.95}Al_2O_4:Eu^{2+}{}_{0.01},Dy^{3+}{}_{0.04}$)

(v) The luminescent properties of $SrAl_2O_4:Eu^{3+}$ phosphors doped with different concentrations of Eu^{3+}, prepared by a sol-gel method.

1.4. THESIS LAYOUT

Chapter 2 provides background information on the fundamentals of phosphors and types of luminescence in solids. Detailed information about the phosphorescence mechanism of long persistent phosphors as well as the electronic transition of rare earth ions (Eu^{2+}, Eu^{3+}) is provided. The structural properties of the alkaline earth aluminates ($MAl_2O_4:Eu^{2+},Dy^{3+}$) are briefly discussed. *Chapter 3* gives a brief description of the experimental techniques used to synthesize and characterize alkaline earth aluminate phosphors. The sol-gel, combustion and solid state reaction methods used to synthesize the phosphors are discussed in detail. Detailed information on the principle and operation of the experimental techniques used to investigate the luminescence and the structure of the phosphors are presented. Luminescent properties of $SrAl_2O_4:Eu^{2+},Dy^{3+}$ phosphors prepared by a solid state reaction method are discussed in *chapter 4*. In chapter 5, the luminescent properties influenced by crystal field changes and the distortion in the host matrix of the phosphors ($MAl_2O_4:Eu^{2+},Dy^{3+}$ (M = Ca, Ba, Sr) prepared by the combustion method is reported. *Chapter 6, 7 and 8* present the effects of the initiating combustion temperatures (500-800^{0}C) in $SrAl_2O_4:Eu^{2+},Dy^{3+}$, $CaAl_2O_4:Eu^{2+},Dy^{3+}$, and $BaAl_2O_4:Eu^{2+}, Dy^{3+}$. The effects of the concentration of the Eu^{2+} and Dy^{3+} in $Sr_{1-x}Al_2O_4:Eu^{2+}_x$, $Sr_{1-z}Al_2O_4:Eu^{2+}_{0.04},Dy^{3+}_z$ and $Sr_{1-y}Al_2O_4:Eu^{2+}_y,Dy^{3+}_{0.04}$ phosphors are presented in *chapter 9*. *Chapter 10* presents the red emitting $SrAl_2O_4:Eu^{3+}$ phosphors prepared by a sol-gel process. *Chapter 11* is about the concluding remarks on the overall study and suggestions for possible future studies.

REFERENCES

1. D. R. Vij, N. Singh, Luminescence and Related Properties of II-IV Semiconductors, Nova Publishers, New York, (1997) 169
2. S. Ekambaram, K.C Patil, M. Maaza, Synthesis of lamp phosphors, Facile combustion approach, Purdue University, USA, 2005
3. J. C. Whitaker, The Electronics Hand Book, CRC Press, USA, (1996) 469
4. O. Kasap, P. Capper, Hand Book of Electronic and Photonic, Springer, Canada, 2006
5. T. Peng, H Yang, X. Pu, B. Hu, Z. Jiang, C. Yan, Materials Letters **58** (2004) 352 -356
6. D. Wang, Y. Li, Y. Xiong, Q. Yin, Journal of The Electrochemical Society, **152 (1)** (2005) H1-H14
7. X. Luo, W. Cao, Z. Xiao, Journal of Alloys and Compounds **416** (2006) 250-255
8. S.K Tokuno, S. Komuro, H. Aizawa, T. Katsumata, T. Morikawa, CISE – ICASE, International Joint Conference, Bexco, Busan, Korea, 18 – 21 Oct, 2006
9. C. Chang, D. Mao, Thin Solid Films **460** (2004) 48-52

CHAPTER 2

LUMIINESCENT AND STRUCTURAL PROPERTIES OF PHOSPHORS

2.1. FUNDAMENTALS OF PHOSPHORS

The word phosphor comes from the Greek language and it means light bearer, and it refers to a luminescent or light emitting material [1]. Phosphors are mostly inorganic solid materials consisting of a host lattice, usually intentionally doped with impurities such as rare earth ions [2]. The impurity concentrations in general are relatively low because of the fact that at higher concentrations the efficiency of the luminescence process usually decreases due to concentration quenching effects. Most phosphors have a white body color, which is an essential feature that prevents absorption of visible light by the phosphors [2].

Ultraviolet (UV) energy can be used to excite a phosphor, and the excitation energy can either be absorbed by the host lattice and then transferred to luminescent centres (usually intentionally introduced rare earth ions or transition metal ions or defects) or it can be absorbed by an impurity ion and transfer to another impurity ion identical to the former. In general, the emission takes place on the impurity ions, and when these impurity ions are used to generate the desired emission, they are referred to as activators [2].

When the absorption efficiency displayed by an activator is too low, a second kind of impurity called sensitizer can be added, which will absorb the energy and subsequently transfer it to the activators as illustrated in figure 2.1.

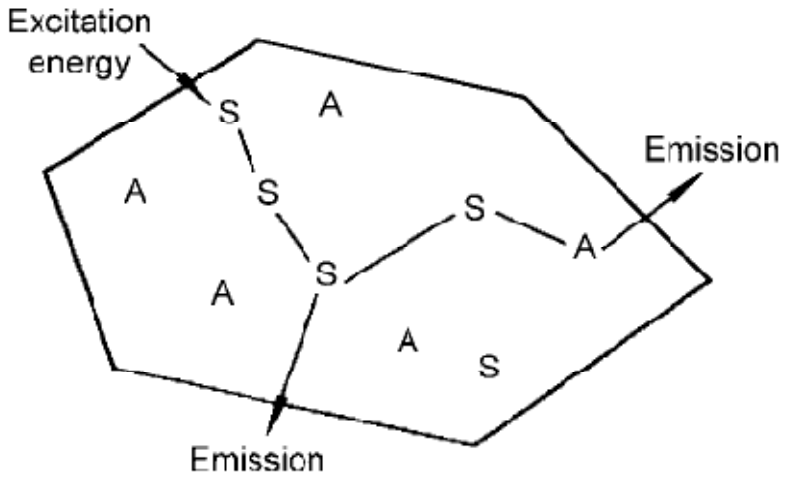

Figure 2.1: Phosphors containing activator ions A (ions showing the desired emission) and sensitizing ions S (on which UV excitation can take place) [2].

The energy transferred involves transport of energy through the luminescent materials, and in most cases, the emission color can be adjusted accordingly by choosing the proper impurity ion, without changing the host lattice in which the impurity is incorporated [3].

It is commonly known that, the emission of light exhibited by the luminescent materials is due to the excited electrons whose quantum state is above the minimum ground state [1]. There are several processes by which electrons can be excited in luminescent in materials. Shown in table 2.1 is a list of the most important types of luminescence processes and corresponding excitation mechanisms.

In this study, light emission by photoluminescence (PL) was investigated when different materials were excited by a fixed laser wavelength or various wavelengths using a monochromatized xenon lamp. Therefore only the photoluminescence (PL) process is discussed extensively in the following section.

Table 2.1: The various types of luminescence [4]

Name	Excitation Source
Cathodoluminiscence	**Electrons**
Photoluminescence	**Light (photons)**
Radioluminescence	**X-rays**
Thermoluminescence	**Heating**
Electroluminescence	**Electric field or current**
Triboluminescence	**Mechanical energy**
Sonoluminescence	**Sound waves in liquids**
Chemiluminescence	**Chemical reactions**

2.1.1. PHOTOLUMINESCENCE (PL)

In solids, PL takes place when the electronic states of the solids are excited by a photon and the excitation energy is released in the form of light [5].The emission process is more complicated than the absorption process, and this is because the generation of light by luminescence is initially tied up with the energy relaxation mechanism in the solid. Furthermore, the shape of the emission spectrum is affected by the thermal distribution of the electrons and holes within their bands [6]. The PL emission in solids, i.e. in inorganic insulators and semiconductors, is classified in terms of the nature of the electronic transitions producing it. In this study the classification of the electronic transition due to this kind of luminescence, such as intrinsic and extrinsic luminescence, are discussed in the next section.

2.1.2. INTRINSIC PHOTOLUMINESCENCE

Intrinsic photoluminescence is a kind of luminescence that may arise due to the presence of a variety of defects in a crystal structure [7**].** This type of luminescence does not involve impurity atoms. There are three kinds of intrinsic photoluminescence namely: band to band, excitons and cross luminescence. In general there are several factors that may influence intrinsic photoluminescence such as:

Non stoichiometry - a state of a material (semiconductor) not having exactly the correct elemental proportion.

Structural imperfections – owing to poor ordering, radiation damage, or shock damage.

2.1.3. EXTRINSIC PHOTOLUMINESCENCE

Extrinsic photoluminescence describes the luminescence that results due to intentionally incorporated impurities in the crystal structure [8]. In this case, defects and trace elements in the crystal lattice responsible for luminescence, known as activators with energy levels in the band gap (forbidden zone) provide additional energy levels for excitation and relaxation processes [8]. This type of luminescence in ionic crystals and semiconductors can be classified into two types: unlocalized and localized. In unlocalized luminescence the electrons and holes participate in the luminescence process (free electrons in the conduction band and free holes in the valence band), whereas in the localized luminescence excitation and emission processes are confined to a localized luminescence center [9].

2.2. TYPES OF LUMINESCENCE IN SOLIDS

The term luminescence refers to the absorption of energy with subsequent emission of light [10]. Luminescence in solids is exhibited by the group of semiconducting materials known collectively as phosphors [11]. In luminescent materials, fluorescence and phosphorescence are distinguished by whether the transition to emit light is allowed or forbidden by spin selection rules. The light emission due to an allowed singlet-singlet transition is called fluorescence, while that due to a forbidden transition which usually shows long afterglow is called phosphorescence [12].

2.2.1. FLUORESCENCE

Fluorescence in phosphors occurs when valence electrons are raised to the conduction band and return immediately via the luminescence centre to fill the holes in the valance band. In fluorescent phosphors there are no traps but many luminescent centers [11]. When the excited electrons return to the ground state, their surplus energy will be emitted in a form of visible light and the process is instantaneous. If the excited electrons return to the ground state in a time not greater than 10^{-6} sec, the resulting emission is described as fluorescence [13]. The energy of light emitted depends on the difference in energy across the luminescence centre. The emitted energy is always less than the energy which originally stimulated the fluorescence. For example, phosphors exited with higher energy in the ultraviolet region will result in emission in the visible spectrum which corresponds to less energy.

Figure 2.2 illustrates the electronic transition of an excited electron to the conduction band, which is followed by a subsequent return to the valance band via the luminescence centers. The photon emitted during this process has an energy that is equivalent to the energy difference across the luminescence centre. This energy difference will determine the emission wavelength and the colour of fluorescence [11].

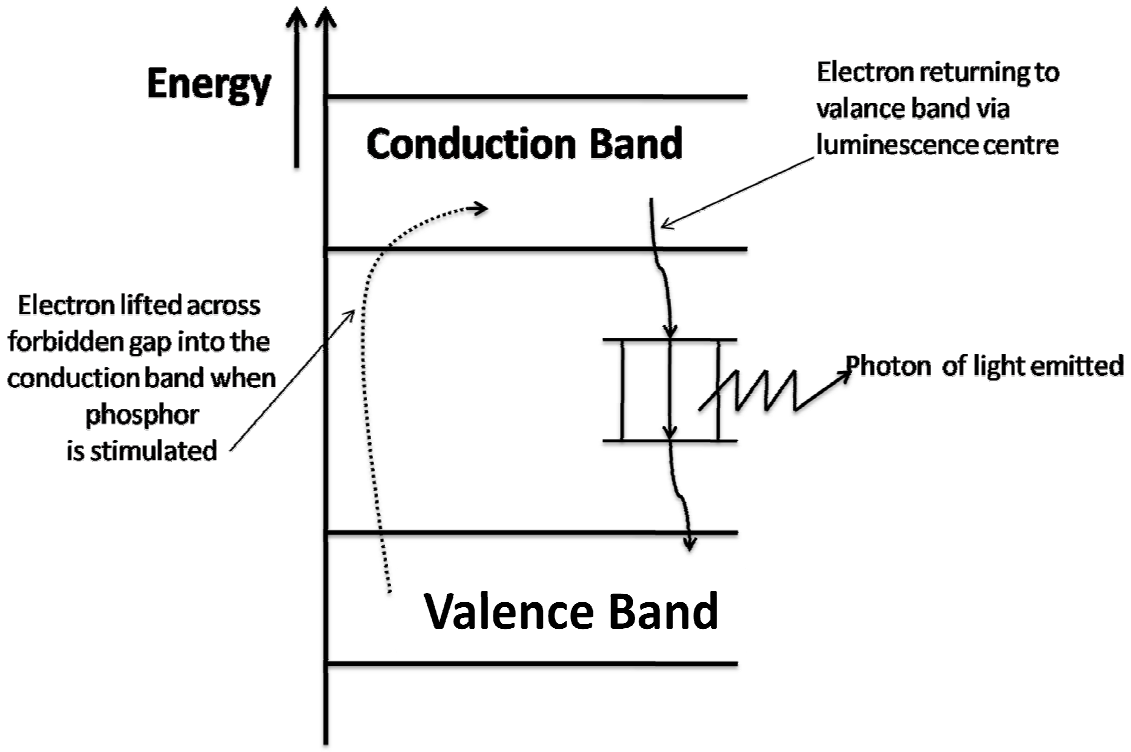

Figure 2.2: Energy band diagram of fluorescent phosphor [11].

2.2.2. PHOSPHORESCENCE

Phosphorescence is when the recombination of the photogenerated electrons and holes is significantly delayed in a luminescent material. If one of the excited states of a luminescent center is a quasistable state (i.e., an excited state with very long life time) a percentage of the centers will be stabilized in that state during excitation. Excited electrons and holes in the conduction and valence bands of a phosphor can often be captured by impurity centers or crystal defects before they are captured by emitting centers. When the probability for the electron (hole) captured by an impurity or defect center to recombine with a hole (electron) or to be reactivated

into the conduction band (valence band) is negligibly small, the center or defect is called a trap [5].

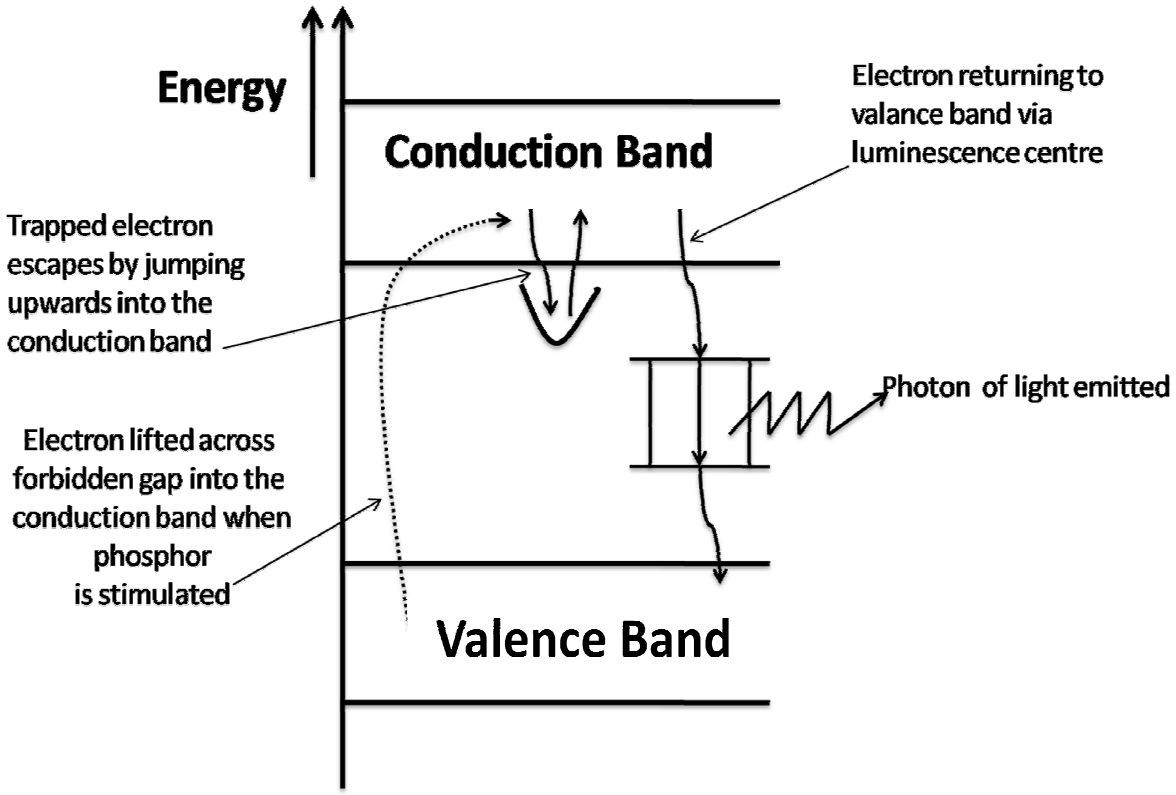

Figure 2.3: An energy band diagram representing a phosphorescent phosphor [11]

Figure 2.3 shows the electrons (holes) captured by traps, which may cause phosphorescence when they are thermally reactivated into the conduction band (valence band) and radiatively recombined at an emitting center. The decay time of phosphorescence due to traps can be as long as several hours and is often accompanied by the photoconductive phenomena [5]. The decay curve of the long afterglow due to traps is not generally represented by a simple exponential function. The form of a decay curve is dependent on the concentration of the traps and on the electron capture cross-sections of the traps and the emitting center. Furthermore, it also depends on the excitation intensity [5].

2.3. LUMINESCENT CENTERS

A wide variety of centers give rise to luminescence in semiconductors and insulating materials, including rare earth ions, transition metal ions, excitons, donor-acceptor pairs, and ions with a d^{10} or s^2 electronic configuration state [14]. The resulting characteristic luminescence can be comprised of either relatively sharp emission lines or a broad band in the visible part of the electromagnetic spectrum [2]. The sharp emission lines that are usually illustrated by most of the rare earth ions arise from purely electronic transitions and the effect of the environment is felt mainly through their effects on the lifetimes of the states [14]. The broad emission bands arise from the interaction between the electronic system of the luminescent centre and the vibrations of the atoms or ions, which surround it. This is due to the simultaneous transitions of both electronic and vibrational systems [14]. Furthermore the broad band spectra are observed when the character of the chemical bonding in the ground and excited states differs considerably. This process goes hand in hand with a change in equilibrium distance between the emitting ion and its immediate environment and is commonly explained with the configuration coordinate diagram shown in figure 2.4 [2].

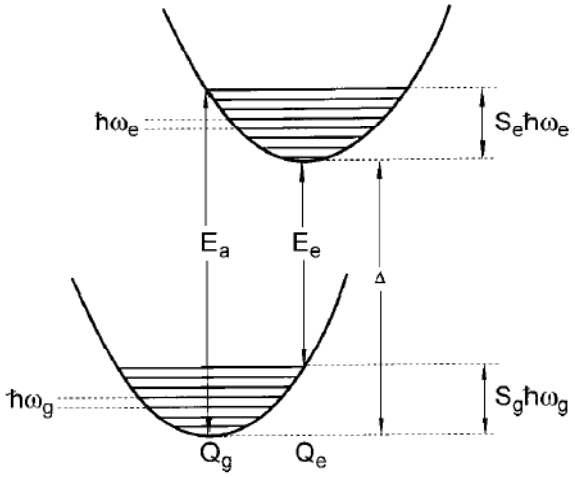

Figure 2.4: Configurational coordinate diagram [2].

As illustrated in the diagram, Q_g and Q_e represent the metal-ligand distances in the ground and excited state, respectively. E_a and E_e are the energies at which the absorption and the emission bands have their maximum intensity, respectively [2].The zero phonon energy given by Δ is the transition which involves the completely relaxed excited and ground states, and no excited photon states are involved- hence the name of this kind of transitions.

The $\hbar\omega_g$ and $\hbar\omega_e$ are the phonon energies in the ground and the excited states, respectively. The relaxation energies in the ground and excited states can be expressed as a product of the phonon energy and the Huang-Rhys factors. The Huang-Rhys factors S_g and S_e in the ground and the excited state, respectively give the mean number of phonons involved in the absorption and emission processes, respectively [2]. According to the harmonic approximation the curvature of the parabolic bands, the phonon frequencies and the Huang-Rhys factors are the same in the ground and excited state [2]. This diagram is very elementary, in the sense that it does not describe the thermal expansion of the lattice. However it does give a lot of insight, for example, it can be used to illustrate that a larger Stokes Shift is expected on increasing lattice relaxation and also in the description of thermal quenching of the emission [2].

2.4. OPTICAL TRANSITION OF RARE EARTH IONS

Rare earth (RE) is a common name for the elements in the Lanthanum group. The specific feature for these elements is the incompletely filled 4f shell [15]. The 4f orbital lies inside the ion and is shielded by the filled $5s^2$ and $5p^6$ orbitals [16].The rare earth ions may be embedded in different host materials in the form of divalent or trivalent ions. The influence of the host materials on the optical transitions within the configuration is small and this is due to shielding [16]. The energy level diagram which is a substantial part of the energy levels originating from the configuration $4f^n$ as a function of n for the trivalent ions is shown in figure 2.5.

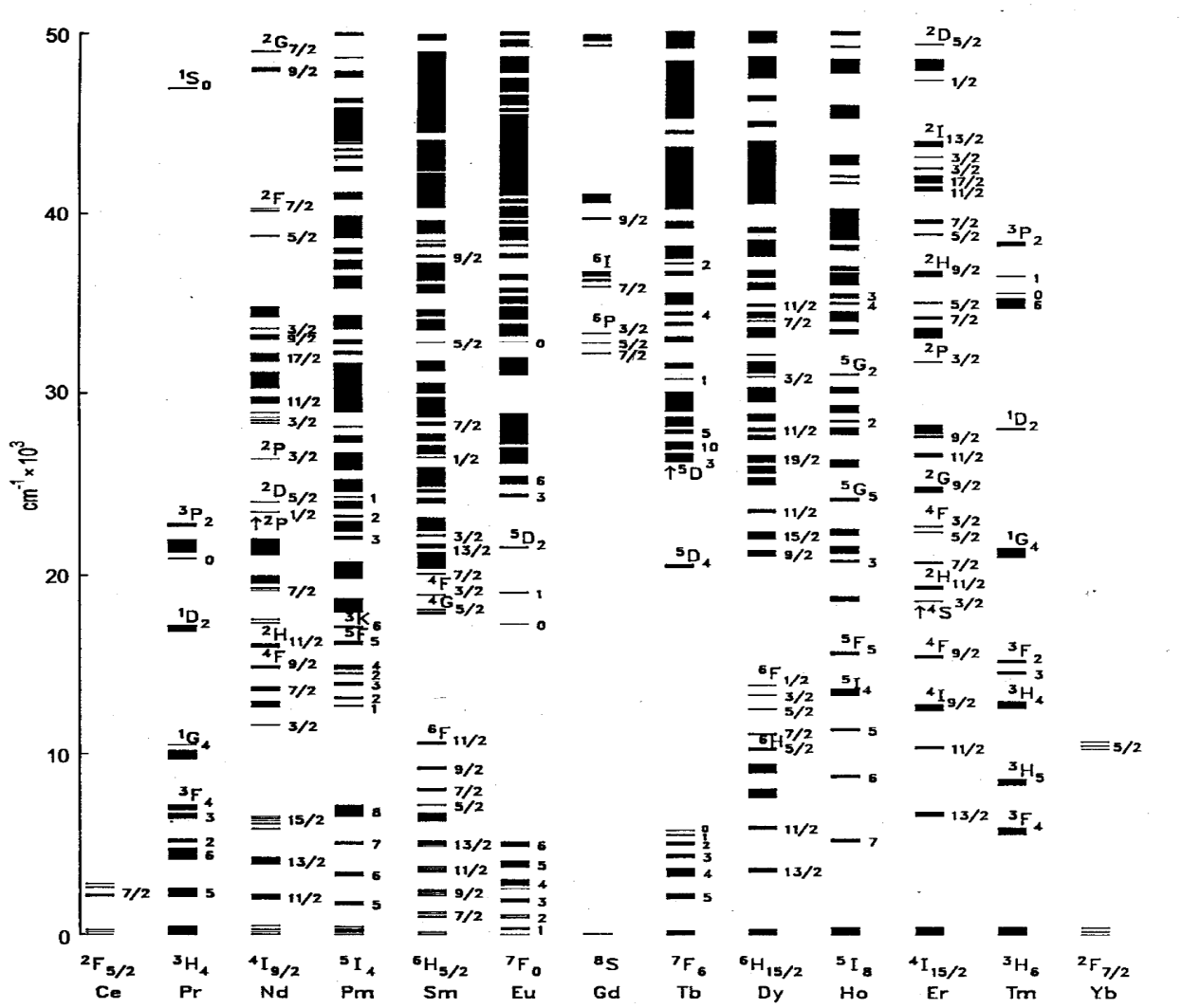

Figure 2.5: Energy level diagrams of the $4f^n$ configurations of the trivalent lanthanides [17].

The width of the bars as illustrated by figure 2.5, gives the order of the crystal field splitting. The optical absorption of these trivalent ions is strongly forbidden by the parity selection rule, which states that for a permitted atomic (ionic) transition the wave function of the initial and final states must have different parity [18]. When doped in a solid, a centric perturbation of the crystal field can create admixture functions with opposite parity (for instance $4f^{n-1}\ 5d^1$) yielding the so called electric dipole transitions [19].

2.4.1. THE f-f TRANSITION OF Eu^{3+} ($4f^6$)

The emission of this ion usually consists of sharp lines in the red spectral region. The sharp emission lines arise from the f-f transition of the Eu^{3+} ions. These emission lines have found an important application in lighting and display (color television) [16]. A simple electronic energy level diagram of Eu^{3+} shown in figure 2.6 illustrates the transitions from the singly degenerate excited state $^5D_0$ to the different sublevels within the terminal states ^7F_J (from J = 0 to 6), which correspond to different emission lines.

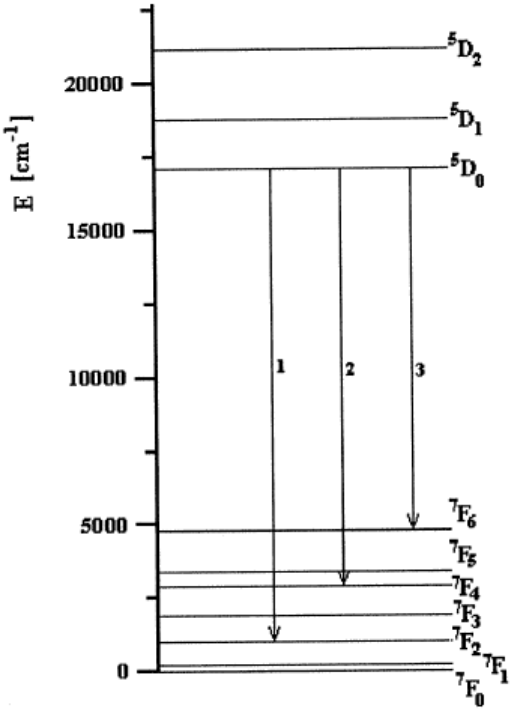

Figure 2.6: A simple electronic energy level diagram of Eu^{3+} [21]

The $^5D_0 \rightarrow {}^7F_0$ emission is forbidden at the electric dipole order and is not observed. Since the $^5D_0$ level is not split by the crystal field (because J=0), the splitting of the emission transition yields crystal field splitting of the ^7F_J [20]. In addition, the emission from higher D-states ($^5D_1$, $^5D_2$ and $^5D_3$) may also be observed and their presence will be determined by several factors

which will not be discussed in this study [16]. The $^5D_0 \rightarrow {}^7F_J$ emission is very suitable to survey the transition probabilities of the sharp spectral lines of the Eu^{3+} ion. In $SrAl_2O_4$ the transitions within Eu^{3+} may give sharp luminescence lines between 580 and 720 nm [21].

2.4.2 THE d-f TRANSITION OF Eu^{2+} ($4f^7$)

Divalent europium (Eu^{2+}) is the most well known and widely applied example of rare earth ions, and gives a very intense and broad emission spectrum in the visible range [22]. The broad bands result from the inter-configurational electronic $f^7(\ ^8S_{7/2}) – f^6d$ transition [23]. The electric dipole transition which is responsible for the promotion of one f electron from an f to d- orbital occurs between two configurations of opposite parity and therefore they are totally allowed at first order [23]. The energy of the $4f^65d^1$ state depends on the crystal field, because unlike the 4f electrons the 5d electron is in the outer shell and not shielded by the $5s^25p^6$ electrons [23]. As a result the excited 5d energy levels are split by the crystal field into t_{2g} and e_g components as illustrated by figure 2.7 [20].

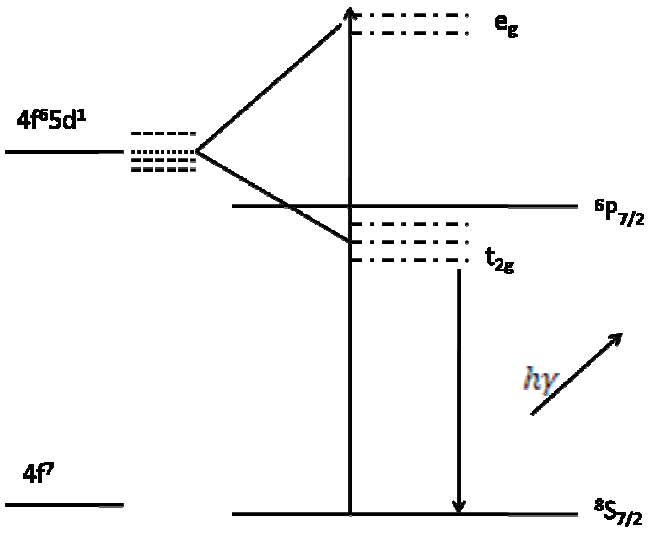

Figure 2.7: Energy level diagram of the $4f^7$ ($^8S_{7/2}$) – $4f^65d^1$ configuration of Eu^{2+} ion [24].

The Eu^{2+} emission is caused by the electronic transition from the lowest excited state to the $4f^7(^8S_{7/2})$ state. The interaction of the crystal field strength will determine whether the lowest $4f^65d^1$ is above or below the excited the $4f^7$ multiplets which are insensitive to the host lattice [25] .When the lowest excited state $^6P_{7/2}$ of $4f^7$ - configuration is located below the lowest state of the $4f^65d^1$ – configuration, a sharp emission line will be observed [23]. On the contrary, when there is no 4f state below the $^6P_{7/2}$ the broad emission band in Eu^{2+} will arise from dipole allowed $4f^65d^1 – 4f^7$. Furthermore, the emission wavelength depends on the strength of the crystal field around the Eu^{2+} ion [23].

2.5. PROPERTIES ASSOCIATED WITH PHOSPHORS.

2.5.1. NOTATION

In order to obtain an efficient phosphor, the notation between the host and the activator is a key factor. Most phosphors consist of a host composition and the activator, added in carefully controlled quantities. The activator itself will act as a substitutional defect and is subject to lattice phonon perturbations [10]. Therefore it is essential that charge transfer on the substitutional cation is equal to that of the host lattice cations, otherwise an efficient phosphor will not be formed. A typical example of phosphors can be denoted by: $M_aYO_b:N_x$ where M is the cation, YO_b is the anion and N is the activator. It is understood that the N- ion is in solid solution in the host matrix, and the above formula is actually: $(1-x)M_aYO_b$: x NYO_b [10]. Thus for europium activated strontium aluminate phosphor, we would write: $SrAl_2O_4:Eu_{0.01}$ = 0.99 $SrAl_2O_4$: 0.01 $EuAl_2O_4$. In this case Sr^{2+} is the cation, and Eu^{2+} is the activator.

2.5.2. QUANTUM EFFICIENCY

In terms of photoluminescence, the quantum efficiency $\boldsymbol{QE}$ ($\boldsymbol{\lambda}$) at a given excitation wavelength is defined as the ratio of emitted quanta to the number of the absorbed quanta at a certain excitation wavelength (λ) [5]. As already mentioned, the proper choice of host and the activator is essential to obtain an efficient phosphor. Now consider a case where one hundred (100) photons are incident upon a phosphor. It is well known that a portion of these photons will be reflected, some will be transmitted and, if the phosphor is an efficient combination of host and activator, most of the quanta will be absorbed [10]. But not all the absorbed quanta will result in an activated center, and once these centers become activated, not all will emit a subsequent phonon. Some become deactivated via relaxation processes. The quantum efficiency of phosphor can be expressed as follows: QE = (photons emitted/photons absorbed). In general, phosphors with quantum efficiency of 80% or greater, are considered as efficient phosphors [10].

2.5.3. BAND SHAPES

During excitation the density states arise due to the random process phonon perturbation of the excited state, both before it relaxes and afterwards as well. It is this random formation of Gaussian energy states that result in broad energy bands, which give rise to a broad band in excitation and to a broad band in emission [10]. The zero phonon line that will arise depends on the nature of the electronic transitions taking place, and is broadened by the vibronic coupling process. As the temperature rises, increased phonon- wave branching – intensities results and the emission band will be broadened further.

Figure 2.8 illustrates that the integrated emission intensities of one band will remain constant, and only the peak intensity will change as the band broadens. To this point it has been accepted that vibronic coupling leads to broadening of the excitation and emission bands of semiconductors (phosphor). The diagram shows that as the temperature increases, the phonon spectrum becomes broader, thereby leading to broadening of the bands [10]. Thus, at -200^0C, the

number of phonon vibrations is restricted and a rather sharper band is observed. As the temperature increases, the number of separate phonon branches increases (the empty phonon levels become occupied) and the emission (excitation) band is further broadened. It is important to mention that as the temperature increases above 300^0C according to this example, the phonon vibrations will increase to the point where the emission intensity will decrease to zero. In this case, what happens is that the relaxation processes through vibronic coupling have dominates the overall electronic excitation and emission processes [10].

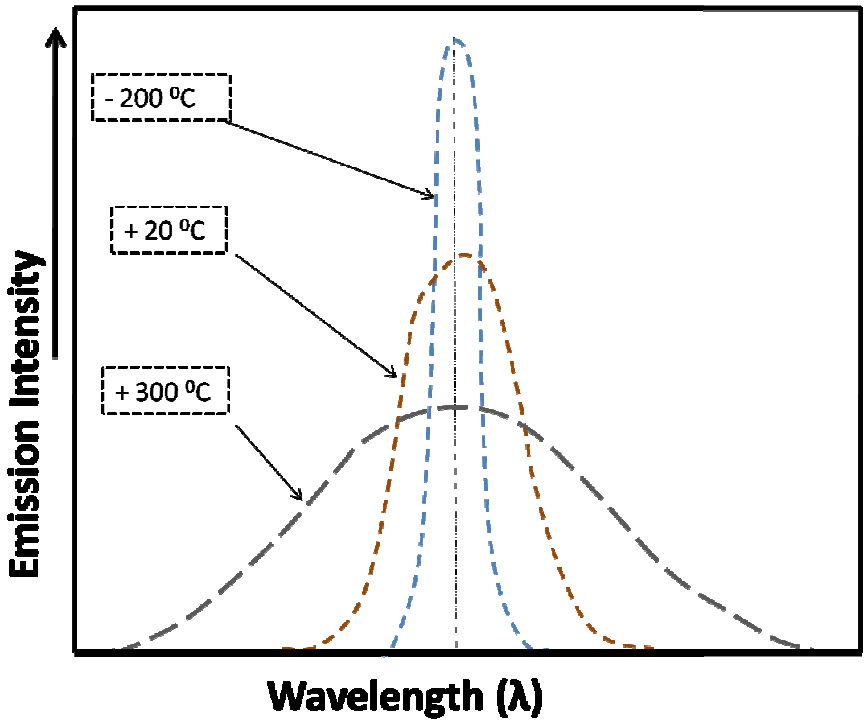

Figure 2.8: Experimental measurements illustrating that an increase in temperature will broaden the emission bands [10].

2.6. LONG PERSISTENT PHOSPHORS

Long persistent phosphors are luminescent materials that have long afterglow emission or phosphorescence. The long persistent phosphors to be discussed in this section are different from the radiation stimulated phosphors which rely on nuclear decay radiation as an excitation source [5]. The long afterglow mechanism of the luminescent materials in this study rather relies on the trapped electrons produced by an excitation source.

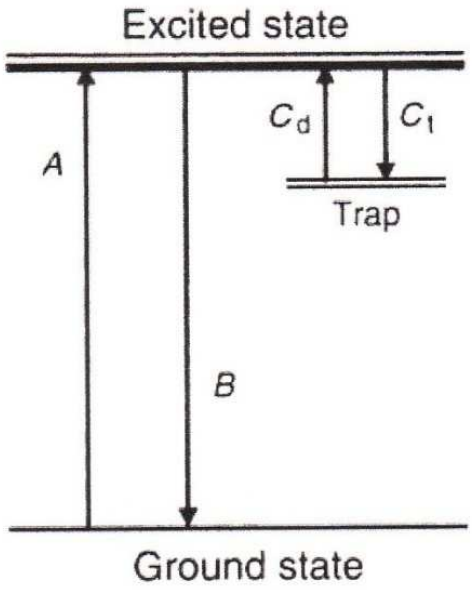

Figure 2.9: Illustration of the long persistent phosphorescence mechanism of a phosphor [5]

Figure 2.9 illustrates the long persistent phosphorescence mechanism which can be explained in terms of a simplified three level diagram, which includes a ground state, an excited state and a metastable trapping state for the active electron [5]. As shown in the figure, C_t and C_d are trapping and detrapping rates, respectively and A and B are the excitation and emission rates respectively. The phosphorescence lifetimes are usually longer than the lifetime of the excited state and depend on the trap depth and trapping-detrapping mechanism. The phosphorescence of the phosphors can be classified according to the lifetime. Very short persistent phosphorescence

has a lifetime of the same order of magnitude as the lifetime of the exited state. Normally this is not longer than a few milliseconds and this is attributed to shallow traps. Short persistent phosphorescence which is noticeable to the human eye generally can last for few seconds [5]. Most common phosphors may show some short time persistence especially after being exposed to the UV, electron beam, plasma beam, X-rays or to gamma rays. On the other hand the persistent phosphorescence and long persistent phosphorescence have lifetimes in minutes or hours respectively [5]. The persistent lifetime of long afterglow phosphors can be defined as the afterglow emission intensity to decay to 0.032mcd/m^2, which is approximately 100 times the limit of human perception with dark adapted eyes [5].

2.7. PHOSPHORESCENCE MECHANISM OF ALKALINE EARTH ALUMINATE ($MAl_2O_4:Eu^{2+},Dy^{3+}$) PHOSPHORS

Phosphorescence, as mentioned earlier, refers to light emission by a material that persists at room temperature after stopping the excitation source (usually UV radiation). The delayed emission in these materials arise from the fact that charge carriers (i.e. electrons and/ or holes) generated by excitation are trapped at certain defect sites and their detrapping is thermally activated [26]. The trapped carriers can be excited out of traps thermally when the temperature is sufficiently high. The rate of electron escape from the trap can be expressed as:

$$\boldsymbol{P = f\, e^{(-\frac{W_t}{k_B T})}} \qquad \textbf{2.1}$$

where W_t is the trap depth and the frequency factor $\boldsymbol{f}$ is given by the product of the density of states of the band into which the carriers are released, the thermal velocity of the carrier and the capture states cross section of the trap [27]. The phosphorescence mechanism of the alkaline earth aluminate phosphors ($MAl_2O_4:Eu^{2+},RE^{3+}$) was first proposed by Matsuzawa *et al.*[28] and was later modified by various researchers such as Clabau *et al.* [26], Aitasalo *et al.* [29],

Beauger *et al.* [30] etc. The widely accepted mechanism is the one proposed by Clabau *et al.* [26]. They reported that the problem with previous phosphorescence mechanisms is that most of them are not consistent with a number of important experimental and theoretical observations. Their new proposed mechanism (figure 2.10) relies on the fact that the d- state of Eu^{2+} is located near the bottom of the conduction band of $SrAl_2O_4$, and also the Eu^{2+} concentration decreases under UV excitation, and that the phosphor samples always have small amounts of Eu^{3+} ions, because it is impossible to reduce all Eu^{3+} ions to Eu^{2+} under the synthetic conditions employed.

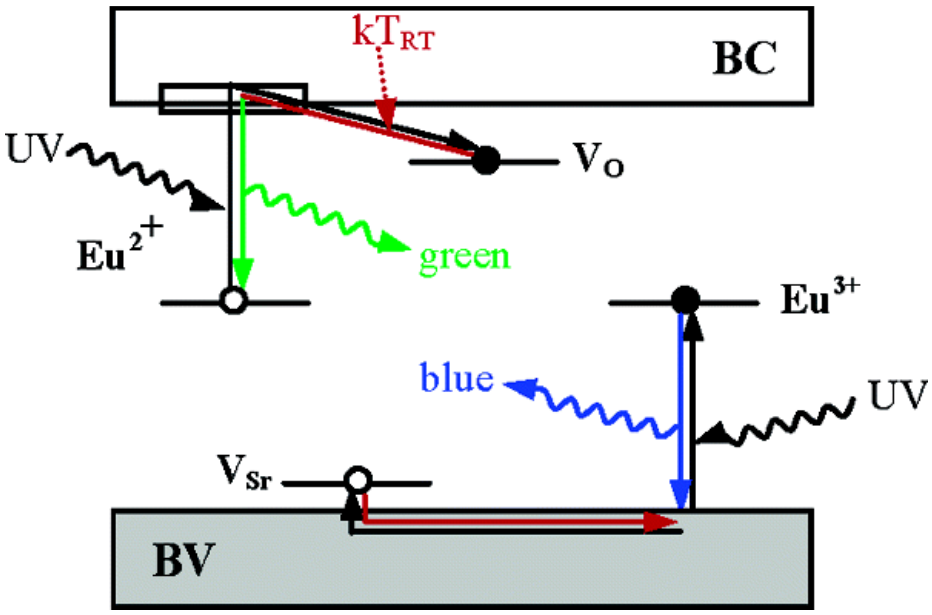

Figure 2.10: Phosphorescence mechanism proposed by Clabau et al. [26]

Under UV excitation, the electrons are promoted from the occupied 4f levels of Eu^{2+} to the empty 5d levels and from the top valence band of the unoccupied 4f levels of residual Eu^{3+} (i.e. charge transfer) [26]. The excited electrons promoted to the 5d level can be trapped at the oxygen vacancy V_O located in the vicinity of the photogenerated Eu^{3+} as illustrated by figure 2.10, while the holes created in the valance band can be trapped at the strontium V_{Sr} or aluminum V_{Al} vacancy. The thermal energy at ambient temperature will lead to detrapping of trapped electrons directly to the conduction band (CB) 5d levels of Eu^{2+}, hence leading to the $4f^6 5d^1 - 4f^7$ ($S_{7/2}$) green phosphorescence. According to Clabau *et al.* [26] the role of the trivalent rare-earth

(Re^{3+}) co - dopant such as Dy^{3+} is to enhance phosphorescence and the trap depth and the number of electron traps in the vicinity of Eu^{2+}[26].

The phosphorescence mechanism of $CaAl_2O_4:Eu^{2+},Dy^{3+}$ proposed by Lin *et al.* [31] is shown in figure 2.11.

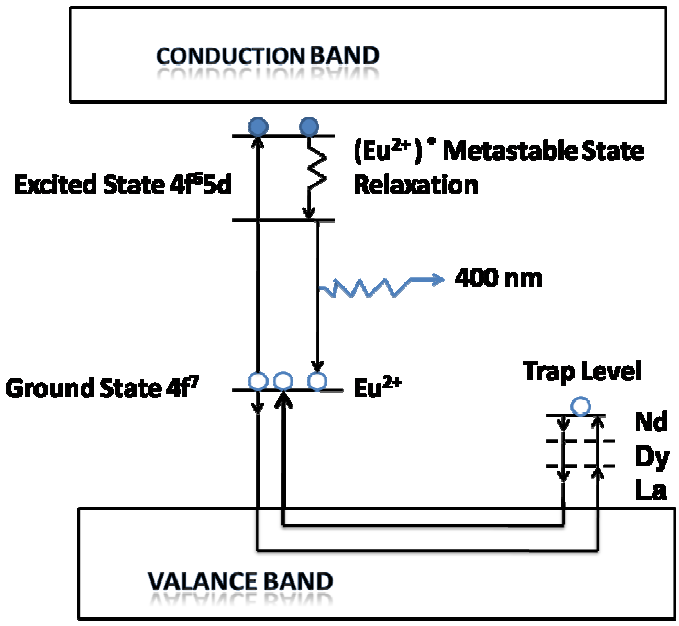

Figure 2.11: Phosphorescence mechanism of $CaAl_2O_4:Eu^{2+},Dy^{3+}$ (Re^{3+}) proposed by Lin *et al.* [31]

As reported earlier, when the Eu^{2+} ions are excited, the electrons will be promoted from the ground state $4f^7$ to the excited state $4f^65d^1$ and the holes will be generated. Some of these free holes are thermally released to the valance band and some of them are trapped by co-doped rare earth ions (Dy, Nd, La).When the excitation source is removed the trapped holes are released by thermal bleaching to recombine with some of the free electrons which leads to long afterglow [31]. The discrepancies in the phosphorescence mechanism of $MAl_2O_4:Eu^{2+}$, Re^{3+} (Dy, Nd, La) proposed by various researchers still require further investigation.

2.8. CRYSTAL FIELD CHANGES AND DISTORTION IN $MAl_2O_4:Eu^{2+}$ (M = Ca, Sr, Ba) HOST LATTICE

The phosphorescence of Eu^{2+} in most aluminate hosts is well known and it is believed to be due to the 4f – 5d transition. The peak positions in the emission spectra depend strongly on the nature of the Eu^{2+} surroundings, and therefore, Eu^{2+} ions can emit visible light of different wavelengths due to the changes in crystal fields [32]. The energy position for the lower d- band edge for Eu^{2+} in various hosts can be calculated by the following empirical relation:

$$E = Q\left[1 - \left(\frac{V}{4}\right)^{1/4} 10^{-(n \times EA \times r)/8}\right] \qquad 2.2$$

and can be used to provide a good fit to the emission peak data. Here Q is the energy position for the lower d- band edge for the free ion; V is the valency of the active cation (for Ca, Ba and Sr, V = 2); n is the number of anions in the immediate shell about this ion; EA is the electron affinity of the atoms; and *r* is the radius of the cation replaced by the active cation in the crystal structure of the host [32]. It is well known that the emission wavelengths of the $MAl_2O_4:Eu^{2+}$ phosphors do not shift from short to long wavelength with increasing ordinal number of the alkaline earth metals (Ca, Sr and Ba), but this is due to the distortion and crystal field changes experienced in the host lattice when Eu^{2+} ions substitute the sites of the cations. When a foreign atom is introduced at an interstitial site, this will be accompanied by a distortion in the host lattice. The distortion arises from a size mismatch between the doped and the substituted ions in the matrix [33]. In the case of MAl_2O_4, an anamorphic crystal lattice will result, when the surroundings of Eu^{2+} ion is changed and so the emission wavelengths will change correspondingly [33]. Figure 2.12 shows the schematic energy level of Eu^{2+} ion in MAl_2O_4 as a function of the crystal field strength and distortion in the host lattice.

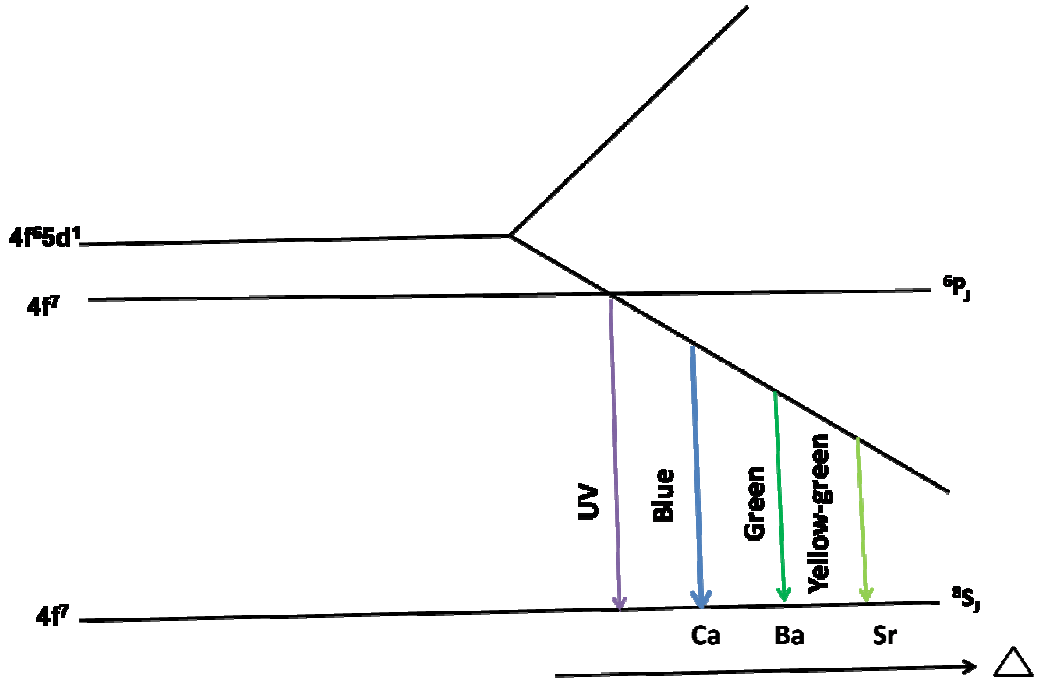

Figure 2.12: Schematic energy level diagram of Eu^{2+} ion due to crystal field and distortion in the MAl_2O_4 (Ca, Ba, Sr) phosphors [32].

2.9. STRUCTURAL CHARACTERISTICS OF ALKALINE EARTH ALUMINATE (MAl_2O_4 (M= Sr, Ca, Ba) HOST.

Alkaline earth aluminate (MAl_2O_4) hosts belong to the stuffed tridymite structure and the three dimensional framework of corner sharing AlO_4 tetrahedra. Each oxygen has one negative charge and the balance is accomplished by divalent cations (Ca, Ba, Sr) which occupy the interstitial sites within the tetrahedral framework [32].

2.9.1. CRYSTAL STRUCTURE OF $SrAl_2O_4$

Strontium Aluminate ($SrAl_2O_4$) exists in two crystallographic forms and a reversible transition occurs at 650^0C. The monoclinic $SrAl_2O_4$, which is stable at lower temperature, is a distorted form of the hexagonal $SrAl_2O_4$.The distortion involves a reduction in the symmetry of trigonally

distorted rings [35]. The low temperature $SrAl_2O_4$ phase (monoclinic, space group $P2_1$, a= 8.447Å, b = 8.816 Å, c = 5.163 Å, b = 93.24 Å) is well established, but that of high temperature (hexagonal, space group $P6_322$, a = 5.140 Å, c = 8.462 Å) is not [26]. The low temperature phase shown in figure 2.13.a has a three dimensional network which is constructed by corner shared AlO_4 tetrahedra forming zigzag strings and Sr penetrating the openings of the structure [36].

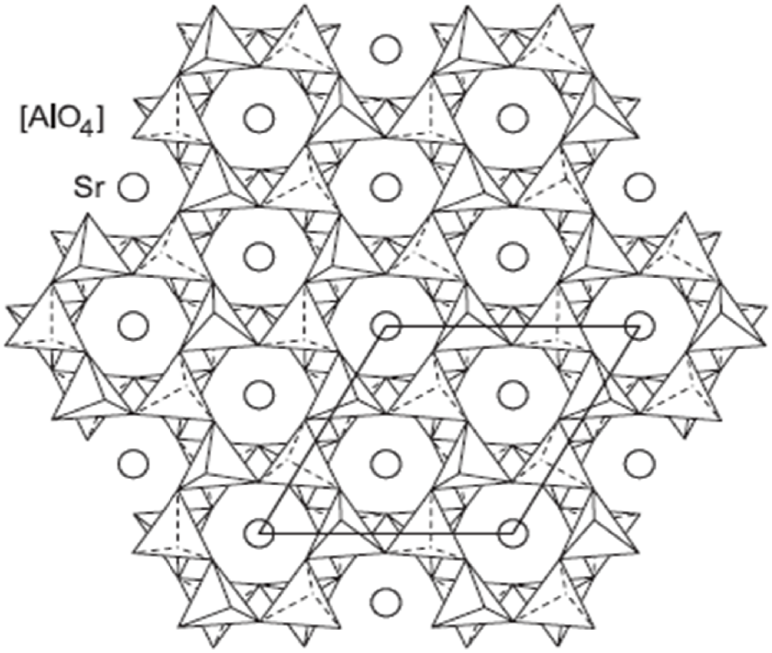

Figure 2.13.a: Monoclinic $SrAl_2O_4$ ($P2_1$) viewed along (100) direction [36].

2.9.2. CRYSTAL STRUCTURE OF $BaAl_2O_4$

$BaAl_2O_4$ has a very high melting point of 1815 ^{0}C and holds a stuff tridymite (hexagonal) structure with lattice parameters a = 10.449 Å and c = 8.793 Å. The $BaAl_2O_4$ structure belongs to the – $P6_3$ space group [37]. Figure 2.14 shows the crystal structure of $BaAl_2O_4$, which consists of two types of tetrahedral rings; trigonal and asymmetrical rings. The trigonal rings, comprising 25% of the total number of rings, contain in their center the Ba atoms with the

special position. This implies that the triad axes exist in the center of the rings and hence they are distorted trigonally [36]. On the other hand the Ba atoms in the asymmetrical rings are located at the general position (6c) site. The alternating arrangement of these two types of rings within the layers leads to doubling of the a-axis with respect to the tridymite unit cell. The solid lines in figure 2.14 represent the unit cell and the closed circles are Ba atoms at special positions (2a sites) [36]. In $BaAl_2O_4$ there two different sites, one site (site -1) is twice as abundant as the other (site -2) [37].

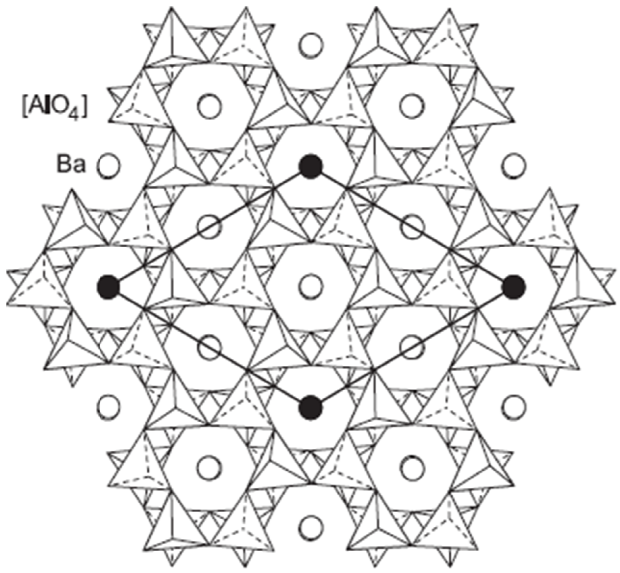

Figure 2.14: $BaAl_2O_4$ crystal structure viewed along (0001) [36].

2.9.3. CRYSTAL STRUCTURE OF $CaAl_2O_4$

Mono-Calcium aluminate, $CaAl_2O_4$ finds potential application as refractory castables, high strength polymer modified cement based materials, optical materials and ceramics [38]. The crystalline structure of mono-aluminate $CaAl_2O_4$ is comprised of channels formed by six-membered rings of aluminium tetrahedra, filled with calcium ions. $CaAl_2O_4$ has a - tridymite type monoclinic structure space group: $P2_1/n$ where $[AlO_4]$ compose a three dimensional

framework as shown in figure 2.15. Each oxygen atom is shared with two aluminium ions. There are three Ca^{2+} sites in the $CaAl_2O_4$ lattice: one is nine-fold coordinated and others are six-fold coordinated with oxygen atoms [39].

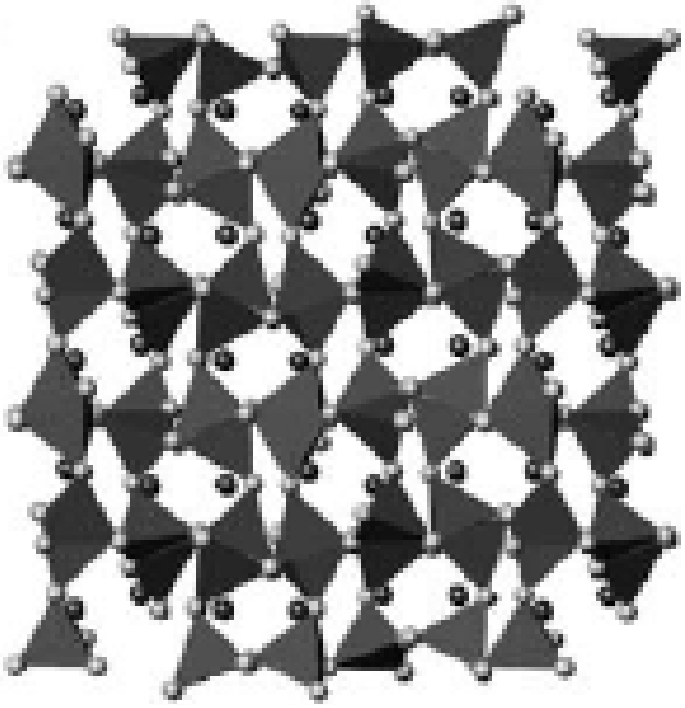

Figure.2.15: A β- tridymite type monoclinic structure of $CaAl_2O_4$ [39]

REFERENCES

1. A. Kitai, Luminescent Materials and Applications, John Wiley & Sons, Canada, 2008 pp 19
2. C. R Ronda, Luminescence from Theory to Applications, Willy-VCH, Germany, (2008) pp 3
3. T. Gacoin, A. Huignard, G. Counio, J. Boilot, Mat. Res. Soc. Symp. Proc **628** (2000) pp 371
4. An Introduction to the Optical spectroscopy of Inorganic Solids, by J.G Sole, L.E Bausa and D. Jaque, ISBN 0-470-86886-4,John Wiley and Sons,Ltd (2005) pp17
5. S. Shionoya, W.M. Yen, Phosphors Handbook, CRC Press,USA, 1998, pp 95
6. M. Fox, Optical Properties of Solids, Oxford University Press, London, 2006, pp 94
7. S. Boggs, D. Krinsley, Application of Cathodoluminescence imaging to the study of sedimentary rocks, Cambridge University Press, England, 2006
8. R.D. Blackledge, Forensic analysis on the cutting edge, John Willey & Sons Publications, USA, 2007
9. D. R. Vij, Luminescence of Solids, Science, Plenum Press, New York & London, 1998
10. R.C. Rop, Luminescence and the Solid state, Elsevier Science Publishers, USA, 1991
11. J. Ball, A. D. Moore Essential physics for radiographers, Blackwell Publishing, First edition, Oxford, 1979
12. W.M Yen, S. Shionoya, Fundamentals of phosphors, CRC Press, USA, 2007
13. J.T .Randall and M.F Wilkins, Proc. R. Soc. Lon.Vol.**184** A (6 November 1945 (347)
14. W. Martienssen, H. Warlimont, Handbook of Condensed Matter and Data Materials, Springer, USA, 2005
15. J. Singh, Optical properties of condensed matter and applications, Willey, USA, 2006
16. G.Blasse ,B.C Grabmaier, Luminescent materials, Springer-Verlag, USA, 1994
17. F. Träger, Handbook of Lasers and Optics, Springer, USA,2007
18. J. Singh, Optical properties of Condensed Matter and Applications, Willey, USA, 2006
19. F. Träger, Handbook of Lasers and Optics, Springer, USA, 2007

20. G. Solé, L.E. Bausá, D. Jaque, An introduction to the optical spectroscopy of inorganic solids, John Willey and Sons, USA, 2005
21. V. Kityk, J. Wasylak, D. Dorosz, J. Kucharski, Optics & Laser Technology **33** (2001) 157–160
22. T. Kobayashi, T. Sekine, N. Hirosaki, Optical Materials **31** (2009) 886–888
23. J. Krupa, N.A. Kulagin, Physics of laser crystals, NATO Science Series, II, Mathematics, Physics and Chemistry, Vol **126** (2003) pp 166
24. S. Galajev, Master's Thesis, University of Tartu (2008)
25. Z. Luo, Y. Huang, X. Chen, Spectroscopy of Solid-State Laser and Luminescent Materials, New York, USA, 2006
26. F. Clabau, X. Rocquefelte, S. Jobic, P. Deniard, M. H. Whangbo, A. Garcia, T. Le Mercier, Chem. Mater, **17** (2005) 3904 -3912
27. S. Sugano, N. Kojima, Magneto - optics, Springer Publishers, USA, New York, 2000
28. T. Matsuzawa, Y. Aoki, N. Takeuchi, N. Maruyama, Y. J. Electrochem. Soc. **143** (1996) 2670
29. T. Aitasalo, J. Hölsa, M. Lastusaari, J. Legendziewicz, J. Niittykoski, J. Radiat. Eff. Defects Solids **158** (2003) 89
30. C. Beauger, Thesis, University of de Nice, France, 1999
31. Y. Lin, Z. Tang, Z. Zhang, C. Nan, Journal of the European Ceramic Society **23** (2003) 175-178
32. Y. Lin, Z. Zhang, Z. Tang, J. Zhang, Z. Zhang,B. Lu, Materials Chemistry and Physics, **70** (2001) 156 -159
33. K. Srinivasa Rao, R. Balasubramaniam, J. Hydrogen Energy **21(7)** (1996) 563-569
34. Z .Qui, Y Zhou, M. Lu, A Zhang, Q. Ma, Acta Materialia **55** (2007) 2615-2620
35. K. Fukuda, K. Fukushima, Journal of Solid State Chemistry **178** (2005) 2709–2715
36. Z. Fu, S. Zhou, S. Zhang, J. Phys. Chem. B **109 (**2005) 12396–14400
37. D. Jia, X. Wang, E. Van der Kolk, W. M Yen, Optics Communications **204** (2002) 247-251
38. K.S Kumar, L.J Berchamans, Ceramics International **35** (2009) 1277-1280

39. Y.J. Park, Y. J. Kim, Materials Science and Engineering B **146** 9 (2008) 84-88
40. P.J. Saines, M.M. Elcombe, B.J. Kennedy, Journal of Solid State Chemistry **17** (2006) 613-622

CHAPTER 3

EXPERIMENTAL TECHNIQUES

3.1. INTRODUCTION

In this chapter a brief description of the experimental techniques used to synthesize and characterize the alkaline aluminate phosphors is presented. The combustion, sol gel process and solid state reaction methods were used to synthesize the alkaline earth aluminate phosphors. X-ray diffraction (XRD) and scanning electron microscopy (SEM) coupled with the energy dispersive X-ray (EDX) spectrometer were used to investigate the crystalline structure, particle morphology and elemental composition of the phosphor powders, respectively. Transmission Electron Microscopy (TEM) was also used to examine the crystalline structure of the phosphors. A 325 nm He-Cd laser fitted with a SPEX 1870 0.5m spectrometer and a photomultiplier detector was used to collect photoluminescence data in air at room temperature. A Cary Eclipse fluorescence spectrometer fitted with a monochromatic xenon lamp was also used to investigate the photoluminescence (excitation and emission) properties and decay characteristics of the phosphors.

3.2. SYNTHESIS TECHNIQUES

The growth of nanosciene and nanotechnology in the last decade has been made possible by the success in the synthesis of nanomaterials. The synthesis of the nanomaterials includes control of size, shape and structure of the materials [1]. Over the past few years, nanoparticles (powders) of ceramic materials have been produced on large scales by employing physical and chemical methods. The considerable scientific progress in preparation of nanomaterials such as ceramics and semiconductors has been made possible by synthesis techniques such as co-precipitation,

sol-gel, combustion method, etc [1]. In this study, combustion, solid state reaction and sol gel methods were used to synthesize the alkaline earth aluminate phosphors doped with rare earth ions.

3.2.1. COMBUSTION METHOD

The combustion method has emerged as an important synthetic route for the synthesis and processing of advanced ceramics (structural and functional), catalysts, composites, alloys, intermetallics and nanomaterials [2]. The combustion process has generated more interest in the field of nanomaterials such as luminescent materials (phosphors) and other ceramic materials, because fine particle sizes, multicomponent, crystalline and homogenous materials can be achieved at relatively low temperature and less time [3].

The combustion process involves a redox (reduction- oxidation) reaction between an oxidiser such as metal nitrates and an organic fuel such as urea (CH_4N_2O), carbonhydrazide (CH_6N_4O), citric acid ($C_6H_8O_7$) or glycerine ($C_2H_5NO_2$). In general good fuels should react non-violently, produce nontoxic gases, and act as a chelating agent for metal cations [3]. Among the well known fuels, urea and glycerine have demonstrated the versatility for combustion synthesis method by the successful preparation of large number of single phase and well crystallized multicomponent oxides.

The combustion process involves an exothermic reaction that occurs with evolution of heat. Once the precursors are ignited the energy necessary for the combustion reaction is supplied from the reaction itself, and hence this process is sometimes called self-propagating low temperature synthesis. [4].

The luminescent materials (phosphors) prepared by the combustion method have low density and have a fluffy texture. Ultra fine particles produced during the combustion reaction are accompanied by the evolution of gases. As more gases are released, either agglomerates are not formed or disintegrated into fine particles [4].

Furthermore, compared to other conventional ceramic processing techniques, the combustion method has shown several advantages such as:

(i) Short reaction times.
(ii) Inexpensive processing equipment.
(iii) Production of final product in one step using the chemical energy of the reactants.
(iv) Liberation of volatile impurities and thus higher purity products.

3.2.2. SOLID STATE REACTION METHOD

The solid state reaction method is the oldest and still the most commonly used method of preparing multicomponent solid materials by direct reaction of solid components at high temperatures. Since solids do not react with each other at room temperature – even if thermodynamics favours product formation-high temperatures are necessary to achieve appreciable reaction rates. The advantage of solid state reaction method is the availability of precursors in abundance and the low cost for powder production on the industrial scale [5].

The solid state reaction method is commonly used for synthesis of luminescent materials at elevated temperatures. During the synthesis of phosphors, a host matrix is formed from high purity starting chemicals and the impurities, also known as activators and co-activators of specified quantities are diffused into the crystal lattice. The formation of a phosphor host and doping process by solid solution is critical and is highly dependent on the reaction temperature and the environmental conditions. During synthesis the purity of the starting chemical is very important, typically 99.9 – 99.999 %. Furthermore, it is important to minimize contaminants such as Fe, Ni, Co etc, which can seriously affect the performance of the phosphor [6].

The starting chemicals are mixed in the presence of an appropriate flux such as B_2O_3 (boric oxide) and fired at high temperatures (900 -1500 ^oC) in air or in a controlled atmosphere (N_2, C, CO_2 or N_2 with 25% of H_2). The flux is added in order to improve the crystal structure of a

material. The presence of flux materials of low melting compounds such as alkali halides helps to complete the doping process at low temperatures [6]. The morphology, particle sizes and shapes are largely influenced by the starting chemicals and the flux. The luminescence efficiency and the crystal structure of the phosphors will also be influenced by the calcination conditions such as the firing temperature, duration of firing, firing atmosphere and the heating rate and cooling process [6]. The solid state reaction method was used in this study to synthesize the alkaline earth aluminate phosphors doped with rare earth ions.

3.2.3. SOL-GEL METHOD

The sol-gel method is a chemical technique that uses metal alkoxides for the synthesis and production of glasses or ceramics, through a series of chemical processes, including hydrolysis, gelation, drying and thermal treatment. The sol-gel method was discovered as early as 1864 by T Graham. The potential of the sol-gel method was rediscovered in the 1980's due to its usefulness during the synthesis of various materials of practical importance such as optical glasses and solid state laser materials [7]. Since then the method has received considerable attention and has been investigated extensively. The starting point of this method is a sol, which is a colloidal dispersion of small particles suspended in a liquid. A sol can be stabilized by peptization, i.e. the addition of peptizing agents (e.g. HNO_3) which form an electrically charged layer around each particle; electrostatic repulsion then prevents the particles to aggregate. Under suitable chemical and thermal conditions, the particles in some sols can be made to react or interact electrostatically so that they form a continuous, three dimensional network of connected particles called gel [8].

The sol-gel method of phosphor preparation is regarded as wet a chemistry method. The metal alkoxides, during preparation, are either in liquid form or are soluble in certain organic solvents. Through the use of appropriate reagents, the processes such as hydrolysis and gelation can be induced to produce heterogeneous gels from mixtures of alkoxides. To obtain a powder or

ceramic samples, the gels can be baked, sintered and powderized as in other traditional methods [7].

Compared to other traditional methods, the sol-gel method presents several advantages such as:

High homogeneity of the chemical composition of the materials produced.

Thin films and multilayer coatings of sol-gel materials can be readily prepared by spinning or dipping methods during the gelation period.

High uniformity of the doping ion distribution exists. No local concentration quenching will occur because of impurity clustering and higher doping concentration becomes possible.

Control of the microstructure of the materials.

Sol gel method was used in this study to synthesize red emitting $SrAl_2O_4:Eu^{3+}$ phosphors.

3.3. CHARACTERIZATION TECHIQUES

3.3.1. SCANNING ELECTRON MICROSCOPY (SEM)

The Scanning election microscope (SEM) is often used as the analytical instrument of choice when the light microscope no longer provides adequate resolution. The SEM consists of an electron optical column mounted on a vacuum chamber with electron gun placed on top of the column, as illustrated in figure 3.1.

The electron gun, which consists of a tungsten or LaB_6 filament or a field emission electron gun is used to generate electrons, when the applied current causes resistance heating which generates the electrons [9].

When a high energy electron beam impinges on the sample, a variety of electrons and/or x-rays will be generated. Depending on the nature of the sample, these can include secondary electrons

(electrons from the sample itself), backscattered electrons (beam electrons from the filament that bounce off nuclei of atoms in the sample) and X-rays. This technique can be used to investigate the topography, morphology, and elemental composition of materials (if coupled with an EDS) on the micrometer to nanometer scale. The secondary electrons can be used to investigate the image and the topographic features of solid samples. The SEM coupled with EDS, is used

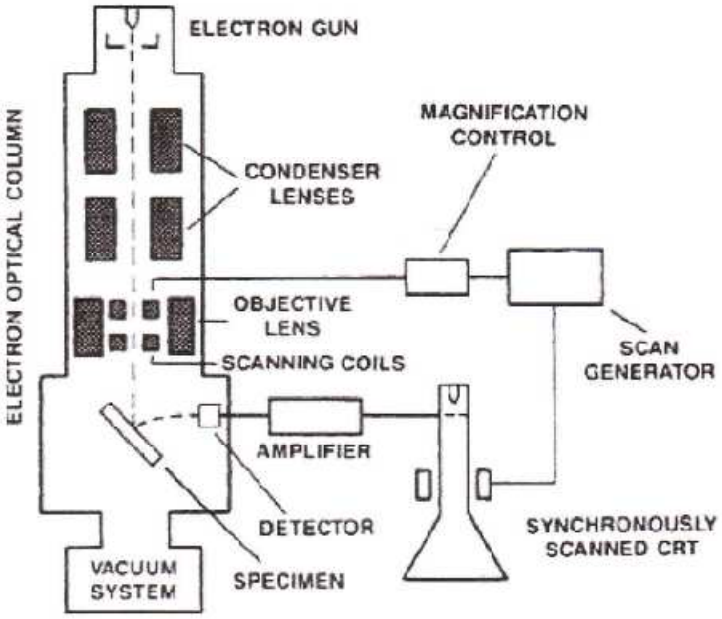

Figure 3.1: Schematic representation of a SEM [9]

during the analysis of the characteristic x-rays emitted as a result of electronic transitions between the inner core levels to provide a quantitative and qualitative elemental composition of the sample [10]. The analysis of elemental compositions can be performed by measuring the energy and intensity distribution of the x-ray signals generated by a focused electron beam. Due to a well defined nature of the various atomic energy levels, it is clear that the energies and associated wavelengths of the set of x-rays will have characteristic values for each of the atomic species present in a sample [10].

The morphologies and elemental compositions of the phosphor powders were obtained by using a Shimadzu Superscan SSX-550 SEM coupled with an EDAX EDS from the Center of Microscopy at the University of the Free State as shown in figure 3.2.

Figure 3.2: Shimadzu Superscan SSX-550 model Scanning Electron Microscope.

3.3.2. TRANSMISSION ELCETRON MICROSCOPY (TEM)

In Transmission Electron Microscopy, the thin solid or diluted sample can be analyzed by bombarding the sample with a focused beam of electrons under high vacuum [11]. The focused electron beam in TEM can be used to produce images and to determine the crystallographic and morphological information of the material under investigation. Owing to its high resolution, TEM is in principle appropriate for providing topographic data in the nanometer range [12]. In addition to the high resolution, TEM provides the advantage that not only the sample surface, but

also the interior, e.g., the arrangement of the layers, is visualized due to the contrasts in the material [12].

In TEM the accelerated electron beam is projected onto the sample by means of the condenser lens system and the beam can be deflected or not as it penetrates the sample. The greatest advantages that TEM offers are high magnification ranging from 50 to 10^6, and its ability to provide both microstructure and diffraction information from a single sample [13].

The scattering processes experienced by electrons during their passage through the specimen can be used to provide information about a sample. Inelastic scattering between the primary electrons and the electrons in the sample at heterogeneities such as grain boundaries, dislocations, second-phase particles, defects, density variations, etc., cause complex absorption and scattering effects, leading to a spatial variation in the intensity of the transmitted electrons. The elastic scattering involves no energy loss and gives rise to diffraction patterns [13]. In this kind of scattering the selected-area diffraction (SAD) offers a unique capability to determine the crystal structure of individual nanomaterials such as nanocrystals, nanorods and the crystal structures of different parts of the sample. The SAD patterns are often used to determine the Bravais lattices and lattice parameters of the crystalline materials using the same procedure as in XRD [13]. Specimens to be examined by TEM are often deposited on or in a thin membrane resting on a grid. The grids are usually made of copper and form a support for the film, which is usually only self-supporting over a small area. The powder samples are usually diluted and a drop is placed on the grid by means of a pipette or hydrometer syringe [14].

In this study the images, particle sizes and the diffraction of alkaline earth aluminate phosphors were obtained using a JEOL JEM-2100 Model Transmission Electron Microscope shown in figure 3.3.

Figure 3.3: JEOL JEM-2100 Model Transmission Electron Microscopy.

3.3.3 X-RAY DIFRACTION (XRD)

X- ray diffraction is a versatile analytical technique for examining the crystalline structure of solid materials, which include ceramics, metals, electronic materials, organics and polymers. The materials may be powders, multilayer thin films, fibers, sheets or irregular shapes, depending on the desired measurements. The X-ray diffractometer fall broadly into two classes: single crystal and powder. The powder diffractometer is routinely used for phase identification and quantitative phase analysis [15]. X-ray diffractometer consist of three basic elements: an X-ray tube, a sample holder, and an X-ray detector. The X-rays are produced in a cathode ray tube by

heating a filament to produce electrons. When the voltage is applied, the electrons will accelerate towards the target material. When electrons have sufficient energy to dislodge the inner shell electrons of the target material, characteristic X-ray spectra will be produced. These X–ray spectra consist of several components and the most common are K_α and K_β. The target materials that are usually used are Cu, Fe, Mo and Cr. Each of these has specific characteristic wavelengths [16].

In order to generate the required monochromatic X-rays needed for diffraction, a filter such as a foil or crystal monochrometers is usually used. Copper is the most commonly used target material for single-crystal diffraction, with Cu K_α radiation = 1.5418Å. The resulting X-rays are collimated and directed onto the sample. As the sample and detector are rotated, the intensity of the reflected X-rays is recorded. When the geometry of the incident X-rays impinging on the sample satisfies the Bragg Equation, constructive interference occurs and characteristic diffraction peaks of the sample will be observed [16].

The X-ray diffractometer Bruker XRD D8 Advance shown on figure 3.4, from University of Zululand, Department of Chemistry was used to analyze the samples in this study.

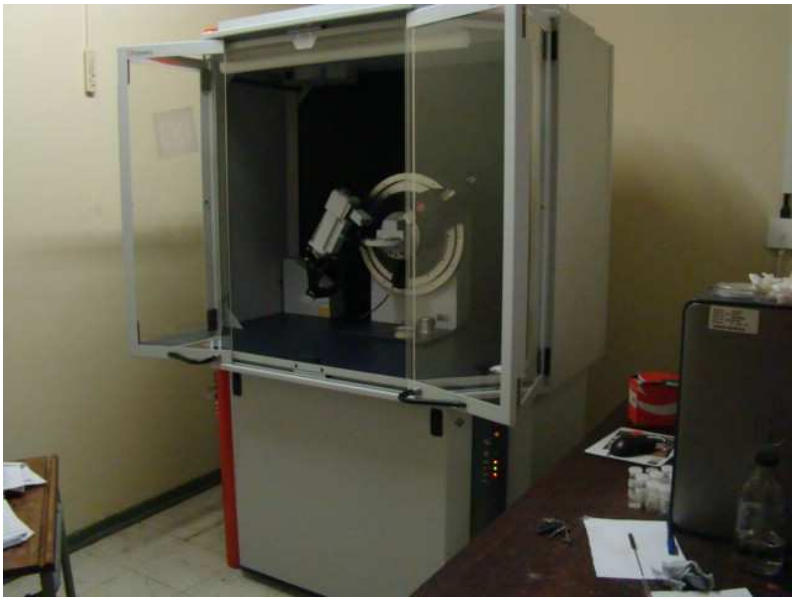

Figure 3.4: BrukerD8 Advance model x-ray diffractometer.

3.3.4 PHOLUMINSCENCE SPECTROSCOPY (HELIUM–CADMIUM LASER)

The Helium–Cadmium (He-Cd) laser is the best known member of a family of lasers that uses a metal with a low vaporization temperature as the active medium [17]. The He-Cd laser consists of a tube, terminated by two Brewster angle windows with two laser mirrors mounted separately from the tube [18]. In a typical setup of the He-Cd laser, the tube is filled with high pressured helium gas at 6 to 8 torr and a cadmium reservoir located near the anode as shown in figure 3.5

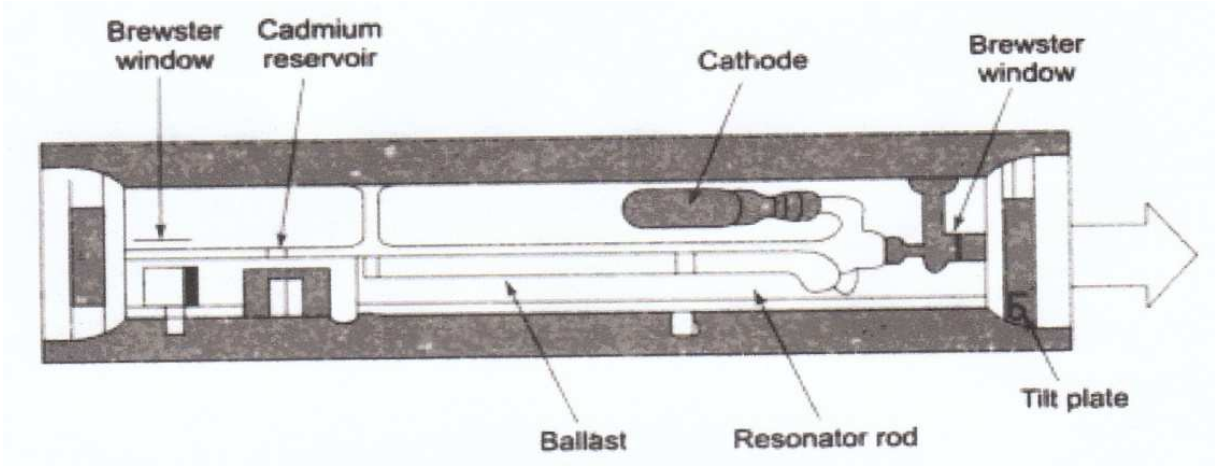

Figure 3.5: The cavity structure of He-Cd Laser [19]

When the temperature of the cadmium reservoir is raised to higher values (e.g. 250^0C) the desired vapour pressure of Cd atoms will be produced in the tube. The net results will cause the He atoms inside the tube to undergo ionization and excitation when they mix with the Cd vapour. The energy transferred from the exited He ions to neutral atoms by collision, will lead to further excitation and ionization of a Cd atom inside a tube [19]. This electronic transition between the exited ionic state and the ground state inside a tube, will lead to the output lines of a laser beam either in the deep blue (441.6nm) or ultraviolet (325nm) range with an output power of 20 - 100mw [20]. Due to its coherence and low optical noise, the He-Cd laser can be used in Raman spectroscopy, fabrication of holographic gratings and photochemical processing of materials. In this study a 325nm He-Cd laser was used to investigate the photoluminescent properties of the

phosphors. This was conducted by directing the laser beam on to a sample by using the optical lenses and mirrors, followed by the chopper that was used to ensure that the light beam is sent in packets as illustrated in figure 3.6. To ensure that only the light beam from the sample is sent through the photomultiplier tube detector, the glass GG 385 was used to block the laser beam. The He-Cd laser system, shown in figure 3.7 used in this study was from Nelson Mandela Metropolitan University (NMMU) in Port Elizabeth.

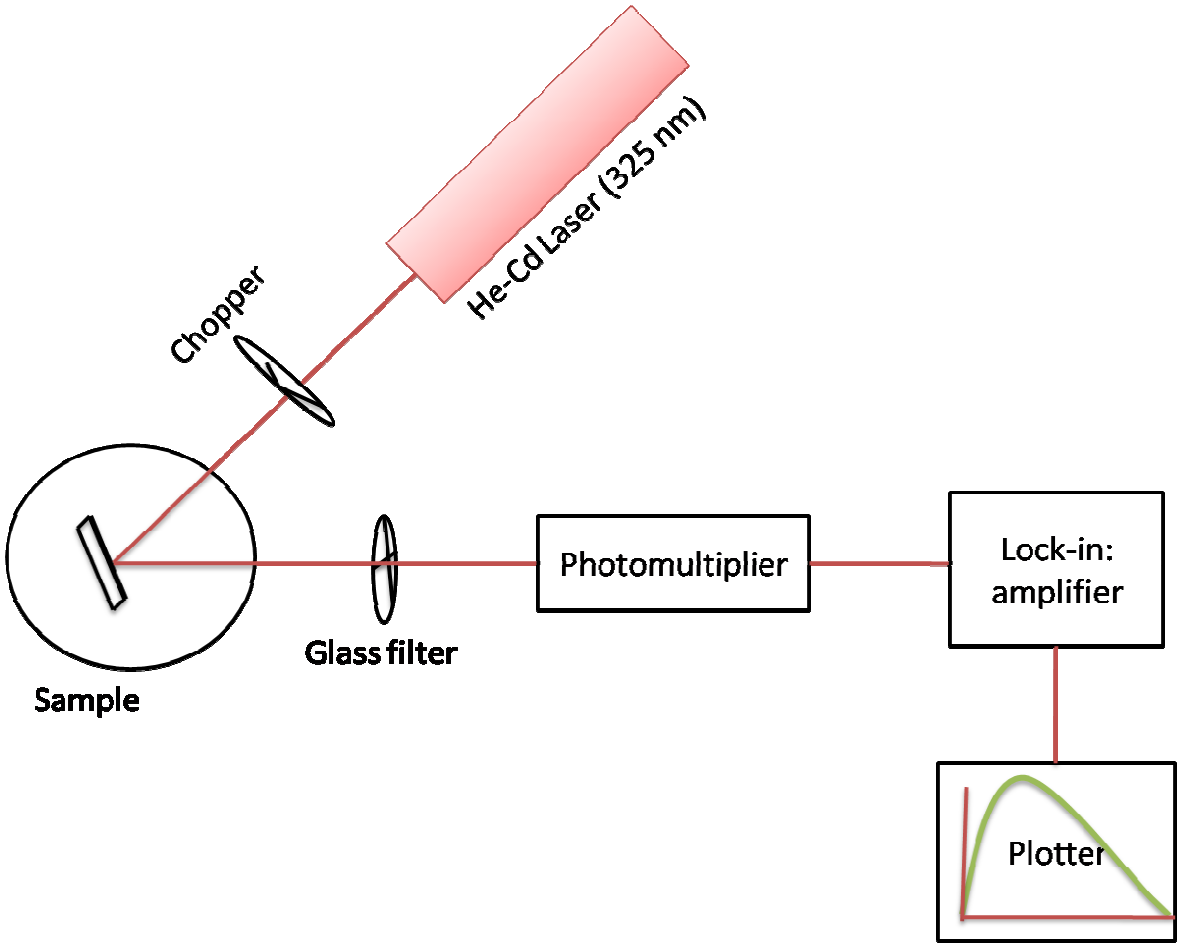

Figure: 3.6 Schematic representation of the PL system [21].

Figure 3.7: PL system used to investigate the luminescent properties of the phosphors.

3.3.5. FLUORESCENCE SPECTROPHOTOMETTRY

Fluorescence spectrophotometry is used to measure the fluorescence or phosphorescence emitted by a substance when exposed to ultraviolet, visible or other electromagnetic radiation. Measurement of the fluorescence intensity can be made by using the fluorescence spectrometer, which consists of a radiation source, monochromator, sample holders and fluorescence detection system as shown in figure 3.8.

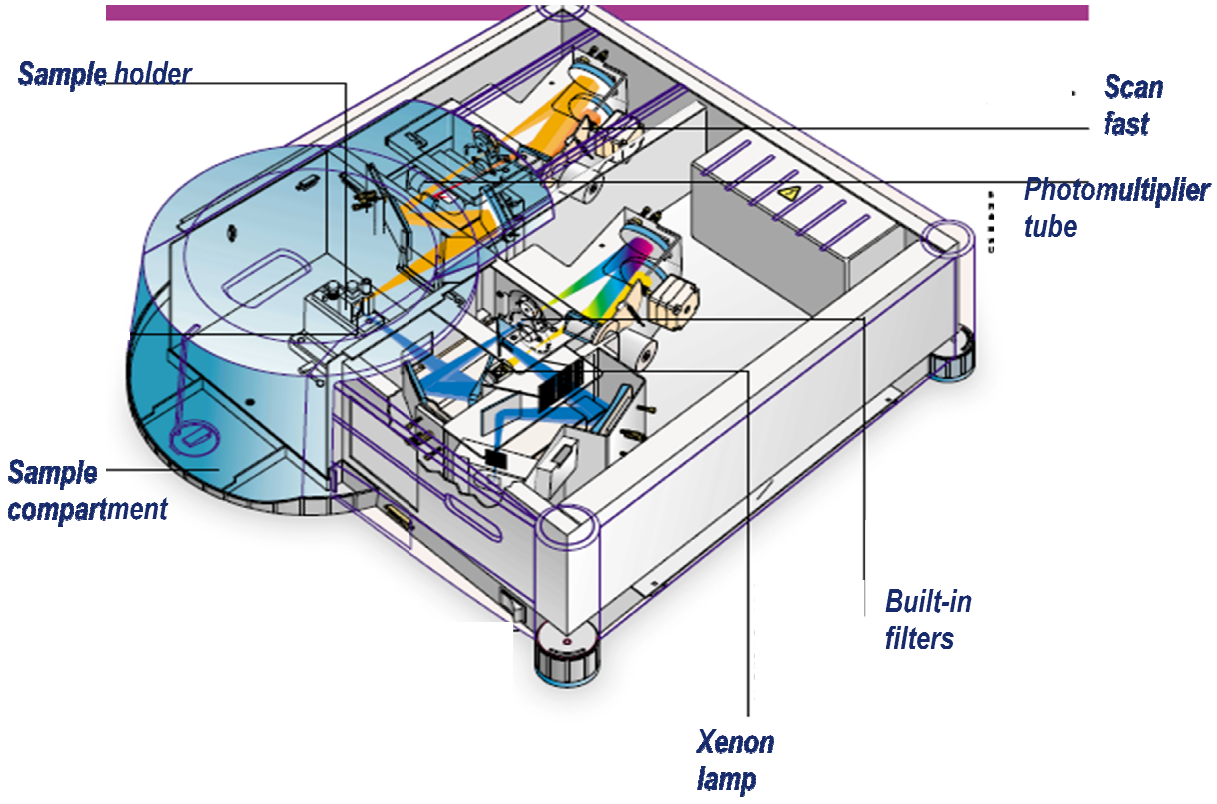

Figure 3.8: Schematic representation of the Cary Eclipse Fluorescence Spectrophotometer.

The monochromators are equipped with narrow slits, which provide high resolution and spectral purity [22]. There are various sources that are used in the fluorescence spectrophotometer such as mercury lamps, tungsten lamp and Xenon arc lamp. The Xenon arc lamp is commonly used, because it has an energy continuum extending from the ultraviolet into the near infrared. The fluorescence spectrophotometer is superior when it comes to fluorescence measurements due to wavelength selectivity, flexibility and convenience [22].

In this study a Cary Eclipse Fluorescence Spectrophotometer (shown in figure 3.9) coupled with monochromator xenon lamp was used to collect fluorescence data in air at room temperature. The photoluminescence excitation and emission spectra as well as exponential decay times of the alkaline earth aluminates phosphor powders were determined.

Figure 3.9: Cary Eclipse Florescence Spectrophotometer

REFERENCES

1. Y. Gogotsi, Nanomaterials Handbook, Materials Science at the Nanoscale, Routledge Publishers, USA, 2006, pp 5
2. K.C. Patil, S.T. Aruna, and T. Mimani, Solid State and Materials Science **6** (2002) 507–512
3. J.J .Kim, J.H. Kang, D.C. Lee and D.Y. Jeon, American Vacuum Society (2003).
4. N. Suriyamurthy and B.S. Panigrahi, Journal of Luminescence, (In Press) SCIENCE-53
5. U. Schubert, N. Hüsing, Synthesis of Inorganic Materials, Second Edition, WILEY-VCH, 2005
6. W.M.Yen, S. Shionoya, H.Yamamoto, Practical Applications of Phosphors, CRC Press, Boca Raton, 2006
7. W.M. Yen, M. J. Weber, Inorganic Phosphors, Routledge Publishers, USA, 2004
8. S. Elliot, The Physics and Chemistry of Solids, John Willey and Sons, New York, 1998, pp 28
9. R. W. Kelsall, I. W Hamley, M. Geoghegan, Nanoscale Science and Technology, Wiley, 2005
10. B. G. Yacobi, D. B. Holt, and L.L. Kazmerski Microanalysis of Solids, New York, Plenum Press, 1994
11. M. Kuno, Introduction to Nanosciene and Nanotechnology: A Workbook, Notre Dame, 2005
12. M. Kohler, W. Fritzsche ,Nanotechnology, An Introduction Nanostructuring Techniques, Wiley-VCH, 2003
13. C. Guozhong, Nanostructures & Nanomaterials, Synthesis, Properties & Applications, University of Washington, Imperial College Press, USA, 2004
14. T. Allen, Particle Size Measurement, Volume **1**, Fifth Edition, Chapman & Hall, USA, 1968

15. F. A. Settle, Handbook of Instrumental Techniques for Analytical Chemistry, Prentice Hall PTR, USA, pp 339-351
16. http://serc.carleton.edu/research_education/geochemsheets/techniques/XRD.html 15/03/2009
17. J .Hecht, The Laser Guidebook, Second Edition, McGraw-Hill Professional Publishing, 1999
18. M. Endo, R.F. Walter, Gas Lasers, CRC Press, New York, 2006
19. K.R. Nambiar, Lasers: Principles, Types and Applications, New Age International Publishers, New Delhi, 2004
20. O. Svelto, D.C. Hanna Principles of lasers, Fourth Edition, Kluwer Academic/Plenum Publishers, 1998
21. T. Katsumata, S. Toyomane, R. Sakai, S. Komuro, and T. Morikawa, J. Am. Ceram. Soc., **89** (3) (2006) 932–936
22. The International Pharmacopoeia, Organization Mondiale de la santé, World Health Organization, Fourth Edition, Volume 1, Geneva, 2006

CHAPTER 4

$Sr_{0.97}Al_2O_4:Eu^{2+}_{0.01},Dy^{3+}_{0.02}$ PHOSPHORS PREPARED BY A SOLID STATE REACTION METHOD

4.1. INTRODUCTION

Strontium aluminate phosphors doped with rare earth ions are of interest in materials science because of their high chemical stability, and bright emission intensity in the visible region of the electromagnetic spectrum [1]. The green luminescence emission is usually observed when the luminescent center ions, such as Eu^{2+}, substitute for Sr in the distorted stuffed tridymite structure of $SrAl_2O_4$ [2]. It is well known that the incorporation of the co-activator ion such as Dy^{3+} will act as a hole trapping center. Its presence will create many trap centers with appropriate depth in the host matrix and consequently, prolong the afterglow at room temperature [2].

Due to their high quantum efficiency and long phosphorescence properties, $SrAl_2O_4:Eu^{2+},Dy^{3+}$ phosphors have high potential to be used in various display devices, such as luminescent paint, screens, glow signs, emergency escape routes, detection of structural damage, etc [3]. It is well known that thermal processing parameters such as heating rates, heating time and cooling rates have great influence on the optical properties of phosphors [4]. In this chapter the photoluminescent and phosphorescent properties $SrAl_2O_4$ doped with 1 mol% Eu^{2+} and 2 mol% of Dy^{3+} prepared by a solid state reaction method at different annealing temperatures(1000 -1200 ^0C were investigated.

4.2. EXPERIMENTAL PROCEDURE

4.2.1. SYNTHESIS

$Sr_{0.97}Al_2O_4:Eu^{2+}_{0.01},Dy^{3+}_{0.02}$ powder phosphors were prepared by a solid state reaction method. The appropriate oxides (Al_2O_3, Dy_2O_3, Eu_2O_3) and the carbonate ($SrCO_3$) all in analytical purity of 99.9% were used as starting materials and 10 mol % of boric oxide (B_2O_3) was added into the mixture in order to improve the crystallinity of the phosphors. The mixture was dissolved in an acetone medium, and then milled until the acetone evaporated completely. This procedure was repeated at least three times in order to ensure a more homogenous sample. The mixture was then calcined in air at 950^0C in a furnace for 3 hours. A white product of a red emitting $SrAl_2O_4:Eu^{3+},Dy^{3+}$ phosphor powder was obtained. The product was then divided into small portions, and then annealed at different temperatures in a reducing atmosphere of N_2 and 25% of H_2. Figure 4.1 shows a flow diagram of $Sr_{0.97}Al_2O_4:Eu^{2+}_{0.01},Dy^{3+}_{0.02}$ phosphor prepared by the solid state reaction method.

4.2.2 CHARACTERIZATION

The samples were annealed in a tube furnace equipped with a microprocessor based temperature controller with an accuracy of $\pm$ 5 ^{0}C. The diffraction patterns of the phosphors before annealing and after annealing were determined with an X'Pert PRO MPD X-ray diffractometer (XRD) with Cu Kα at λ = 1.5406 Å. The photoluminescent and phosphorescent properties of the phosphors were investigated at room temperature with a PSI PL system and a Cary Eclipse Spectrophotometer both equipped with a Xenon lamp.

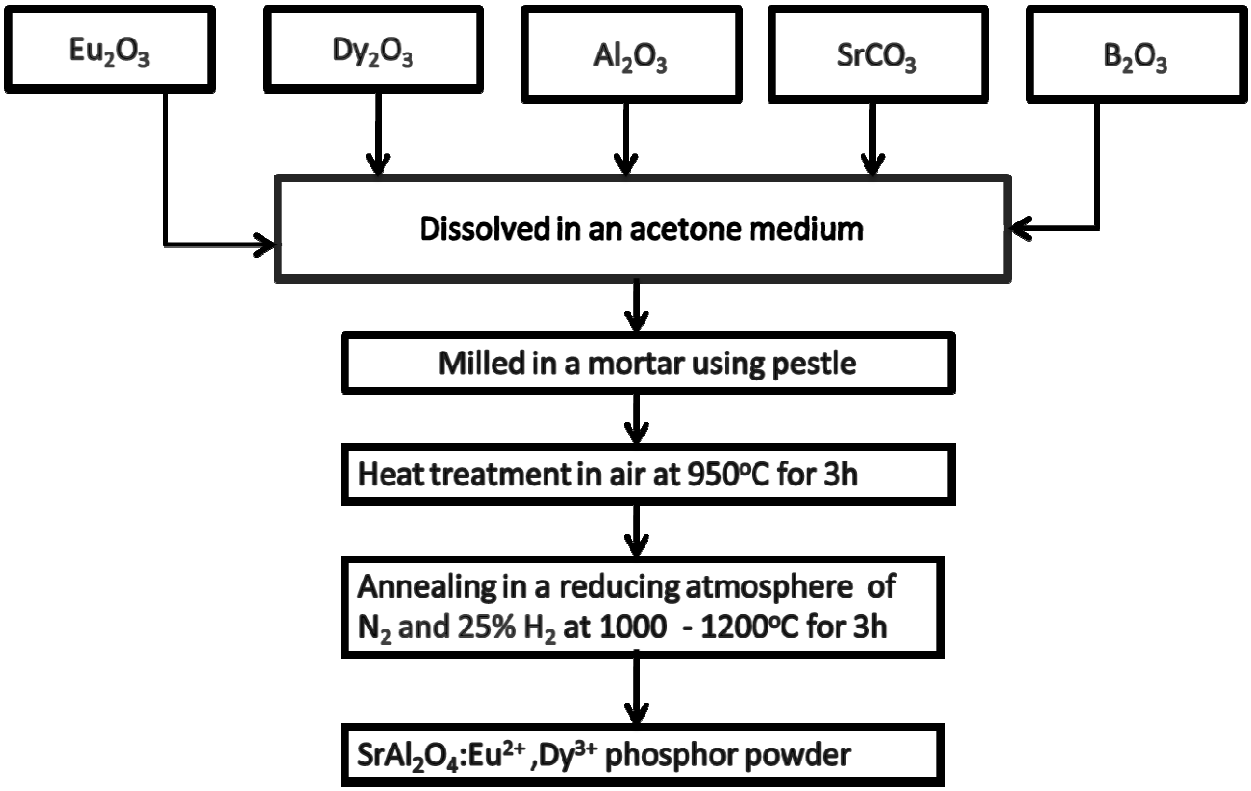

Figure 4.1: Flow diagram of $Sr_{0.97}Al_2O_4:Eu^{2+}_{0.01},Dy^{3+}_{0.02}$ phosphor prepared by a solid state reaction method.

4.3. RESULTS

Figure 4.2 shows the XRD patterns of the phosphors annealed at different temperatures. The main diffraction peaks correspond to the $SrAl_2O_4$ monoclinic phase according to JCPDS card number 34 – 0379. Some unknown diffraction peaks denoted by stars in figure 4.2 were observed in some of the samples and may be attributed to impurity phases such as $Sr_3Al_2O_6$, etc.

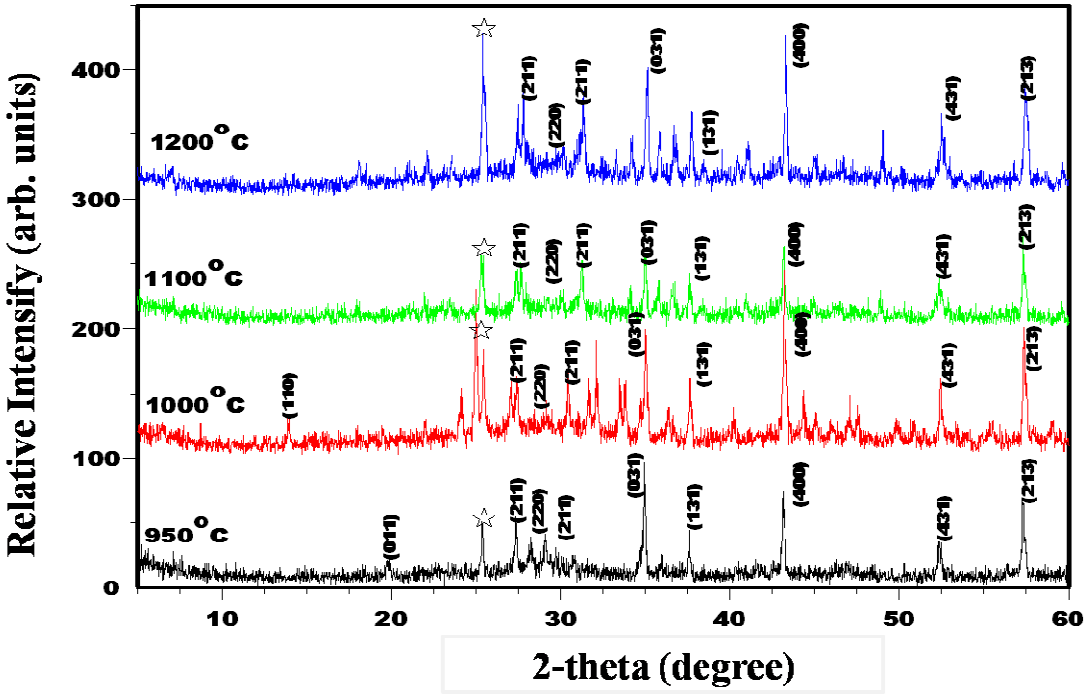

Figure 4.2: XRD patterns of $Sr_{0.97}Al_2O_4:Eu^{2+}_{0.01},Dy^{3+}_{0.02}$ annealed at different temperatures.

4.3.1 PHOTOLUMINESCENCE

Figure 4.3(a) shows the emission spectrum of $SrAl_2O_4:Eu^{3+},Dy^{3+}$ annealed in air at 950 ^{0}C. The red emission lines observed are due to the f-f transition of the Eu^{3+} ions in the host lattice. Typical emission lines of Eu^{3+} ions in various hosts can be observed in the range of 550 – 750 nm and can be assigned to the transitions from $^5D_0$ -^7F_J (J = 0,1,2,3,4) respectively [5]. As observed in the figure, the emission peaks at 615 nm ($^5D_0$ -$^7F_2$) and 700 nm ($^5D_0$ -$^7F_4$) are much stronger than the other emission peaks. Peng *et al.* [5] reported the strongest emission peak at 610 nm ($^5D_0$ -$^7F_2$) for $BaAl_2O_4:Eu^{3+}$, and attributed that to the fact that $^5D_0$ -$^7F_2$ is a

hypersensitive transition and is strongly influenced by the surrounding environment. Furthermore, they reported that when Eu^{3+} ions occupy the sites with higher symmetry, the emission from the $^5D_0$-$^7F_2$ becomes very weak; otherwise the emission will be strong [5]. In this study the strong emissions observed may be attributed to the Eu^{3+} ions when they occupy lower symmetry Sr sites [6].

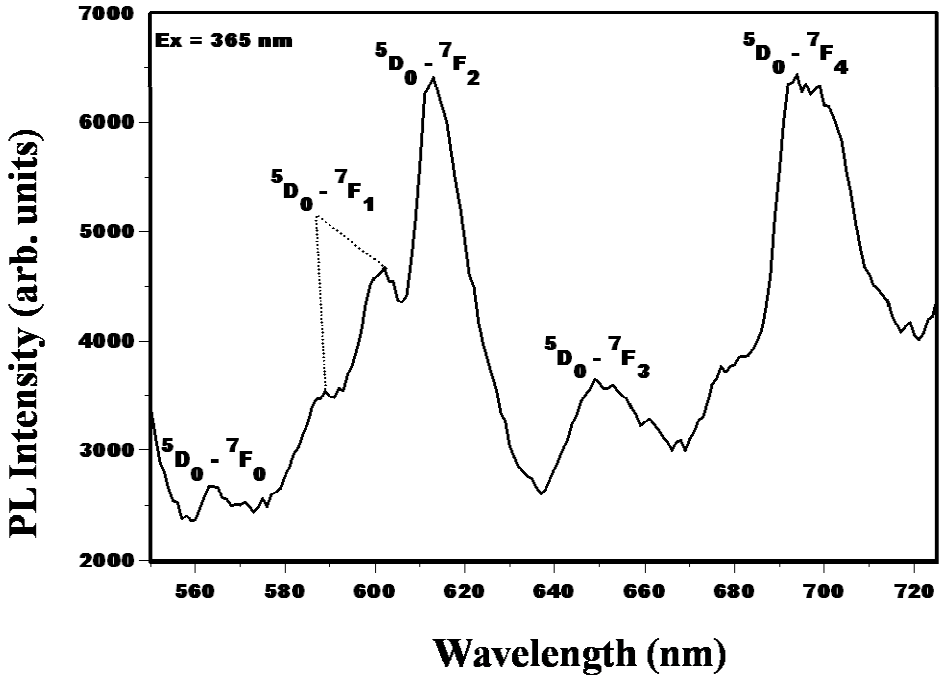

Figure 4.3.a: PL emission of $Sr_{0.97}Al_2O_4:Eu^{3+}_{0.01},Dy^{3+}_{0.02}$ annealed at 950 ^{0}C in air.

The emission spectra of the phosphors annealed in a reducing atmosphere at different temperatures are shown in figure 4.3(b). The samples were excited with a xenon lamp at a wavelength of 365 nm. The phosphor prepared at 1000 ^{0}C showed the lowest intensity. This may be attributed to the fact that Eu^{3+} was not completely reduced. Furthermore, when the phosphor was observed after being irradiated with the UV source, the orange-red color, which is related to the transitions $^5D_0$ -^7F_J of the Eu^{3+}ions, was still dominant. For the samples annealed at 1100 ^{0}C

and 1200 ^{0}C a broad emission band at 497 nm was observed. The emission at 497 nm is attributed to the transition from the excited state $4f^6 5d^1$ to the ground state $4f^7$ of the Eu^{2+} ions. The maximum intensity was observed for the phosphor annealed in a reducing atmosphere at 1100 ^{0}C. It has been reported in the literature [7] that as the annealing temperature increases the luminescence intensity will increase due to a more crystalline structure of the host. Zhang *et al*. [8] further pointed out that an increase in the treatment temperature, will allow the doping rare earth element to easily transfer into the lattice of the matrix, which may result in the enhancement of the luminescence intensity. On the contrary, the highest intensity in this study was observed from the sample prepared at a temperature lower than 1200 ^{0}C. The lower luminescence intensity observed on the sample prepared at 1200 ^{0}C compared to the one prepared at 1100 ^{0}C may be attributed to the impurities or some defects. During synthesis of the phosphors, it was observed that as the annealing temperature increases (1200 ^{0}C and above), the samples were starting to melt and it was very difficult to remove them from the crucibles. Furthermore, formation of large particles with low surface area and hence mechanical particle size reduction by milling was required. This may introduce impurities and defects, which may degrade the luminescence intensity of the phosphors. Zhang *et al.*[8] prepared $SrAl_2O_4:Eu^{3+},Dy^{3+}$ with the gel combustion method at different temperatures (900 - 1200 ^{0}C) in a reducing atmosphere, and the maximum intensity was observed from a sample prepared at 1150 ^{0}C . They [8] attributed the lower intensity from the samples treated at higher temperatures to defects that might have been dispersed on the surface of the phosphors, which may result in a relatively smaller amount of the luminescent centre Eu^{2+} in the $SrAl_2O_4$ lattice available for direct radiation, thus causing the weaker luminescence.

As mentioned earlier, the broad emission bands observed from the samples annealed at 1100 ^{0}C and 1200 ^{0}C both peak at 497 nm. This may be attributed to the fact that only one luminescent center, which is the Eu^{2+}, is present in both phosphors. Tang *et al.* [9] reported an emission peak at 500 nm for $SrAl_2O_4:Eu^{2+},Dy^{3+}$ prepared by a gel method, which is slightly higher wavelength than the results obtained in this study. The variations in the emission peak energies as mentioned may be attributed to the preparation techniques. Another reason for these variations may be due

to changes in the crystal field environment of the Eu^{2+} ions [10]. Since the excited state $4f^6\ 5d^1$ is sensitive to changes in the crystal environment, in contrast to the shielded $4f^7$ state configurations due to the shielding function of the inner electrons [10]. The difference in peak energy in this study may also be attributed to the fact that the 5d couple strongly to the lattice. Hence the mixed state of the 4f and 5d states will be split by the crystal field which may lead to the blue shift in the emission peaks [11].

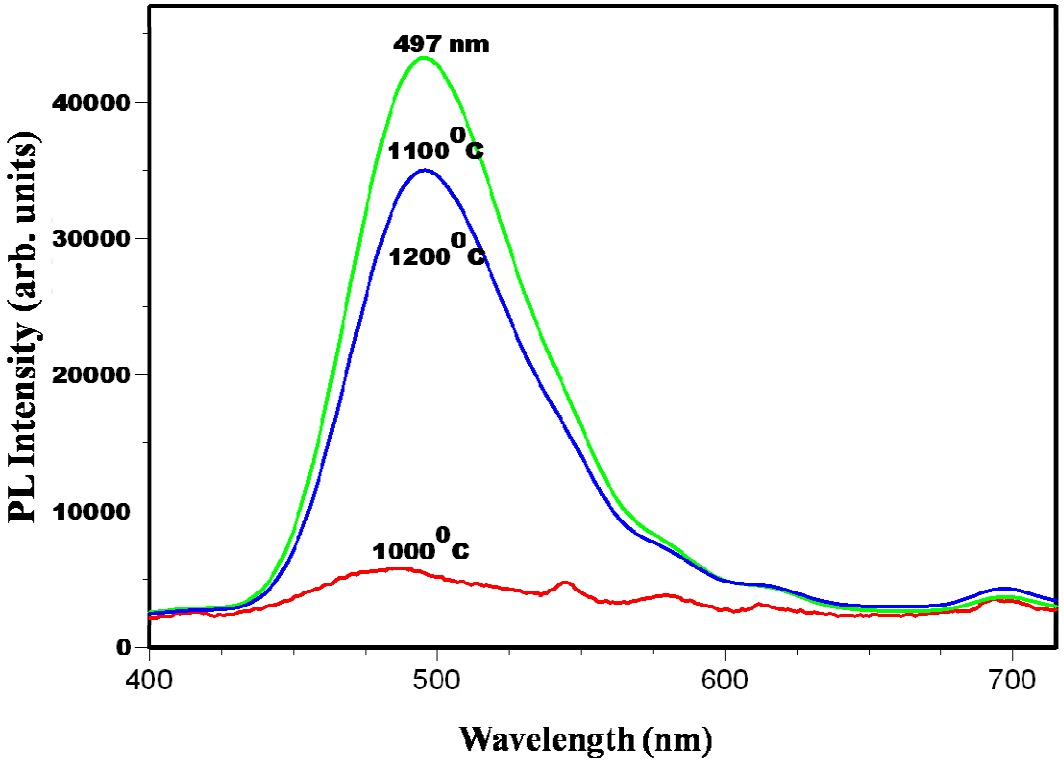

Figure 4.3(b): PL emission of $Sr_{0.97}Al_2O_4:Eu^{2+}_{0.01},Dy^{3+}_{0.02}$ annealed at different temperatures

4.3.2 PHOSPHORESCENCE

Figure 4.4 shows the phosphorescence spectra of the $SrAl_2O_4:Eu^{2+}$, Dy^{3+} phosphor annealed at 1100 ^{0}C. The sample was excited with a deuterium lamp until the saturation point was reached then the source was switched off and the afterglow data was averaged after every 2.5 seconds.

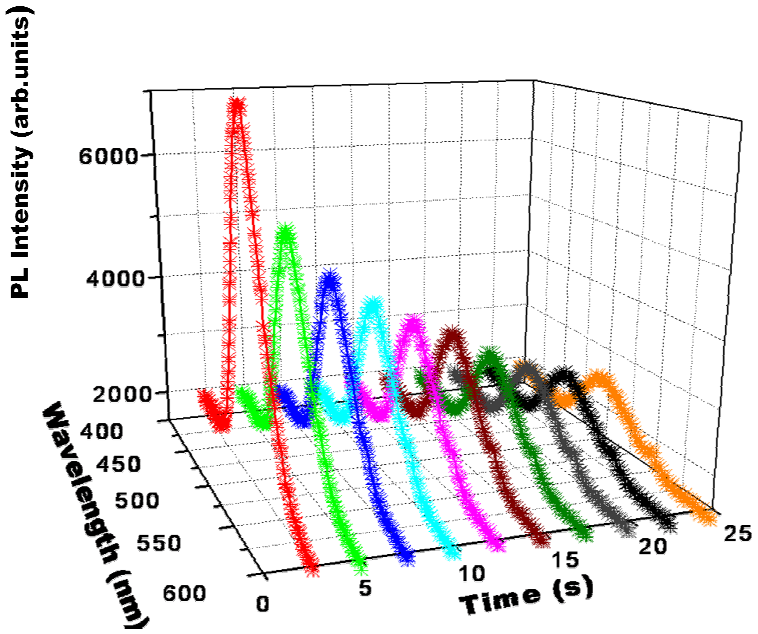

Figure 4.4: Three dimensional decay time of $Sr_{0.97}Al_2O_4:Eu^{2+}_{0.01},Dy^{3+}_{0.02}$ annealed at 1100 ^{0}C.

Figure 4.5 shows the phosphorescence decay curves of the phosphors annealed at different temperatures. The phosphor samples were irradiated with a monochromatized xenon lamp and the sample annealed at 1100 ^{0}C showed the optimum and phosphorescence intensity.

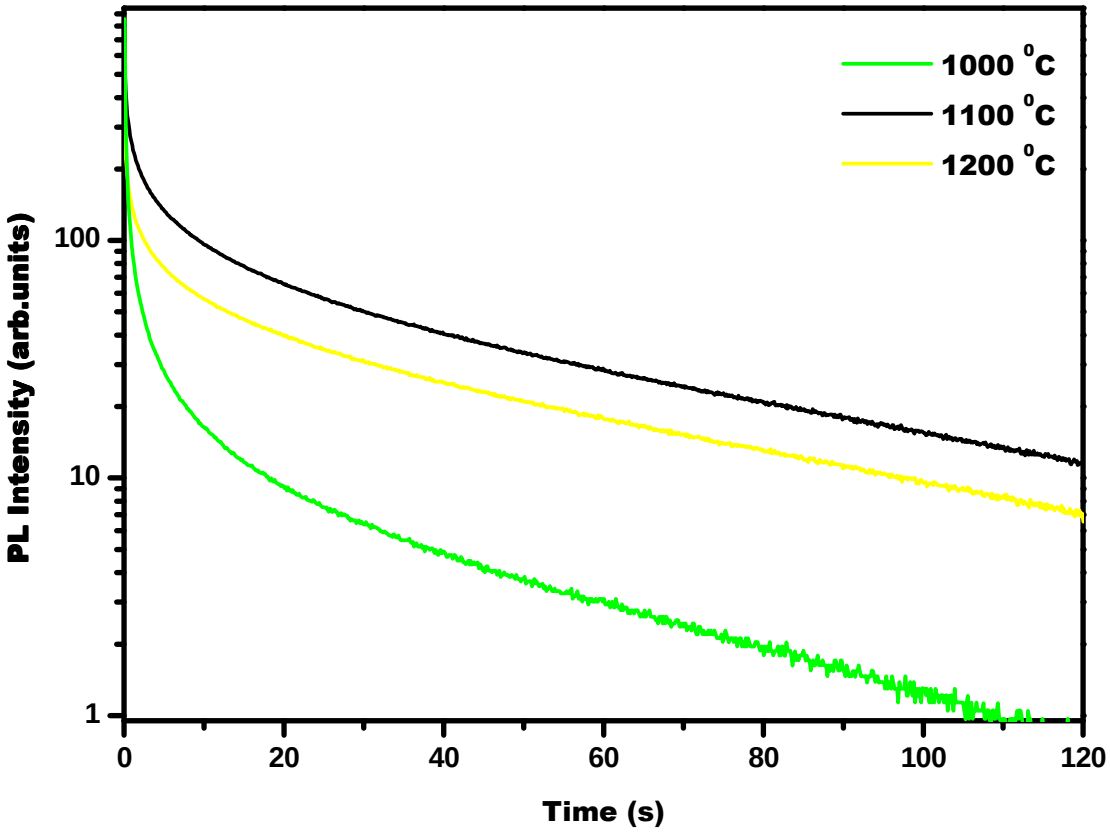

Figure 4.5: Decay curves of the $Sr_{0.97}Al_2O_4:Eu^{2+}_{0.01},Dy^{3+}_{0.02}$ annealed at 1100 and 1200 ^{0}C.

The decay curves in figure 4.5 were fitted by the three order exponential decay equation (4.1):

$$I = A_1 exp\left(-\frac{t}{\tau_1}\right) + A_2 exp\left(-\frac{t}{\tau_2}\right) + A_3 exp\left(-\frac{t}{\tau_3}\right) \qquad (4.1)$$

where I is the phosphorescence intensity at any time t after cutting off the UV excitation, A_1, A_2 and A_3 are constants and τ_1, τ_2 and τ_3 are decay times for the exponential components. The decay parameters for the fitting data are listed in table 4.1.

The phosphorescence decay times as shown in table 4.1 and are described as follows: initial rapid decay, intermediate transitional and then long lasting phosphorescence [12] of the phosphors. The curve fitting and the phosphorescence mechanism for the abovementioned three exponential decay curves will be illustrated in chapter 7.

Table .4.1: Decay parameters of the phosphors.

Phosphor	τ_1**(sec)**	τ_2**(sec)**	τ_3**(sec)**
$Sr_{0.97}Al_2O_4:Eu^{2+}_{0.01},Dy^{3+}_{0.02}$ **(1000 ^{0}C)**	**0.3**	**2.6**	**38.0**
$Sr_{0.97}Al_2O_4:Eu^{2+}_{0.01},Dy^{3+}_{0.02}$ **(1100 ^{0}C)**	**1.0**	**9.8**	**66.1**
$Sr_{0.97}Al_2O_4:Eu^{2+}_{0.01},Dy^{3+}_{0.02}$ **(1200 ^{0}C)**	**0.8**	**8.1**	**61.6**

4.4. CONCLUSION

$Sr_{0.97}Al_2O_4:Eu^{2+}_{0.01},Dy^{3+}_{0.02}$ phosphors prepared at different temperatures were synthesized successfully by the solid state reaction method. The main diffraction peaks of the monoclinic structure of $SrAl_2O_4$ were observed in all the samples. Eu^{3+} was successfully reduced to Eu^{2+} in the reducing atmosphere of N_2 and 25% of H_2.The broad emission band peaking at 497 nm may be attributed to the $4f^65d^1$ - $4f^7$ transition of the Eu^{2+} ions. The long afterglow displayed by the phosphors annealed at different temperatures may be attributed to the Dy^{3+} ions, which play an important role in prolonging the lifetime of luminescence.

REFERENCES

1. Y. Xu, W. Peng, S. Wang, X. Xiang, P. Lu, Materials Chemistry and Physics **98** (2006) 51-54
2. X. Luo, W. Cao, Z. Xiao, Journal of Alloys and Compounds **416** (2006) 250 – 255
3. P. Sharma, D. Haranath, H. Chander, S. Singh, Applied Surface Science **254** (2008) 4052 – 4055
4. X .Li, Y. Qu, X. Xie, Z. Wang, R. Li, Materials Letters **60** (2006) 3673- 3677
5. M. Peng, G. Hong, Journal of Luminescence **127** (2007) 735–740
6. T. Nakamura, K. Kaiya, N. Takahashi, T. Matsuzawa, C. Rowlands,V. Beltra´n-Lo´ pez, G. Smith, P. Riedi, Phys. Chem. (1999) 4011
7. Y. Liu, C Nau, J.Phys. Chem.B, **107 (17)** (2003) 3991- 3995
8. R. Zhang, G. Han, L. Zhang, B. Yang, Materials Chemistry and Physics **113** (2009) 255-259
9. Z. Tang, F. Zhang, Z Zhang, Q. Huang, Y Lin, Journal of the European Ceramic Society **20** (2000) 2129 – 2132
10. T. Peng, L. Huanjun, H. Yang, C. Yan, Materials Letters **58** (2004) 352 -356
11. T. Peng, L. Huanjun, H. Yang, C. Yan, Materials Letters **85** (2004) 68-72
12. H. Zhong, X. Zeng, S. Afr. J. Chem, **61** (2008) 22–25

CHAPTER 5:

PHOTOLUMINESCENT AND PHOSPHORESCENT PROPERTIES OF $MAl_2O_4:Eu^{2+},Dy^{3+}$ (M = Ca, Ba, Sr) PHOSPHORS PREPARED AT AN INTIATING COMBUSTION TEMPERATURE OF 500 ^{0}C

5.1. INTRODUCTION

The photoluminescent properties of divalent europium ion (Eu^{2+}) doped alkaline earth aluminates $MAl_2O_4:Eu^{2+}$(M = Ca, Ba, Sr) have been widely studied by various researchers due to their high quantum efficiency in the visible region [1]. It is well known that the Eu^{2+} emission can be tuned from blue to red depending on the host lattice (MAl_2O_4). The fine tuning is possible because the optical transition involved is $4f^65d^1 – 4f^7$ where the outer d-orbitals can experience the crystal effects more than the inner 4f orbitals [2].$MAl_2O_4:Eu^{2+},Dy^{3+}$ (M = Ca, Ba, Sr) are potential persistent materials to replace ZnS based phosphors used e.g. in luminous paints. The luminescence is characterized by a rapid decay from the Eu^{2+} ion followed by a long afterglow due to the Dy^{3+} ion which acts as the auxiliary activator [3]. Katsumata *et al.* [4] proposed that the long afterglow persistence from Eu^{2+} ions in the aluminates is based on the hole trapping due to the Dy^{3+} ions.

It is well known that the quality of a luminescent material is largely influenced by the synthesis technique [5]. Over the years, MAl_2O_4:Eu2+ (M = Ca, Sr, Ba) phosphors were mostly synthesized by the high temperature solid-state reaction method, which requires quite long reaction times at high temperatures. In recent years the combustion method has displayed unique advantages of lower synthesis temperatures, shorter synthesis times and controlled size of the particles, and it is a more reliable method for preparing long afterglow phosphors [5]. In this chapter photoluminescent and phosphorescent properties the phosphor powders of $CaAl_2O_4$,

$BaAl_2O_4$ and Sr Al_2O_4 doped with 1 mol% of Eu^{2+} and 2 mol% prepared at an initiating combustion temperature of 500 ^{0}C were investigated..

5.2. EXPERIMENTAL

5.2.1. SYNTHESIS

The powder samples of $Ca_{0.97}Al_2O_4:Eu^{2+}_{0.01},Dy^{3+}_{0.02,}$ $Ba_{0.97}Al_2O_4:Eu^{2+}_{0.01},Dy^{3+}_{0.02}$ and $Sr_{0.97}Al_2O_4:Eu^{2+}_{0.01},Dy^{3+}_{0.02}$ phosphors were synthesized using the combustion method. The precursors calcium nitrate ($Ca(NO_3)_3.4H_2O$), barium nitrate ($Ba(NO_3)_3.4H_2O$), strontium nitrate ($Sr(NO_3)_3.4H_2O$), aluminum nitrate ($Al(NO_3)_2.9H_2O$), europium nitrate ($Eu(NO_3)_3.6H_2O$), dysprosium nitrate ($Dy(NO_3)_3.5H_2O$) and urea ($CO(NH_2)_2$) all in analytical purity were weighed according to the stoichiometry. The precursors for each phosphor were mixed and milled in a mortar using a pestle, and a thick white paste was formed from water of crystallization present in metal nitrates. The resulting paste was then heated in a muffle furnace at an initiating combustion temperature of 500 ^{0}C. The paste melted, underwent dehydration, and finally decomposed with the evolution of gases (oxides of nitrogen and ammonia). The mixture frothed and swelled, forming the foam that ruptured with a flame and glowed to incandescence. The entire combustion process was completed in less than 5 minutes. The voluminous combustion ashes of the $Ca_{0.97}Al_2O_4:Eu^{2+}_{0.01},Dy^{3+}_{0.02,}$ $Ba_{0.97}Al_2O_4:Eu^{2+}_{0.01},Dy^{3+}_{0.02}$ and $Sr_{0.97}Al_2O_4:Eu^{2+}_{0.01},Dy^{3+}_{0.02}$ were grounded using a pestle and mortar to make fine powders. **Note:** The sintering process is not required for this method. The reducing atmosphere created during combustion is enough to change the ionization state of Eu^{3+} to Eu^{2+}. A flow diagram for the preparation of $MAl_2O_4:Eu^{2+},Dy^{3+}$ (M = Ca, Ba, Sr) phosphors is shown in figure. 5.1

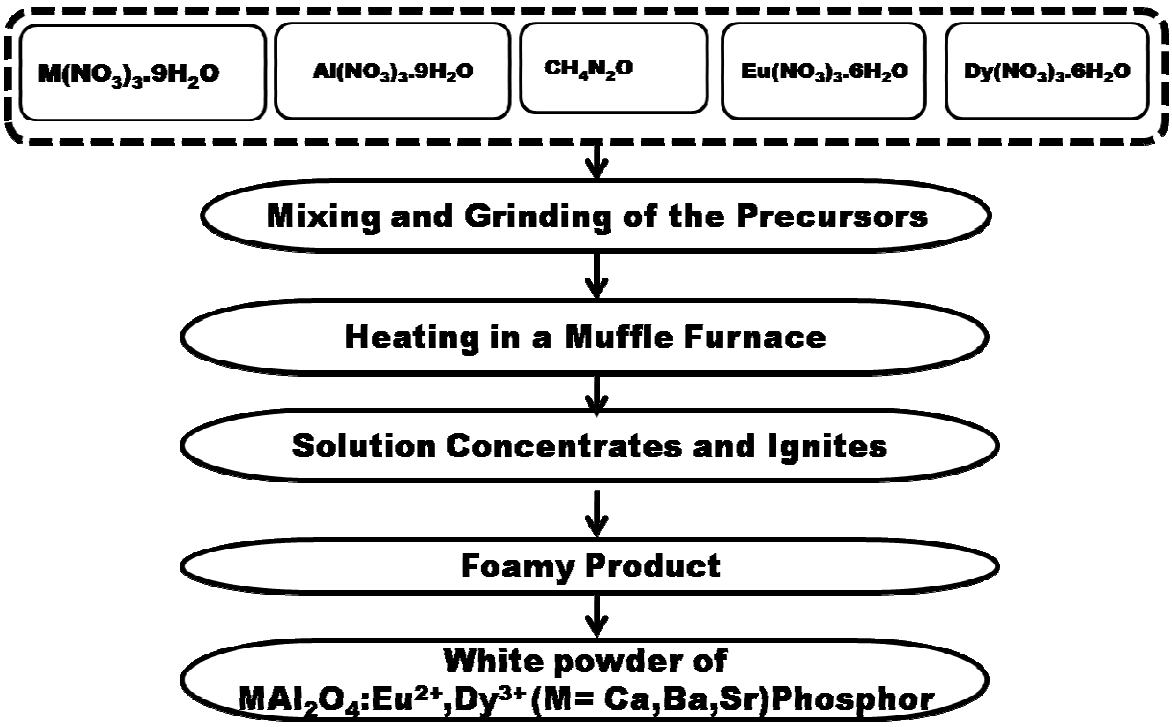

Figure 5.1: A flow diagram for the preparation of $MAl_2O_4:Eu^{2+},Dy^{3+}$ (M = Ca, Ba, Sr) phosphors

5.2.2. CHARACTERIZATION

The crystalline structure, particle morphology and elemental composition of the phosphor powders were investigated using a Burker D8 (Burker Co, German) X-ray diffractometer (XRD) with Cu Kα at = 1.5406 Å and Shimadzu Superscan SSX-550 system for scanning electron microscopy (SEM) coupled with the energy dispersive X-rays spectrometer (EDS) respectively. A 325 nm He-Cd laser and a SPEX 1870 0.5 m monochromator and a photomultiplier detector was used to collect the photoluminescence data. A Cary Eclipse florescence spectrometer coupled with a xenon lamp was also used to investigate the phosphorescence decay curves of the phosphors. The photoluminescence data were collected in air at room temperature.

5.3. RESULTS AND DISCUSSION

The XRD spectra of the samples are shown in figure 5.2. Figure 5.2 (a) shows a monoclinic structure of $CaAl_2O_4$, and the main diffraction peaks index well with the card file (JCPDS: 70 - 0134) [6]. Similar results were reported in the literature [6], where the samples were also prepared by an initiating combustion temperature of 500 ^{0}C. The diffraction peaks indicated by a star may be attributed to other phases and impurities formed during the combustion process.

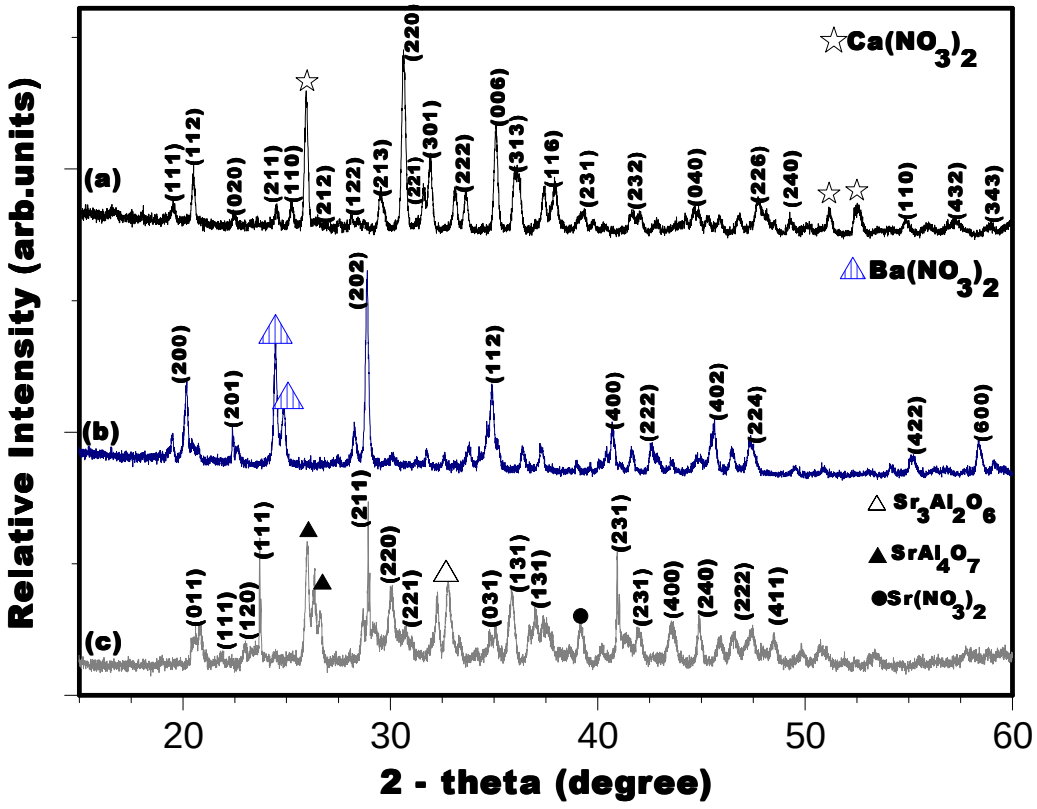

Figure 5.2: XRD patterns of (a) $CaAl_2O_4:Eu^{2+},Dy^{3+}$; (b) $BaAl_2O_4:Eu^{2+},Dy^{3+}$ and $SrAl_2O_4:Eu^{2+},Dy^{3+}$

Figure 5.2 (b) represents the hexagonal structure of $BaAl_2O_4$, and the main diffraction peaks index well with the card file (JCPDS: 17 - 0306). Similar results were also reported [7]. The

monoclinic crystal structure of $SrAl_2O_4$, with the main diffraction peaks indexed according to the card file (JCPDS: 34 – 0379) is shown in figure 5.2 (c). The monoclinic phase of $SrAl_2O_4$ was also reported [8], when the samples were prepared at an initiating combustion temperature of 600 ^{0}C.

Although the main peaks of the crystal structures were observed, there were also additional peaks which may be attributed to un-reacted $Ca(NO_3)_3.4H_2O$, $Ba(NO_3)_3.4H_2O$, $Sr(NO_3)_3.4H_2O$ and $Al(NO_3)_2.9H_2O$ precursors or other impurity phases. Haiyen *et al.* [9] reported that the presence of other phases or some of the precursors can be attributed to the fact that the combustion wave is not uniform and a portion of the precursors might not react completely during the combustion process.

The average particle sizes of the phosphors were estimated from the XRD reflections using the Scherrer's equation:

$$d = \frac{k\lambda}{\beta \cos\theta} \qquad 5.1$$

where d= diameter, k = Scherrer constant ≈ 0.9, λ = wavelength of x-ray radiation, β= full width at half maximum of the diffraction peak and θ = angle of diffraction. From figure 5.2 the estimated particle sizes for $CaAl_2O_4:Eu^{2+},Dy^{3+}$, $BaAl_2O_4:Eu^{2+},Dy^{3+}$ and $SrAl_2O_4:Eu^{2+},Dy^{3+}$ were 40.8 nm, 41.3 nm and 26.0 nm respectively.

Figure 5.3 shows the powder morphologies that were taken at a magnification of 3000 X. The surfaces of the powder samples show lots of voids and pores formed by the escaping gases during the combustion process. These are more significant on (a) $CaAl_2O_4$ and (b) $BaAl_2O_4$. When a gas is escaping under high pressure, pores are formed with the formation of small particles near the pores [6], and this is clearly illustrated by figure 5.3(a). The microstructure of these samples reflects the inherent nature of the combustion process. The non uniform and irregular shapes of the particles shown can be attributed to the non-uniform distribution of temperature and mass flow in the combustion flame.

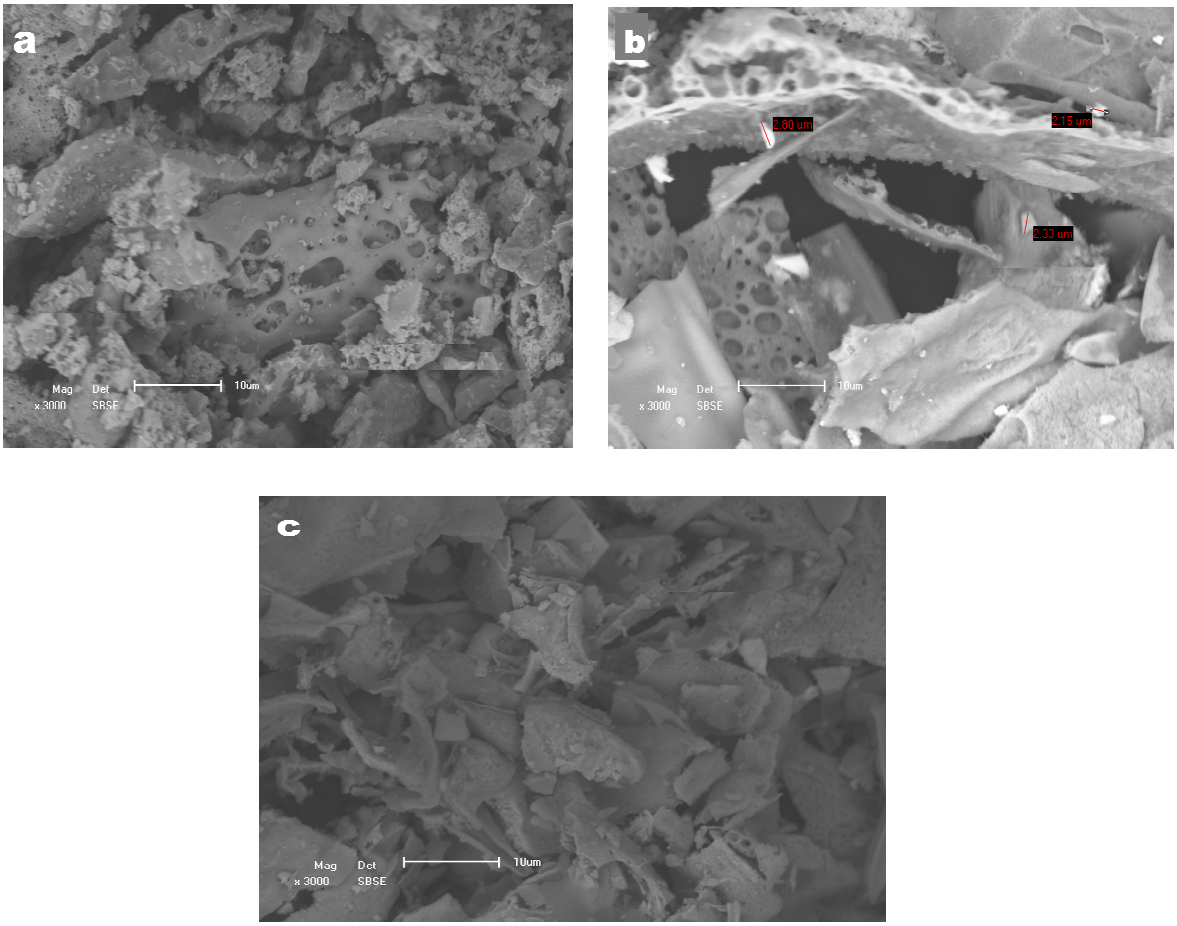

Figure 5.3: SEM micrographs of (a) $CaAl_2O_4:Eu^{2+},Dy^{3+}$, (b) $BaAl_2O_4:Eu^{2+},Dy^{3+}$ and (c) $SrAl_2O_4:Eu^{2+},Dy^{3+}$respectively.

All the elements incorporated in $MAl_2O_4:Eu^{2+}{}_{0.01},Dy^{3+}{}_{0.02}$(M=Ca, Ba, Sr) phosphors prepared at the initiating temperature of 500 ^{0}C were detected in the EDS spectra, except the dopants (spectra not shown) whose concentrations were far too low to be detected.

Figure 5.4 shows the PL emission spectra of $CaAl_2O_4:Eu^{2+},Dy^{3+}$, $BaAl_2O_4:Eu^{2+},Dy^{3+}$ and $SrAl_2O_4:Eu^{2+},Dy^{3+}$ phosphors prepared by the combustion method. Figure 5.4 (a) depicts a relatively narrow emission band of $CaAl_2O_4:Eu^{2+},Dy^{3+}$ which is symmetric around 449 nm.

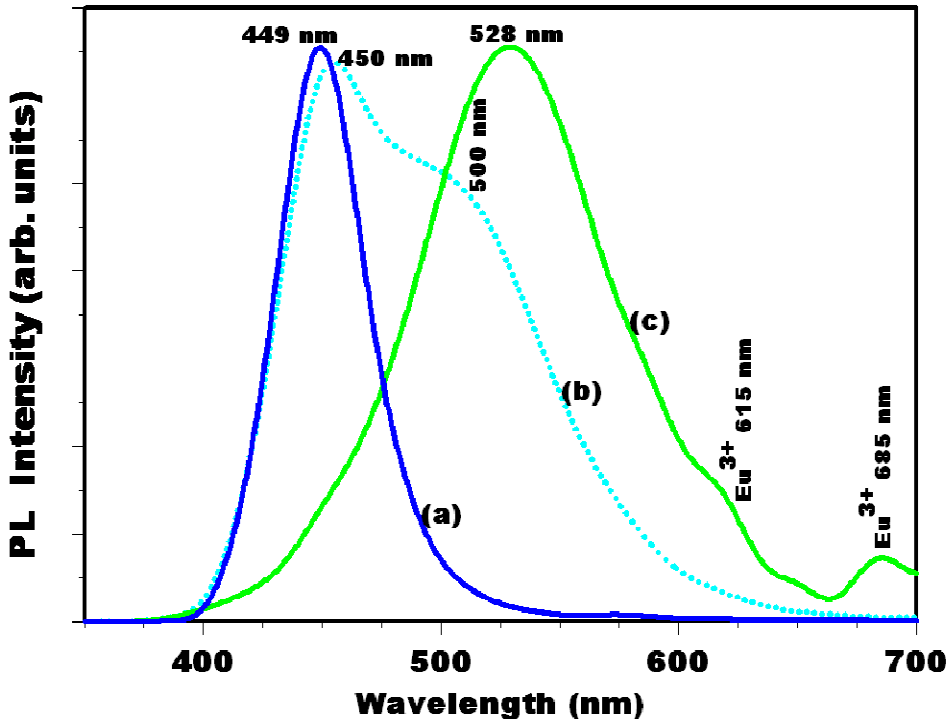

Figure 5.4: Emission spectra of as prepared samples: (a) $CaAl_2O_4:Eu^{2+},Dy^{3+}$, (b) $BaAl_2O_4:Eu^{2+},Dy^{3+}$ and (c) $SrAl_2O_4:Eu^{2+},Dy^{3+}$

The narrowing of the emission spectrum was also reported by Chen *et al.* [10], and they proposed that this may be due to the existence of only one kind of luminescent centre in $CaAl_2O_4:Eu^{2+},Dy^{3+}$, namely Eu^{2+} substituting on the nine fold-coordinated Ca^{2+} sites [10]. Figure 5.4 (b) shows the emission spectrum of $BaAl_2O_4:Eu^{2+},Dy^{3+}$ with main peak at 450 nm and a shoulder at 500 nm. In a host lattice with Eu^{2+} ions on different crystallographic sites, more

than one emission band may occur [11]. In $BaAl_2O_4$ there are two different sites, one occurring 3 times more frequently than the other. Both barium sites are coordinated by nine oxygen ions, one is slightly more regular than the other [12]. Suriyamurthy *et al*. [13] reported that the bond length difference of Ba-O at Ba (1) and Ba (2) sites, may cause the crystal field strength at one site to be stronger than at the other site, which will result in the difference in their emission intensities. The broad emission spectrum of $SrAl_2O_4:Eu^{2+},Dy^{3+}$,which peaks at 528 nm, is shown in figure 5.4(c). An additional peak observed at 685 nm is attributed to the unreduced Eu^{3+} ions in the host lattice. The broad emission spectra displayed by these phosphors as depicted in figure 5.4, are attributed to the transition between the excited ($4f^65d^1$) and ground ($4f^7$) states of the Eu^{2+} ion[10]. Chen *et al*. [10] whom used a solution phase synthesis and post annealing process to prepare the phosphors, reported the emission at 440 nm, 495 nm and 512 nm for $CaAl_2O_4:Eu^{2+},Dy^{3+}$,$BaAl_2O_4:Eu^{2+},Dy^{3+}$ and $SrAl_2O_4:Eu^{2+},Dy^{3+}$ respectively. However the 440 nm and 512 nm for $CaAl_2O_4:Eu^{2+},Dy^{3+}$ and $SrAl_2O_4:Eu^{2+},Dy^{3+}$ are shorter than the wavelengths obtained in this study of 449 nm and 528 nm, respectively. These variations in the emission wavelengths may be related to electric dipole – allowed transition, $4f^65d^1 – 4f^7$, originating from Eu^{2+} doped MAl_2O_4, which seem to depend profoundly on the particle size [10]. This is because the 5d energy level has a closer relation with the conduction band, so when the grain size changes , the band gap may become wider or narrower, and the 5d energy level may change correspondingly [14].

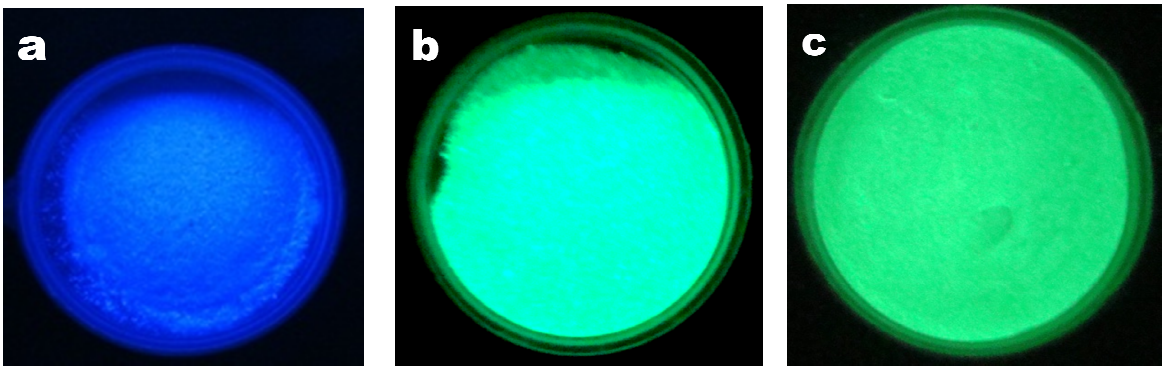

Figure 5.5: Snapshots of (a) $CaAl_2O_4:Eu^{2+},Dy^{3+}$, (b) $BaAl_2O_4:Eu^{2+},Dy^{3+}$ and (c) $SrAl_2O_4:Eu^{2+},Dy^{3+}$.

Figure 5.5 shows the snap shots of the purple-blue, blue-green and green emissions from $CaAl_2O_4:Eu^{2+},Dy^{3+}$, $BaAl_2O_4:Eu^{2+},Dy^{3+}$ and $SrAl_2O_4:Eu^{2+},Dy^{3+}$ after being excited with a UV lamp. Chen *et al*.[10] pointed out that the emission wavelengths of the $MAl_2O_4:Eu^{2+},Dy^{3+}$ phosphors do not shift from short to long wavelength with increasing ordinal number of the alkaline earth metals (Ca, Sr and Ba), but this is due to different crystal field strength (Ca < Ba <Sr) and the distortion experienced by the host lattice when Eu^{2+} ions substitute the sites of the cations (M^{2+}) [10]. When a foreign atom is introduced at an interstitial site, this will be accompanied by a distortion in the host lattice. The distortion arises from a size mismatch between the doped and the substituted ions in the matrix [15]. In the case of MAl_2O_4 ,an anamorphic crystal lattice will result, when the surroundings of Eu^{2+} ions is changed and so the emission wavelengths will change correspondingly [16].This is supported by different emission colors depicted by figure 5.5 when Eu^{2+} ion substitutes the sites of the cations in the MAl_2O_4 (M= Ca, Ba and Sr) host lattice. The ionic radii of Ca^{2+}, Ba^{2+}, Sr^{2+} and Eu^{2+} are 1.0 Å, 1.38 Å, 1.21 Å and 1.20 Å, respectively [16]. When a large Eu^{2+} ion substitutes for Ca^{2+} in $CaAl_2O_4$, Eu^{2+} experiences lesser repulsion owing to the expansion of the crystal lattice, which shifts the emission peak to a short wavelength [10,16].On the contrary, when a smaller Eu^{2+} ion substitutes for Ba^{2+} in $BaAl_2O_4$,Eu^{2+} endures lesser attraction owing to the shrinkage of the crystal lattice [10]. The atomic radii variations between Ba^{2+} and Ca^{2+} ions explain why $BaAl_2O_4:Eu^{2+},Dy^{3+}$ is emitting at a slightly longer wavelength compared to $CaAl_2O_4:Eu^{2+},Dy^{3+}$ when their respective sites are substituted by Eu^{2+} ions. On the other hand the atomic radii of Sr^{2+} and Eu^{2+} are very similar, so when the Eu^{2+} ion occupies the Sr^{2+} sites in $SrAl_2O_4:Eu^{2+},Dy^{3+}$ the local distortion will be similar and the influence in the crystal structure will be quite minimal [16].

Comparative decay curves of the phosphors, after being irradiated with a monochromatized xenon lamp are shown in figure 5.6. The logarithmic plots of the curves were fitted by a three order exponential decay equation as discussed in chapter 4. The parameters for the fitting data are listed in table 5.1.

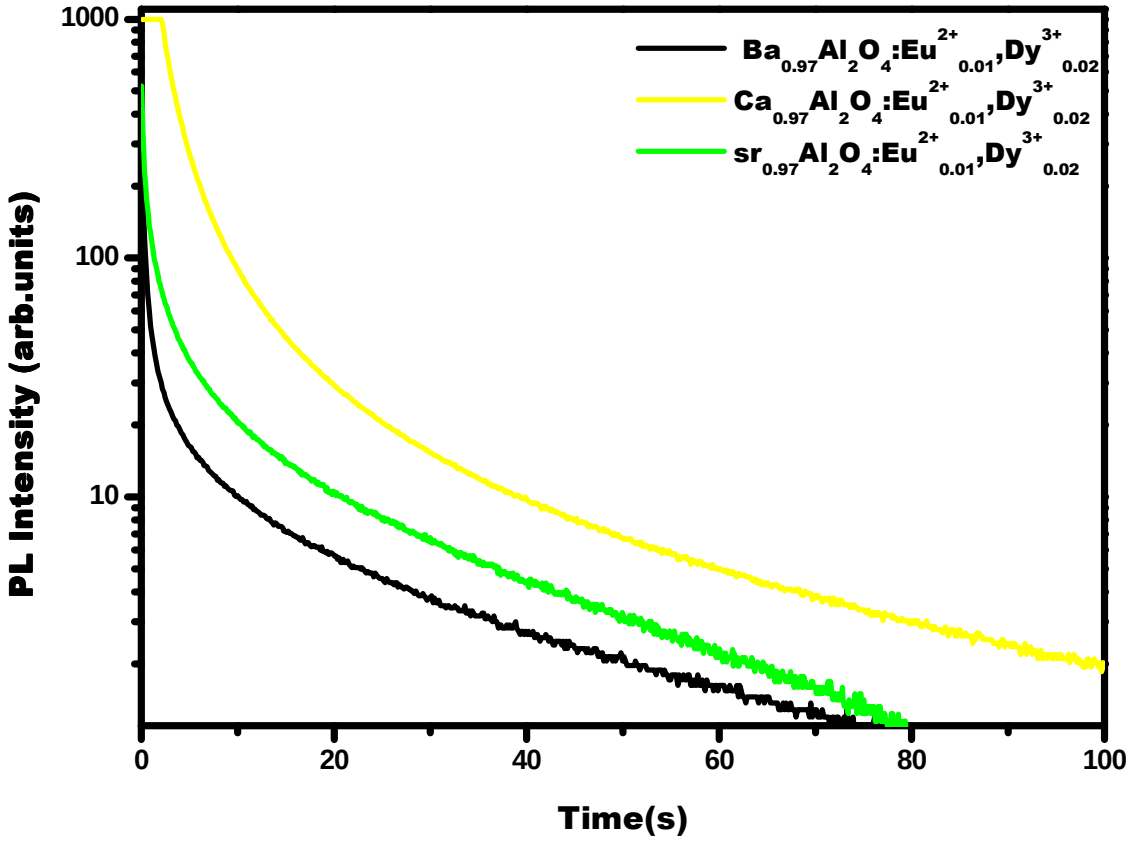

Figure 5.6: Decay curves of (a) $CaAl_2O_4:Eu^{2+},Dy^{3+}$, (b) $BaAl_2O_4:Eu^{2+},Dy^{3+}$ and (c) $SrAl_2O_4:Eu^{2+},Dy^{3+}$.

Table 5.1: Decay parameters of the phosphors.

Phosphors	τ_1(sec)	τ_2(sec)	τ_3(sec)
$Ca_{0.97}Al_2O_4:Eu^{2+}_{0.01},Dy^{3+}_{0.02}$	3.61	3.85	48.80
$Ba_{0.97}Al_2O_4:Eu^{2+}_{0.01},Dy^{3+}_{0.02}$	0.16	1.42	23.29
$Sr_{0.97}Al_2O_4:Eu^{2+}_{0.01},Dy^{3+}_{0.02}$	0.24	2.34	26.89

The exponential decay times as shown in table 5.1 are described as (1) initial rapid decay, (2) intermediate transitional and then (3) long lasting phosphorescence [17]. The initial rapid decay is due to the short survival time of an electron in Eu^{2+}, the intermediate transitional decay might be the capture of Eu^{2+} by a shallow trap energy centre and the very long-lasting decay could be attributed to the deep trap energy centre of Dy^{3+} [17]. It is well known that, for long afterglow persistence , Eu^{2+} acts as a luminescent center and Dy^{3+} acts as trap levels which capture the free electrons, release the trapped holes and recombine with electrons, which give rise to luminescence [17]. The emission lifetime will be influenced by the depth of the trap level and the trap types [17]. Owing to Dy^{3+} added as a co-dopant and partly substituting the alkaline earth metals M^{2+} of MAl_2O_4 and their energy levels have a close relationship to the composition of the structure of the host. In this case $CaAl_2O_4$ and $SrAl_2O_4$ have monoclinic crystal structures, so more appropriate traps will be produced which will be followed by the long afterglow phenomena [16,18]. However the hexagonal crystal structure of $BaAl_2O_4$ will produce shallow traps [17], which are attributed to the shorter decay times shown in figure 5.6

5.4. CONCLUSION

Phosphors of $CaAl_2O_4:Eu^{2+},Dy^{3+}$, $BaAl_2O_4:Eu^{2+},Dy^{3+}$ and $SrAl_2O_4:Eu^{2+},Dy^{3+}$ were successfully synthesized at an initiating combustion temperature of 500 ^{0}C. The low temperature monoclinic structure for both $CaAl_2O_4$ and $SrAl_2O_4$ and the hexagonal structure of $BaAl_2O_4$ were observed. The broad band emission spectra observed at 449 nm, (450nm – with a shoulder peak at 500nm) and 528 nm for $CaAl_2O_4:Eu^{2+},Dy^{3+}$, $BaAl_2O_4:Eu^{2+},Dy^{3+}$and $SrAl_2O_4:Eu^{2+},Dy^{3+}$ respectively, are attributed to the distortions experienced in the host lattice when Eu^{2+} ions substitute the sites of the cations. The monoclinic crystal structures of both $CaAl_2O_4$ and $SrAl_2O_4$ are more appropriate in creating the traps, and this is directly related to the long afterglow phenomena. However the hexagonal structure of $BaAl_2O_4$ can only produce shallow traps.

REFERENCES

1. Z. Fu, S. Zhou, Y. Yu, S. Zhang, Chemical Physics Letters **395** (2004) 285–289
2. N. Lakshminarasimhan , U.V. Varadaraju, Materials Research Bulletin xxx (2008) xxx–xxx , Received 28 June 2007; received in revised form 28 November 2007; accepted 14 December 2007.
3. T. Aitasalo, J. Hölsä, H. Jungner, M. Lastusaari, J. Niittykoski, J. Lumin. **94–95** (2001) 59–63
4. T. Katsumata, S. Toyomane, R. Sakai, S. Komuro, and T. Morikawa, J. Am. Ceram. Soc. **89 (3)** (2006) 932–936
5. H. Zhong, X. Zeng, S. Afr. J. Chem. **61** (2008) 22–25
6. V. Singh, T.K. Gundu Rao, D. Kim, Radiation Measurements **43** (2008) 1198 – 1203
7. H. Ryu, B.K. Singh, K.S. Bartwal, Physica B **403** (2008) 126-130
8. R. Chen, Y. Wang, Y. Hu, Z. Hu, C. Liu, J. Lumin. **128** (2008) 1180–1184
9. D. Haiyen, L. Gengshen, S. Jaiyue, J.Rare earths **25** (2007) 19-22
10. X. Y. Chen, C. Ma, X. X. Li, C. W. Shi, X. L. Li, and Dao Rong Lu , *J. Phys. Chem. C* **113 (7)** (2009) 2685-2689
11. C. Zhao, D. Chen, Y .Yuan, M .Wu, Materials Science and Engineering B **133** (2006) 200-204
12. S. H. M. Poort, W. P. Blokpoel, and G. Blasse, *Chem. Mater.* **7** (1995) 1547-1551
13. N. Suriyamurthy, B.S Panigrahi, J. Lumin. **127** (2007) 483 – 488
14. Z . Fu, S. Zhou, Y. Yu, S. Zhang, Chemical Physics Letters **395** (2004) 285- 289
15. K. Srinivasa Rao, R. Balasubramaniam, J. Hydrogen Energy Vol. **21(7)** (1996) 563-569
16. Z .Qui, Y Zhou, M Lu, A Zhang, Q Ma, Acta Materialia **55** (2007) 2615-2620
17. H. Zhong, X. Zeng, S. Afr. J. Chem. **61**(2008) 22–25
18. J. M. Ngaruiya, S. Nieuwoudt, O. M. Ntwaeaborwa, J. J. Terblans, H.C. Swart, Materials Letters **62** (2008) 3192 – 3194.

CHAPTER 6

LUMINESCENT PROPERTIES OF $Sr_{0.97}Al_2O_4:Eu^{2+}_{0.01},Dy^{3+}_{0.02}$ AND $Sr_{0.95}Al_2O_4:Eu^{2+}_{0.01},Dy^{3+}_{0.04}$ PHOSPHORS PREPARED AT DIFFERENT INITIATING COMBUSTION TEMPERATURES

6.1. INTRODUCTION

The green luminescence from $SrAl_2O_4$ co-activated with divalent europium ions (Eu^{2+}) and trivalent dysprosium ions (Dy^{3+}) have attracted much interest in recent years because of their persistent phosphorescence, high quantum efficiency, and good chemical stability [1]. It is well known that the blue-green emission from these phosphors arises from the $4f^65d \rightarrow 4f^7(^8S_{7/2})$ transitions of Eu^{2+} ions while Dy^{3+} ions are only responsible for the long afterglow behaviour of the phosphors. It is widely reported that the long afterglow is a result of trapping and detrapping of charge carriers (electron and/or holes) by trap levels in the lattice [1]. In this chapter $SrAl_2O_4:Eu^{2+}$ phosphors doped with of different concentrations of Dy^{3+} prepared by the combustion method at different initiating combustion temperatures were investigated. The procedure was illustrated with a flow diagram in chapter 6. TEM and XRD were used to investigate the microstructure and the crystal structure of the phosphors. A 325 nm He-Cd laser and a SPEX 1870 0.5 m monochromator and a photomultiplier detector and a Cary Eclipse UV-Vis spectrophotometer equipped with a monochromatized xenon lamp to collect photoluminescence (PL) data in air at room temperature.

6.2. RESULTS

6.2.1. MORPHOLOGY AND STRUCTURES

Figure 6.1 shows the TEM images of $SrAl_2O_4:Eu^{2+},Dy^{3+}$ phosphors prepared at an initiating combustion temperature of 500 ^{0}C. The irregular shapes, as shown by figure 6.1 (a), clearly illustrate the inherent nature of the combustion method. Figure 6.1(b) shows the particles at higher resolution.

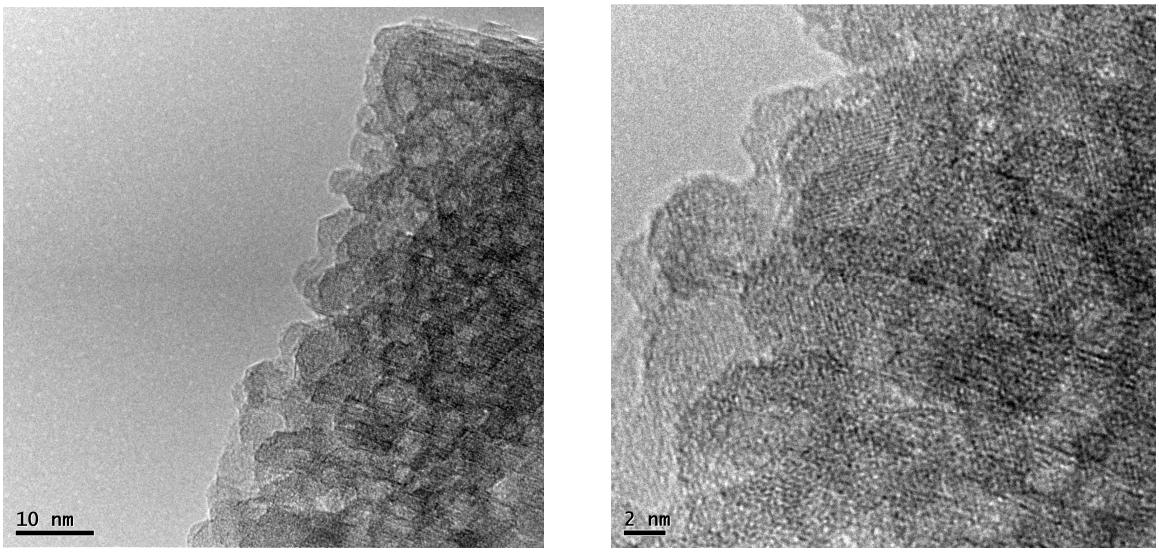

Figure 6.1: TEM images of $SrAl_2O_4:Eu^{2+},Dy^{3+}$ phosphors prepared at an initiating combustion temperature of 500 ^{0}C

Figure 6.2.a shows the XRD $Sr_{0.95}Al_2O_4$ prepared at different initiating combustion temperatures. The main diffraction peaks of these samples matched well with the standard JCPDS file 34 - 0379. The XRD also indicates some peak which may be related to other impurity phases such as $SrAl_4O_7$ [2] and $Sr_3Al_2O_6$ [3] and some may be due to unreacted precursors such as $Sr(NO_3)_2$ [4] during the combustion process.

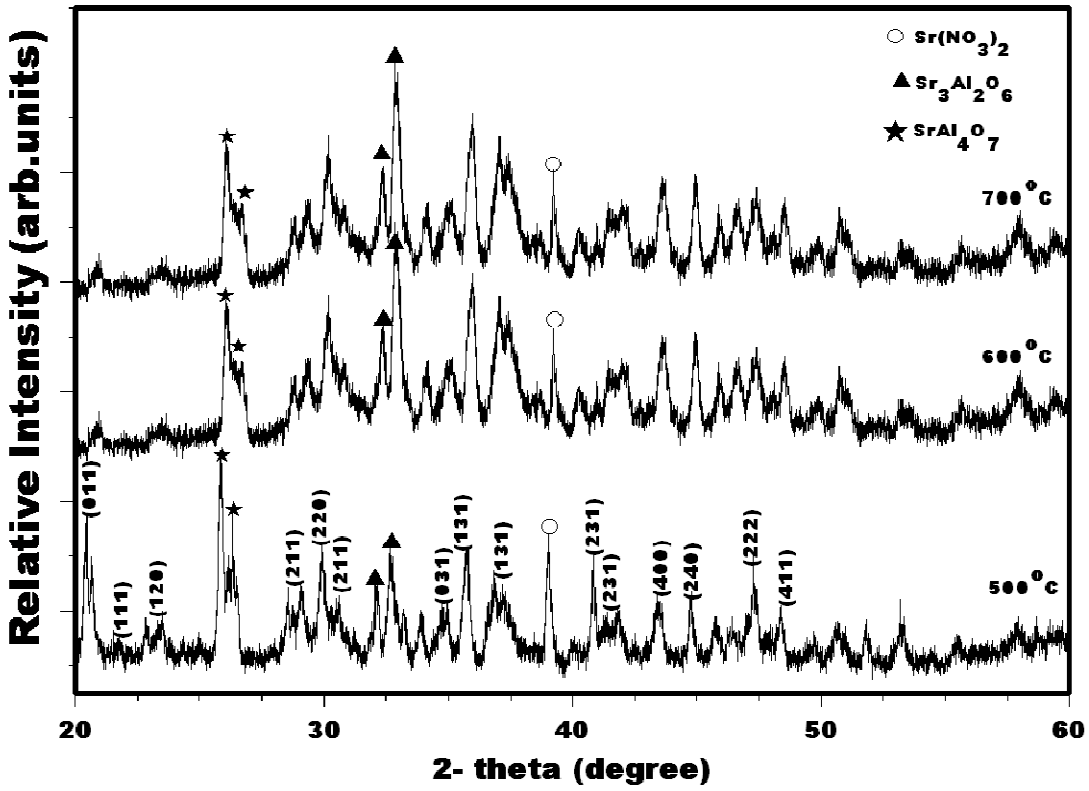

Figure 6 .2.a: XRD patterns of $Sr_{0.95}Al_2O_4$ prepared at different initiating combustion temperatures

Figure 6.2.b shows the XRD patterns of $Sr_{0.97}Al_2O_4$ prepared at different initiating combustion temperatures. The peaks indicated by stars at = 26^0 may be attributed to other impurity phases such as $SrAl_4O_7$.

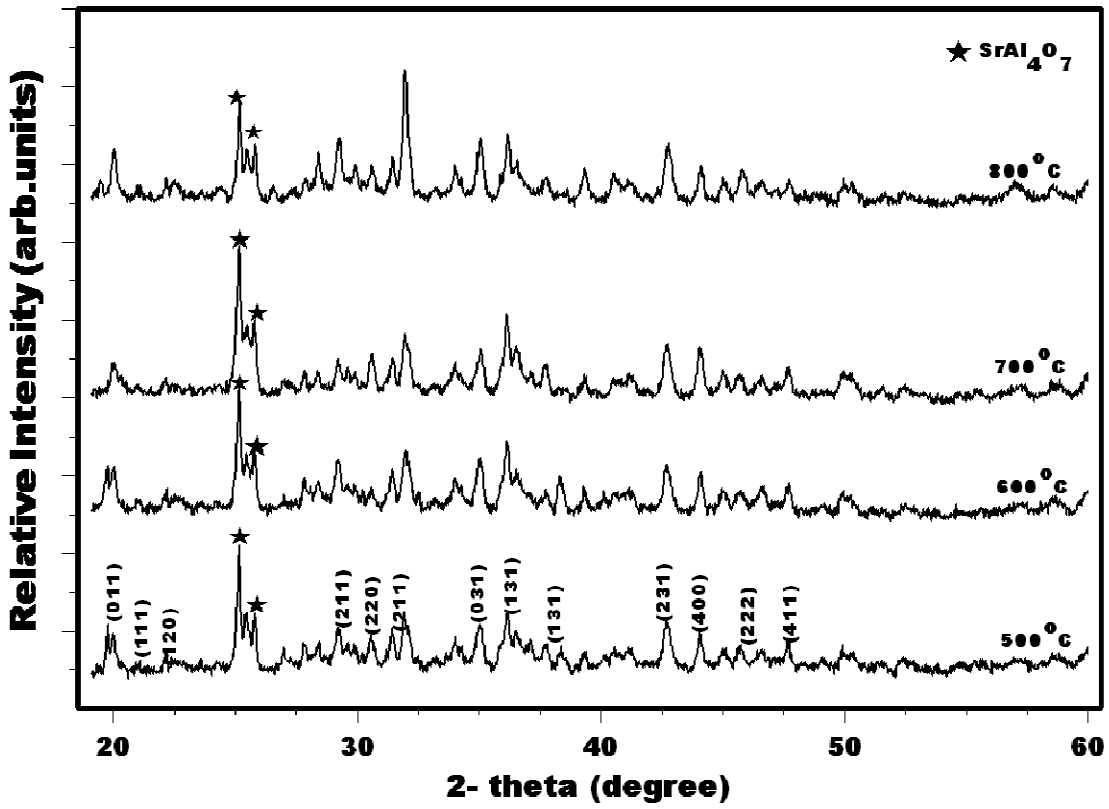

Figure 6.2.b: XRD patterns of $Sr_{0.97}Al_2O_4$ prepared at different initiating combustion temperatures.

6.2.2. PHOTOLUMINESCENCE

Figure 6.3 shows the foamy product of $Sr_{0.97}Al_2O_4$: $Eu^{2+}_{0.01}$,$Dy^{3+}_{0.02}$ phosphors prepared by the combustion method. Figure 6.3.a shows the foamy product with a white body colour before excitation and the greenish product as shown by figure 6.3.b was observed after the sample was excited with a UV lamp in the darkroom. The green emission colour can be attributed to the electronic transition from the excited $4f^6 5d^1$ to the ground state $4f^7$ of the Eu^{2+} [5].

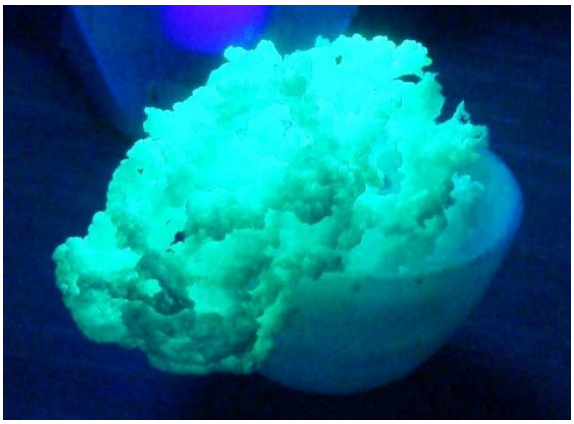

Figure 6.3: (a) Foamy product before excitation and (b) foamy product after excitation.

Figure 6.4 show the broad emission spectra of $Sr_{0.97}Al_2O_4$: $Eu^{2+}_{0.01}$,$Dy^{3+}_{0.02}$ phosphors prepared at different initiating combustion temperatures. The optimum PL intensity was observed on a sample prepared at an initiating combustion temperature of 500 ^{0}C. Furthermore, the samples prepared at 500 – 600^{o}C showed emission peaks at 528 nm, which can be attributed to the electronic transition of the Eu^{2+} ions [6].

The samples prepared at initiating combustion temperatures of 700 - 800 ^{0}C showed the lowest intensity with sharp emission lines instead of a broad emission spectra which may be attributed to the fact that as the temperature increases, the environment may not be conducive to reduce Eu^{3+} to Eu^{2+}. The sharp emission lines observed from these samples can be attributed to the parity - forbidden intra-configurational $4f^7$ - $4f^7$ transitions of un-reduced Eu^{3+} ions present in the host matrix [5].

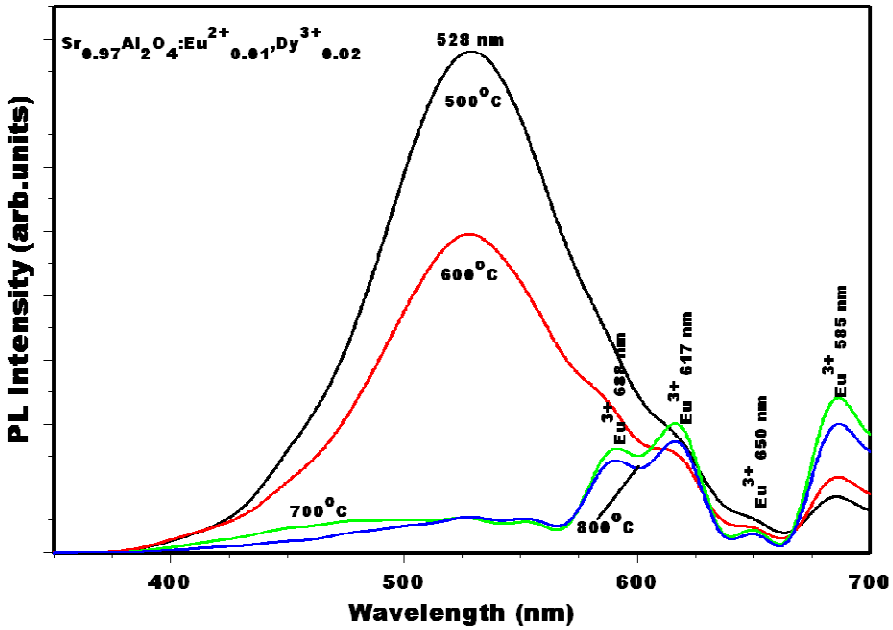

Figure 6.4.a: Emission spectra of $Sr_{0.97}Al_2O_4$: $Eu^{2+}_{0.01}$,$Dy^{3+}_{0.02}$ phosphors prepared at different initiating combustion temperatures.

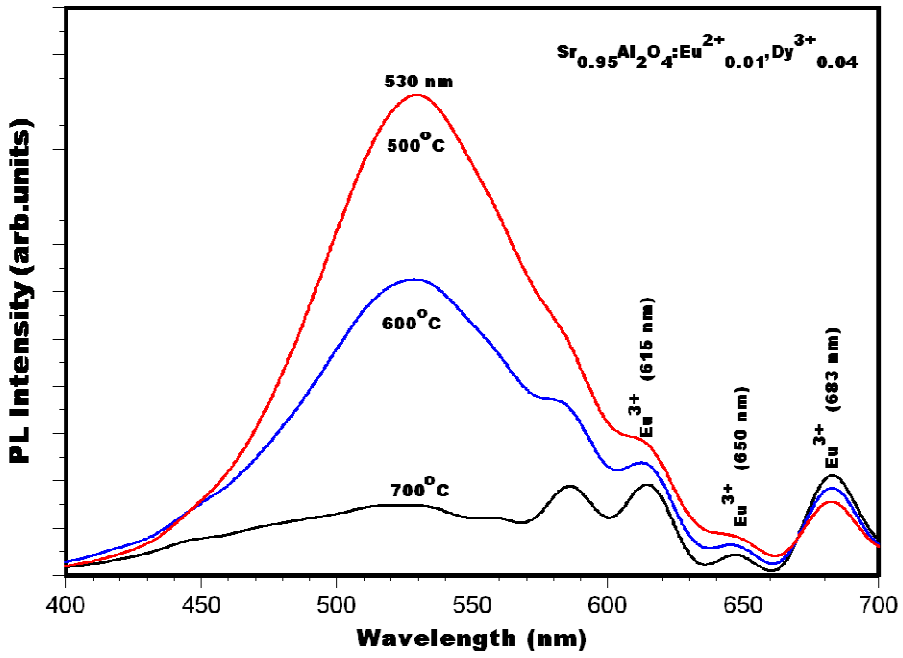

Figure 6.4.b: Emission spectra of $Sr_{0.95}Al_2O_4$: $Eu^{2+}_{0.01}$,$Dy^{3+}_{0.04}$ phosphors prepared at different initiating combustion temperatures.

Figure 6.4.b shows the emission spectra of $Sr_{0.95}Al_2O_4$: $Eu^{2+}_{0.01}$,$Dy^{3+}_{0.04}$ phosphors prepared at different initiating combustion temperatures. The optimum PL intensity was found for the sample prepared at 500 ^{0}C. As the initiating combustion temperature increases the intensity tends to decrease. The emission lines shown by these samples confirm the presence of the Eu^{3+} ions, and from these results we may deduce that the higher initiating temperatures are not a suitable environment to reduce Eu^{3+} to Eu^{2+}.

6.2.3. PHOSPHORESCENCE

In general the stoichiometry of Sr:Al can be expressed as 1:2 according to the empirical formula $SrAl_2O_4$. It is well known that stoichiometry and methods of preparation can significantly affect the luminescence properties of phosphors [7]. Figures 6.5 (a) and (b) show the afterglow curves of phosphors with different stoichiometric composition. In figure 6.5 (a) according to $Sr_{0.97}Al_2O_4$: $Eu^{2+}_{0.01}$,$Dy^{3+}_{0.02}$, the ratio of Sr: Al is 0.97: 2 and in figure 6.5 (b) as shown by the formula $Sr_{0.95}Al_2O_4$: $Eu^{2+}_{0.01}$,$Dy^{3+}_{0.04}$, the ratio is 0.95: 2. The variations in Sr content in these phosphors were done in order to accommodate the concentration variations of luminescent ions (Eu^{2+}) and the co- activator ions (Dy^{3+}). The concentration of the luminescent ions (Eu^{2+} 1 mol %) were kept constant in both phosphors, but the concentration of the co- activator ion (Dy^{3+}) was varied from 2 - 4 mol%. The samples doped with 2 mol% of Dy^{3+} ions showed much higher intensity and the longer decay times than those samples doped with 4 mol% of Dy^{3+} as shown in figure 6.5 (a) and figure 6.5 (b), respectively. This clearly shows that non-stoichiometric composition and the concentration variation of the co - activator ions may result in either enhancing or quenching of the luminescence of the phosphors [7].

Figure 6.5 shows the decay curves of $Sr_{0.97}Al_2O_4$: $Eu^{2+}_{0.01}$,$Dy^{3+}_{0.02}$ phosphors prepared at different initiating combustion temperatures. All these samples were prepared in almost a similar environment with the initiating combustion temperatures ranging from 500 – 800 ^{0}C. In figure 6.5 the optimum phosphorescence intensity was illustrated by a sample prepared at an initiating

combustion temperature of 500 ^{0}C. Similar trends were observed for the samples shown by the $Sr_{0.95}Al_2O_4$: $Eu^{2+}_{0.01}$,$Dy^{3+}_{0.04}$ samples where the optimum PL intensity was illustrated by a sample prepared at lower temperature. As the temperature increases the PL intensity decreased rapidly as a function of time.

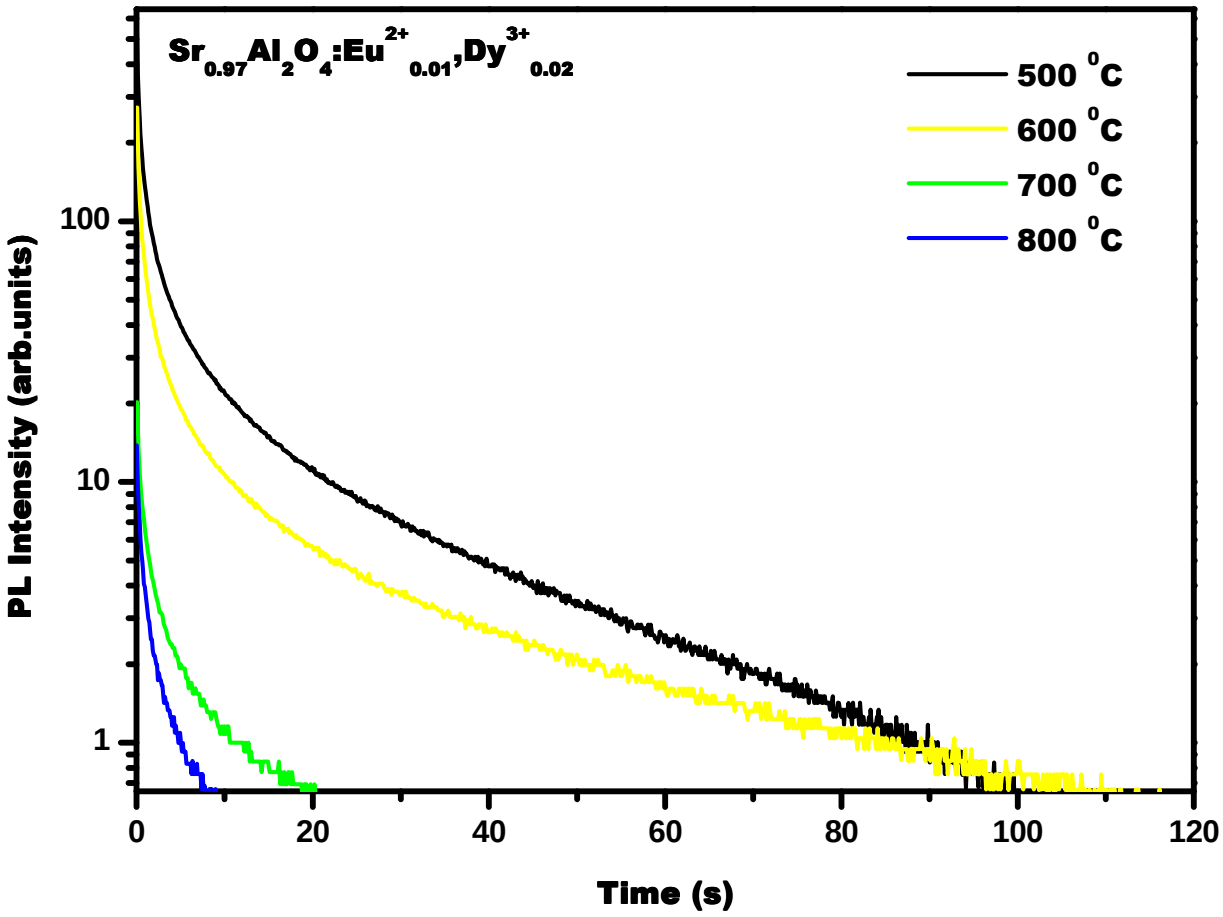

Figure 6.5: Decay curves of $Sr_{0.97}Al_2O_4$: $Eu^{2+}_{0.01}$,$Dy^{3+}_{0.02}$ phosphors prepared at different initiating combustion temperatures.

The decay times of the phosphors as shown in table 6.1 were obtained by fitting the decay curves using the three order exponential decay equation as discussed in chapter 7.

Table.6.1: Decay times of $Sr_{0.97}Al_2O_4$: $Eu^{2+}_{0.01}$,$Dy^{3+}_{0.04}$ phosphors prepared at different initiating combustion temperatures.

Phosphors	τ_1 **(sec)**	τ_2 **(sec)**	τ_3 **(sec)**
$Sr_{0.97}Al_2O_4$:$Eu^{2+}_{0.01}$,$Dy^{3+}_{0.02}$ (500 ^{0}C)	**0.9**	**8.0**	**48.9**
$Sr_{0.97}Al_2O_4$:$Eu^{2+}_{0.01}$,$Dy^{3+}_{0.02}$ (600 ^{0}C)	**0.7**	**5.14**	**30.3**

It is well known that for long afterglow persistence, Eu^{2+} acts as a luminescent center and Dy^{3+} acts as trap levels which capture the free holes, release the trapped holes and recombine with electrons, which accompanies luminescence [8]. The emission lifetime will be influenced by the depth of the trap level and the trap types [8]. In this study the concentration of Dy^{3+} ions, the stoichiometric ratio of Sr: Al and the initiating combustion temperature play an important role in the phosphorescent and photoluminescent properties of the phosphors.

6.3. CONCLUSION

$Sr_{0.97}Al_2O_4$:$Eu^{2+}_{0.01}$,$Dy^{3+}_{0.02}$ and $Sr_{0.95}Al_2O_4$: $Eu^{2+}_{0.01}$,$Dy^{3+}_{0.04}$ phosphors were successfully prepared at different combustion temperatures. The broad emission spectra illustrated by these phosphors can be attributed to the electronic transition of the Eu^{2+} ions from the excited state $4f^65d^1$ to the ground state $4f^7$. $Sr_{0.97}Al_2O_4$:$Eu^{2+}_{0.01}$,$Dy^{3+}_{0.02}$ showed better luminescent properties compared to $Sr_{0.95}Al_2O_4$: $Eu^{2+}_{0.01}$,$Dy^{3+}_{0.04}$ and this may be attributed to the concentration of the Dy^{3+}.

REFRENCES

1. H. Song, S.D. Singh, K.C. Cho, T.-Y. Lee, H.-S. Jakhar, D. Hulme, J.P. Han, C.-H. Gwak, J., J. Lumin. **128 (3)** (2008) 301
2. T. Katsumata, K. Sajima, T. Nabae, S. Komuro, T. Morikawa,J.Am. Ceram. Soc, **81 (2)** (1998) 413 - 416
3. X. Qiu, Y. Xu, X. Qiao, Mater. Lett. **61** (2007) 2731-2734
4. D. Wang, Y. Li, Y. Xiong, Q. Yin, J. Electrochem. Soc. **152 (1)** 2005 H12 - H14
5. S.H.M Poort, A. Meyerink,G. Blasse, J.Phys.Chem Solids, Vol **58** (1997) 1451-1456
6. Z. Tang, F. Zhang. Z Zhang, Q. Huang, Y Lin, J.European Ceram. Soc. **20** (2000) 2129 – 2132
7. N. Suriyamuthy, B.S. Panigrahi, J.Lumin. **128** (2008) 1809–1814
8. H. Zhong, X. Zeng, S. Afr. J. Chem., **61** (2008) 22–25

CHAPTER 7

LUMINESCENT PROPERIES OF $Ca_{0.97}Al_2O_4:Eu^{2+}_{0.01},Dy^{3+}_{0.02}$ PHOSPHORS PREPARED BY THE COMBUSTION METHOD AT DIFFERENT INITIATING COMBUSTION TEMPERATURES

7.1. INTRODUCTION

$CaAl_2O_4:Eu^{2+},Re^{3+}$ phosphors have been considered as a useful violet phosphor in the application of luminous clocks and watches, as well as potential outdoor night time displays [1]. $CaAl_2O_4$ has a stuffed tridymite structure with two sites for the large cation, each with 9-fold coordination [2]. Zhong *et al*. [3] reported that the quality of the luminescent material is largely influenced by the synthesis technique. Over the years, MAl_2O_4:Eu2+ (M = Ca, Sr, Ba) phosphors were mostly synthesized by high temperature solid-state and sol-gel methods, which require quite long reaction times at high temperatures. In recent years the combustion method has displayed unique advantages, such as shorter synthesis times and controlled size of the particles, and it is a more reliable method for preparing long afterglow phosphors [3].In this chapter the luminescent properties and the XRD patterns of $CaAl_2O_4:Eu^{2+}_{0.01},Dy^{3+}_{0.02}$ phosphors prepared at different initiating combustion temperatures (500 – 800 ^{0}C) were investigated .

7.2. EXPERIMENTAL

The powder samples of $Ca_{0.97}Al_2O_4:Eu^{2+}_{0.01},Dy^{3+}_{0.02,}$ phosphors were synthesized at different initiating combustion temperatures (500 – 800 ^{0}C). The precursors Calcium nitrate ($Ca(NO_3)_3.4H_2O$), Aluminum nitrate ($Al(NO_3)_2.9H_2O$), Europium nitrate ($Eu(NO_3)_3.6H_2O$), Dysprosium nitrate ($Dy(NO_3)_3.5H_2O$) and Urea ($CO(NH_2)_2$), all in analytical purity were

weighed according to the stoichiometry. The combustion process used to synthesis these phosphors at different initiating combustion temperatures have been illustrated with a flow diagram in chapter 5. The crystalline structure, particle morphology and elemental composition of the phosphor powders were investigated using a Panalytical X-ray diffractometer (XRD) with Cu Kα at λ = 1.5406 Å and Shimadzu Superscan SSX-550 system for scanning electron microscopy (SEM) coupled with an energy dispersive X-rays spectrometer (EDS) respectively. A 325 nm He-Cd laser and a SPEX 1870 0.5 m monochromator and a photomultiplier detector and a Cary Eclipse UV-Vis spectrophotometer equipped with a monochromatized xenon lamp to collect photoluminescence (PL) data in air at room temperature.

7.3. RESULTS AND DISCUSSION

Figure 7.1 shows the XRD $CaAl_2O_4$ phosphors prepared at different initiating combustion temperatures. There is no significant change in the diffraction peaks of the phosphors prepared at different initiating temperatures. The main diffraction peaks indexed well with the monoclinic structure of $CaAl_2O_4$ according to the card file (JCPDS: no: 70 - 0134), with additional impurity phases (marked with stars) that can be attributed to $CaAl_4O_7$ [4] or some of the unreacted precursors during the combustion process. Haiyen *et al.* [5] reported that the presence of other phases or some of the un-reacted precursors may be attributed to the fact that the combustion wave is not uniform and a portion of some of the precursors might not react completely in the process. It must also be noted that the small amount of doped rare earth ions has almost no effect on the $CaAl_2O_4$ phase composition. Singh *et al*. [6] reported similar XRD results when they prepared similar phosphors by the combustion method at an initiating combustion temperature of 600 ^{0}C.

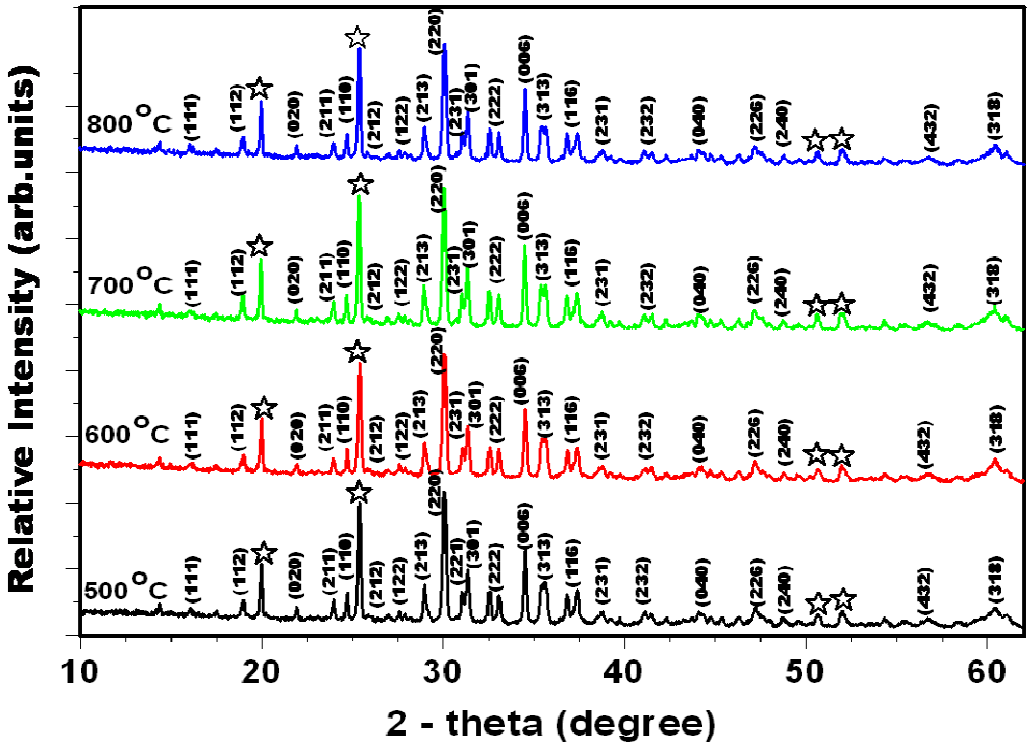

Figure 7.1: XRD patterns of $Ca_{0.97}Al_2O_4:Eu^{2+}_{0.01},Dy^{3+}_{0.02}$ samples prepared at different initiating combustion temperatures.

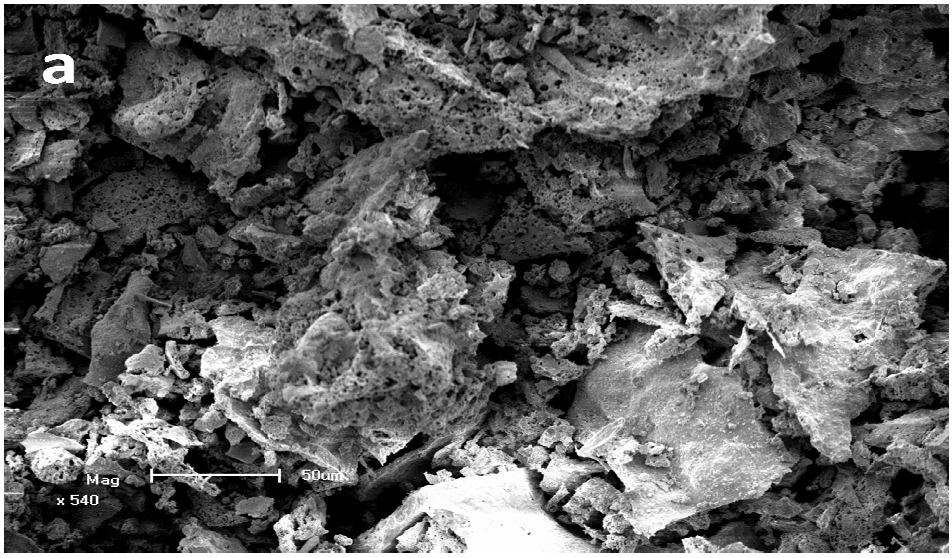

Figure 7.2.a: Lower resolution SEM micrograph of $Ca_{(0.97)}Al_2O_4:Eu^{2+}_{0.01},Dy^{3+}_{0.02}$ prepared at 600 ^{0}C

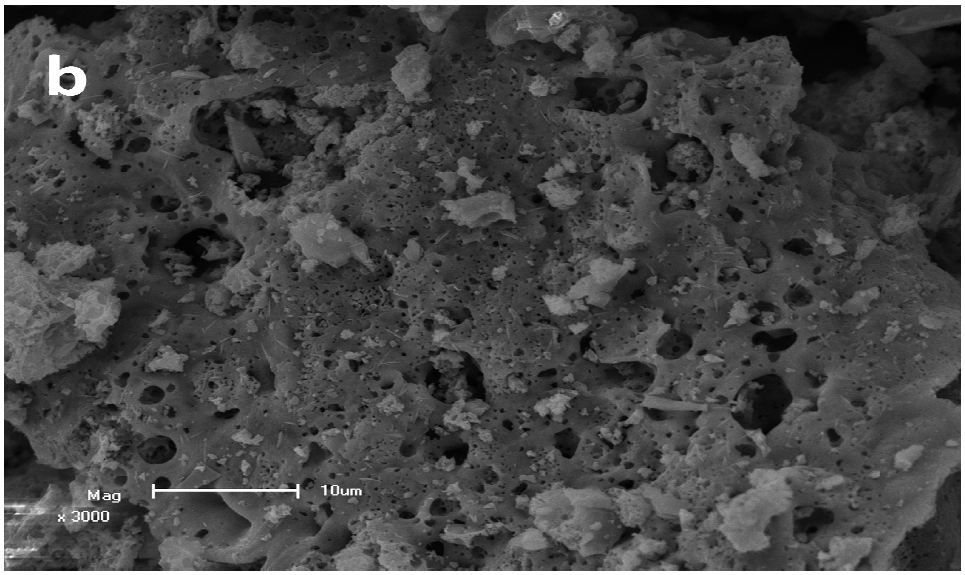

Figure 7.2: Higher resolution SEM micrograph of $Ca_{0.97}Al_2O_4:Eu^{2+}_{0.01},Dy^{3+}_{0.02}$ prepared at 600 ^{0}C.

Figure 7.2 shows the SEM micrographs of the phosphors prepared by combustion method at 600^{o}C. The non-uniform and irregular shapes of particles shown in figure 7.2(a) illustrate the inherent nature of the combustion method. Singh *et al.* [7] ascribed the irregular particle shapes to the non-uniform distribution of temperature and mass flow in the combustion flame. The morphology of a porous product with the small particles close to the pores at higher resolution as shown by figure 7.2(b) occurs during the combustion process when the gases escape under high pressure. Although the samples were prepared at different initiating combustion temperatures there were no significant variations in the surface morphology of the phosphors.

Figure 7.3 shows the PL emission spectra of $Ca_{0.97}Al_2O_4:Eu^{2+}_{0.01},Dy^{3+}_{0.02}$ phosphors prepared at different initiating combustion temperatures. The narrow emission bands at 449 nm for all the phosphors can be attributed to the $4f^6 5d^1$ to $4f^7$ transition of the Eu^{2+} ion. The similar narrow band spectra were also reported by Chen *et al*. [8] and they proposed that this may be due to the existence of only one kind of luminescent centre in $CaAl_2O_4:Eu^{2+},Dy^{3+}$. Furthermore, Park *et al.* [9] reported that there are three Ca^{2+} sites in the $CaAl_2O_4$ lattice, one is nine-coordinated and the others are six - coordinated by oxygen atoms. In the $CaAl_2O_4$ host lattice, Eu^{2+} ions prefer the

nine - fold coordinated Ca^{2+} sites (*r*Ca: 1.18 Å) to two six- fold coordinated ones (*r*Ca: 1.0 Å), because larger spaces are demanded for the substitution of Eu^{2+} ions (*r*Eu: 1.30 Å) due to the ionic size difference [10].

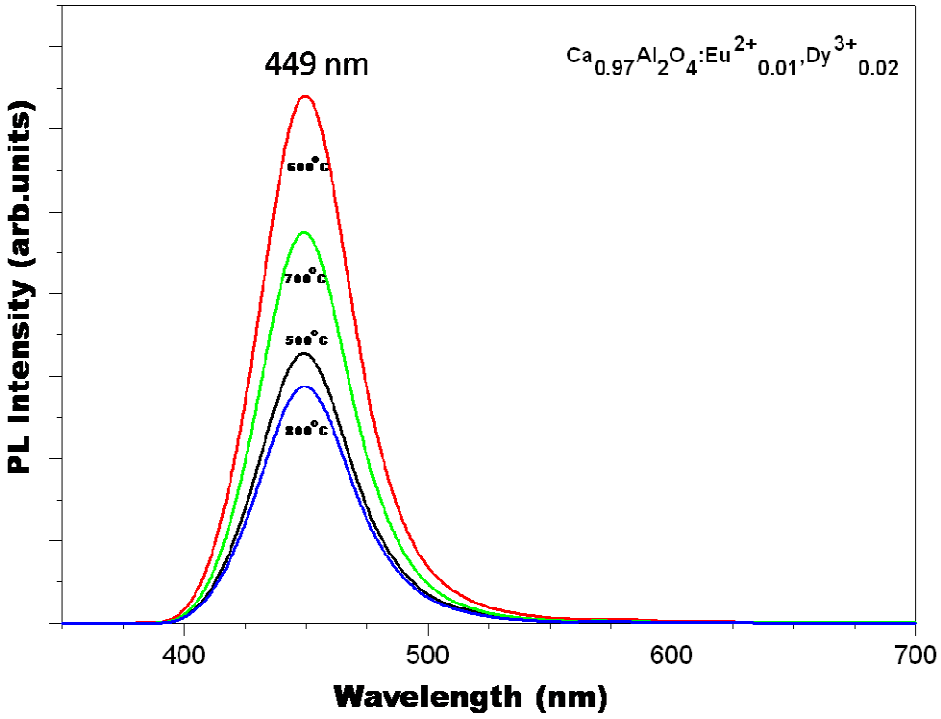

Figure 7.3: PL emission spectra of the $Ca_{0.97}Al_2O_4:Eu^{2+}_{0.01},Dy^{3+}_{0.02}$ phosphor powder samples prepared at different initiating combustion temperatures.

As illustrated in figure 7.3 the sample prepared at an initiating combustion temperature of 600 ^{0}C showed the highest intensity. The PL intensity decreased drastically when the temperature was increased to 700 and 800 ^{0}C. The difference in the PL intensity as a function of the initiating combustion temperature may be attributed to the fact that at lower initiating temperatures (500 ^{0}C), the lower reaction heat may lead to the incomplete reaction of raw materials. On the other hand higher initiating combustion temperatures may release more heat which may not be

favorable for the formation of a more crystalline phosphor [11].Yu *et al*. [14] prepared $SrAl_2O_4:Eu^{2+}$ at different initiating combustion temperatures ranging from 400 -1000 ^{0}C, and the highest luminescence intensity was observed for a sample prepared at 600 ^{0}C. Liu *et al*. [12] reported an emission peak at 443 nm for $CaAl_2O_4:Eu^{2+},Dy^{3+}$ phosphors prepared at an initiating combustion temperature of 600 ^{0}C.

Figure 7.4 shows the decay curves of the samples after being irradiated with the monochromatized xenon lamp. As can be seen, the intensity of the decay curve of the sample prepared at the initiating combustion temperature of 600 ^{0}C is higher than the intensity of all other samples. This clearly shows that the initiating combustion temperature plays a major role in determining the luminescent properties of these phosphors.

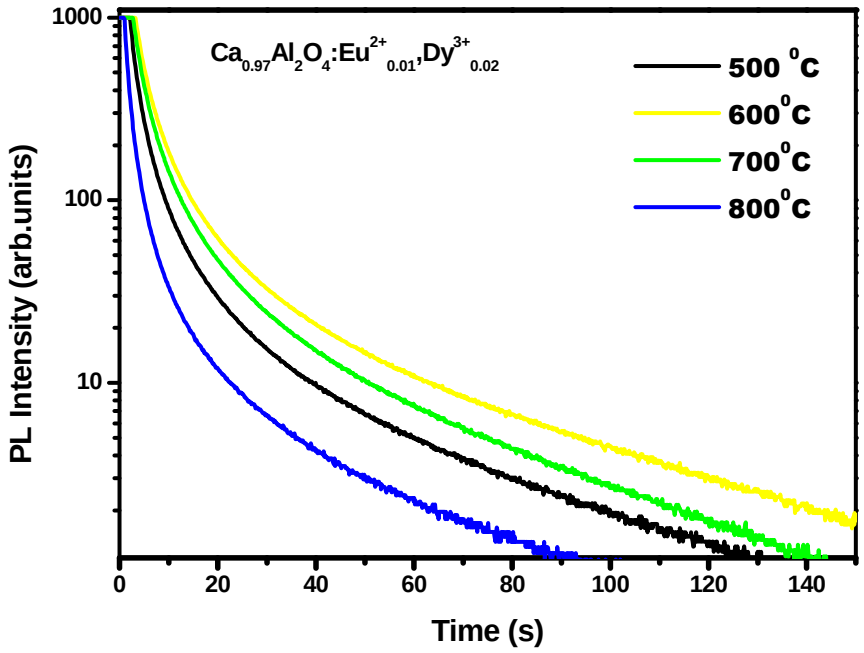

Figure 7.4: Decay curves of $Ca_{0.97}Al_2O_4:Eu^{2+}{}_{0.01},Dy^{3+}{}_{0.02}$ phosphors prepared at different initiating combustion temperatures.

In order to illustrate different decay times, the fittings of the decay profiles of the phosphors were performed based on equation 7.1

$$I = A_1 exp\left(-\frac{t}{\tau_1}\right) + A_2 exp\left(-\frac{t}{\tau_2}\right) + A_3 exp\left(-\frac{t}{\tau_3}\right) \qquad (7.1)$$

where I is the phosphorescence intensity at any time t after cutting off the UV excitation, A_1, A_2 and A_3 are constants and τ_1, τ_2 and τ_3 are decay times for the exponential components. A typical curve fitting results of $Ca_{0.97}Al_2O_4:Eu^{2+}_{0.01},Dy^{3+}_{0.02}$ phosphor prepared at an initiating combustion temperature of 600 ^{0}C is shown in figure 7.5. The three parameters with different decay times described as exp 1, exp 2 and exp 3 are clearly shown in figure 7.5.

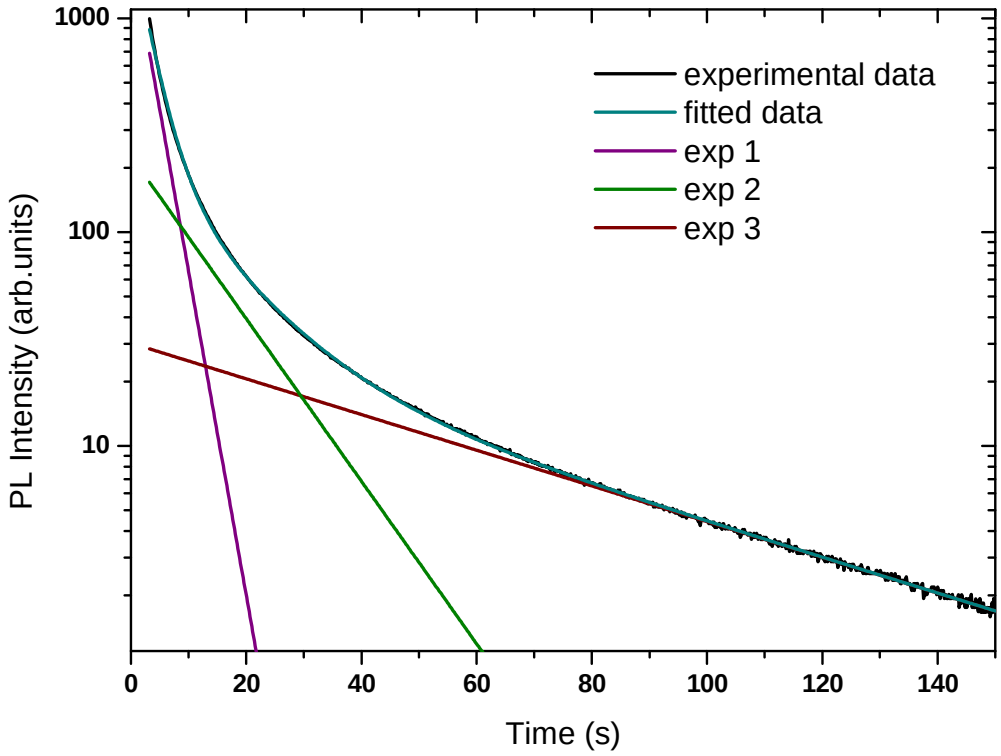

Figure 7.5: A typical curve fitting results of the $Ca_{0.97}Al_2O_4:Eu^{2+}_{0.01},Dy^{3+}_{0.02}$ prepared at an initiating combustion temperature of 600 ^{0}C.

As mentioned in the previous chapters, the three exponential decay times of the long persistent phosphors can be described as (1) initial rapid decay, (2) intermediate transitional and then (3) long lasting phosphorescence. The initial rapid decay is due to the short survival time of an electron in Eu^{2+}, the intermediate transitional decay might be the capture of Eu^{2+} by a shallow trap energy centre and the very long-lasting decay could be attributed to the deep trap energy centre of Dy^{3+}. Table 7.1 shows the decay parameters of the phosphors calculated using equation 7.1.

Table 7.1: Decay parameters of the phosphors calculated by curve fitting technique.

Phosphors	τ_1 **(sec)**	τ_2 **(sec)**	τ_3 **(sec)**
$Ca_{0.97}Al_2O_4:Eu^{2+}_{0.01},Dy^{3+}_{0.02}$ **(500 ^{0}C)**	**2.4**	**10.8**	**49.7**
$Ca_{0.97}Al_2O_4:Eu^{2+}_{0.01},Dy^{3+}_{0.02}$ **(600 ^{0}C)**	**3.9**	**13.5**	**54.0**
$Ca_{0.97}Al_2O_4:Eu^{2+}_{0.01},Dy^{3+}_{0.02}$ **(700 ^{0}C)**	**2.5**	**10.3**	**44.3**
$Ca_{0.97}Al_2O_4:Eu^{2+}_{0.01},Dy^{3+}_{0.02}$ **(800 ^{0}C)**	**1.7**	**10.5**	**49.00**

The results in table 7.1 reveal that the phosphor prepared at an initiating combustion temperature of 600 ^{0}C has better afterglow properties than the other phosphors. The difference in the afterglow properties of $Ca_{0.97}Al_2O_4:Eu^{2+}_{0.01},Dy^{3+}_{0.02}$ prepared at different initiating combustion temperatures can be explained in terms of the different types of traps..

7.4. CONCLUSION

$Ca_{0.97}Al_2O_4:Eu^{2+}_{0.01},Dy^{3+}_{0.02}$ phosphors were successfully prepared by combustion at different initiating temperatures. The monoclinic structures of $Ca_{0.97}Al_2O_4$ were obtained for all initiating combustion temperatures. The broad emission spectra for all the phosphors were all symmetric at 449 nm, which confirms that the emitting center is still the same, which is a Eu^{2+} ion. The decay curves of the long persistent phosphors were fitted successfully fitted using the three exponential decay times.

REFERENCES

1. C. Zhao, D. Chen, Mater. Lett. **61** (2007) 3673–3675
2. N. Suriyamurthy a, B.S. Panigrahi, J. Lumin. **128** (2008) 1809– 1814
3. H. Zhong, X. Zeng, S. Afr. J. Chem. **61** (2008) 22–25
4. C.Zhao, D. Chen, Mater. Lett. **61** (2007) 3673–3675
5. D. Haiyen, L. Gengshen, S. Jaiyue, J.Rare Earths **25** (2007) 19-22
6. V. Singh, T.K. G. Rao, D Kim, Radiation Measurements **43** (2008) 1198–1203
7. V.Singh, T.K.G Rao, J Zhu, Journal of Luminescence **128** (2008 583-588
8. X. Y. Chen, C. Ma, X. Li, C. W. Shi, X. L. Li, and Dao Rong Lu, *J. Phys. Chem. C*, **113 (7)** (2009) 2685-2689
9. Y. Jin Park, Y. J. Kim, Mater. Sci. Eng **B 146** (2008) 84–88
10. T. Aitasalo, P. Deren, J. Hölsä, H. Jungner, M. Lastusaari, J. Niittykoski,. Strek, Radiat. Meas **38** (2004) 515–518
11. Xibin Yu, Chunlei Zhou, Xianghong He, Zifei Peng and Shi-Ping Yang, Materials Letters **58** (2004) 1087–1091
12. C. Liu, Y. Wang, Y. Hu, R.Chen, F. Liao, Journal of Alloys and Compounds **470** (2009) 473–476
13. H. Ryu, K.S. Bartwal, Journal of Alloys and Compounds **464** (2008) 317–321
14. J. M. Ngaruiya, S. Nieuwoudt, O. M. Ntwaeaborwa, J. J. Terblans, H.C. Swart, Mater. Lett **62** (2008) 3192–3194.

CHAPTER 8

LUMINESCENT PROPERTIES OF $Ba_{0.97}Al_2O_4:Eu^{2+}_{0.01},Dy^{3+}_{0.02}$ PHOSPHORS PREPARED AT DIFFERENT INITIATING COMBUSTION TEMPERATURES

8.1. INTRODUCTION

Persistent luminescent materials such as $BaAl_2O_4,Eu^{2+},Dy^{3+}$ are a ubiquitous part of everyday life, finding use in a wide range of commercial applications such as luminescent watch dials and emergency lighting [1]. In this study, the effects of initiating temperature on photoluminescent and phosphorescent properties of $Ba_{0.97}Al_2O_4:Eu^{2+}_{0.01},Dy^{3+}_{0.02}$ phosphor powders prepared by the combustion method were investigated.

8.2. EXPERIMENTAL

The powder samples of $Ba_{0.97}Al_2O_4:Eu^{2+}_{0.01},Dy^{3+}_{0.02}$ phosphors were prepared at different initiating combustion temperatures ranging from 500 to 800 ^oC . The following precursors: Barium nitrate ($Ba(NO_3)_3.4H_2O$) and Aluminum nitrate ($Al(NO_3)_2.9H_2O$), Europium nitrate ($Eu(NO_3)_3.6H_2O$), Dysprosium nitrate ($Dy(NO_3)_3.5H_2O$) and Urea ($CO(NH_2)_2$), all in analytical purity, were weighed according to the desired stoichiometry. The samples were prepared by the combustion method as illustrated by a flow diagram in chapter 5. The crystalline structure, particle morphology and elemental composition and the luminescent properties of the phosphors were investigated as mentioned in chapter 5.

8.3. RESULTS AND DISCUSSION

The XRD patterns of $Ba_{0.97}Al_2O_4:Eu^{2+}_{0.01},Dy^{3+}_{0.02}$ powder samples prepared at initiating combustion temperatures of 500 - 800^{0}C are shown in figure 8.1. $BaAl_2O_4$ has a very high melting point and holds a stuffed tridymite (hexagonal) structure with lattice parameters a = 10.449 Å and c = 8.793 Å [2]. The hexagonal structures of $BaAl_2O_4$ were observed in all

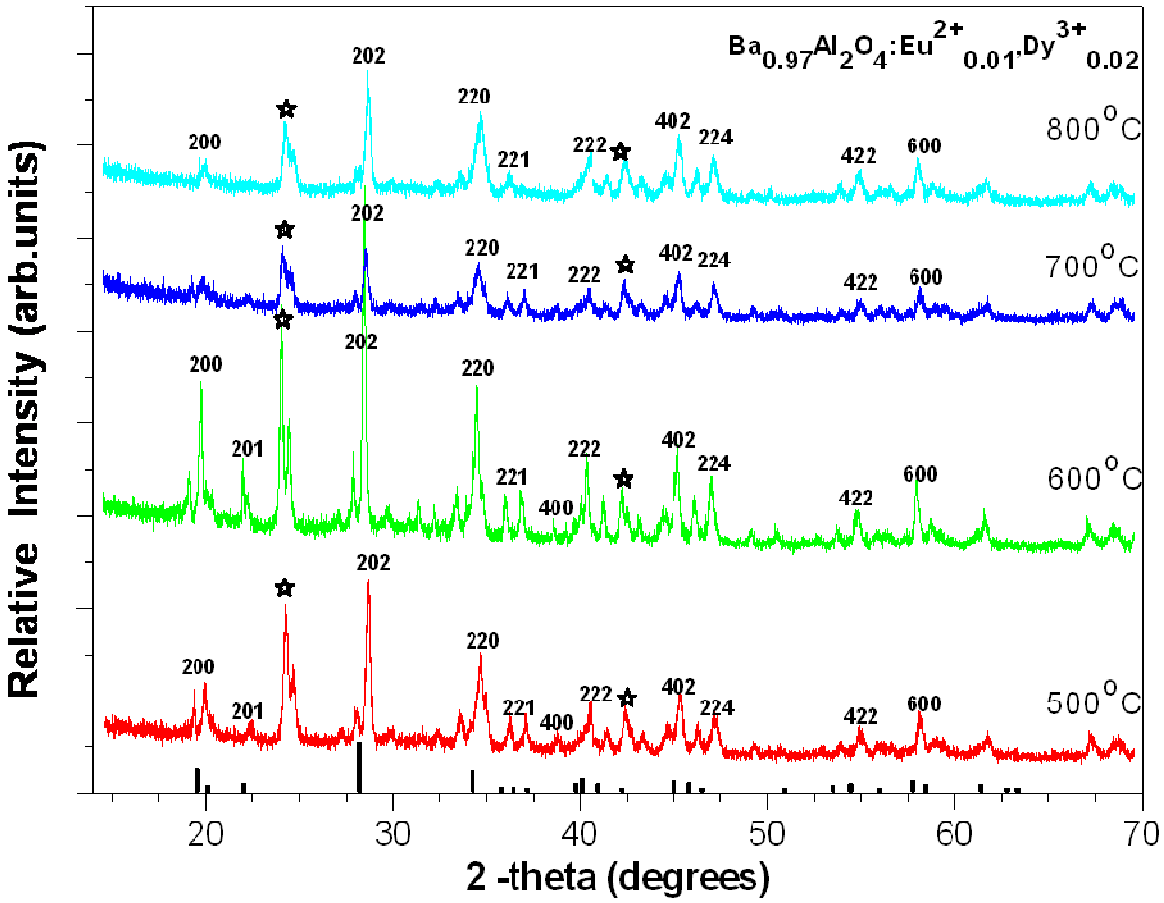

Figure 8.1: XRD patterns of $Ba_{0.97}Al_2O_4:Eu^{2+}_{0.01},Dy^{3+}_{0.02}$ prepared at different initiating combustion temperatures.

samples, and the JCDPS file no.17- 306 was used to match the characteristic peaks. Although the main peaks of the crystal structures were observed there were some additional peaks which can be attributed to unreacted $Ba(NO_3)_3.4H_2O$ and $Al(NO_3)_2.9H_2O$ precursors or other impurity phases. Haiyen *et al.* [3] reported that, the presence of other phases or some of the precursors can be attributed to the fact that the combustion wave is not uniform and a portion of some of the precursors might not react completely during the combustion process. The X-ray diffraction spectra of the samples prepared at 500 – 600 ^{0}C show more intense peaks than those prepared at 700 – 800^{0}C. This clearly illustrates that better crystalline samples can also be obtained at lower combustion temperatures.

Figure 8.2(a) shows the low and high resolution SEM images of $Ba_{0.97}Al_2O_4:Eu^{2+}_{0.01},Dy^{3+}_{0.02}$ phosphor powder prepared at the initiating combustion temperature of 500^{o}C. In general, the morphologies of the phosphors did not change significantly with different initiating combustion temperatures. The non- uniform and irregular shapes of particles observed in figure 8.2(a) may be attributed to the non-uniform distribution of temperature and mass flow in the combustion flame [4].

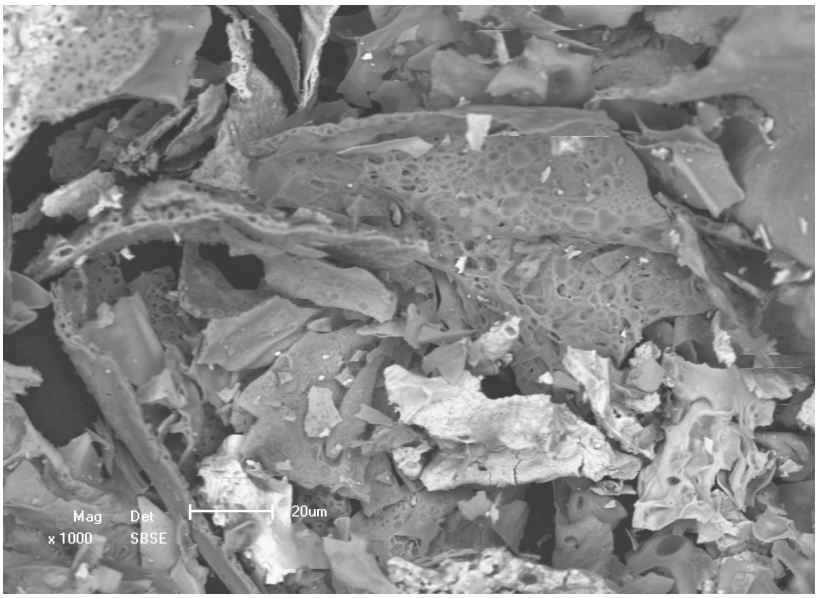

Figure 8.2.a: SEM morphology at lower resolution for $Ba_{0.97}Al_2O_4:Eu^{2+}_{0.01},Dy^{3+}_{0.02}$ prepared at 500 ^{0}C .

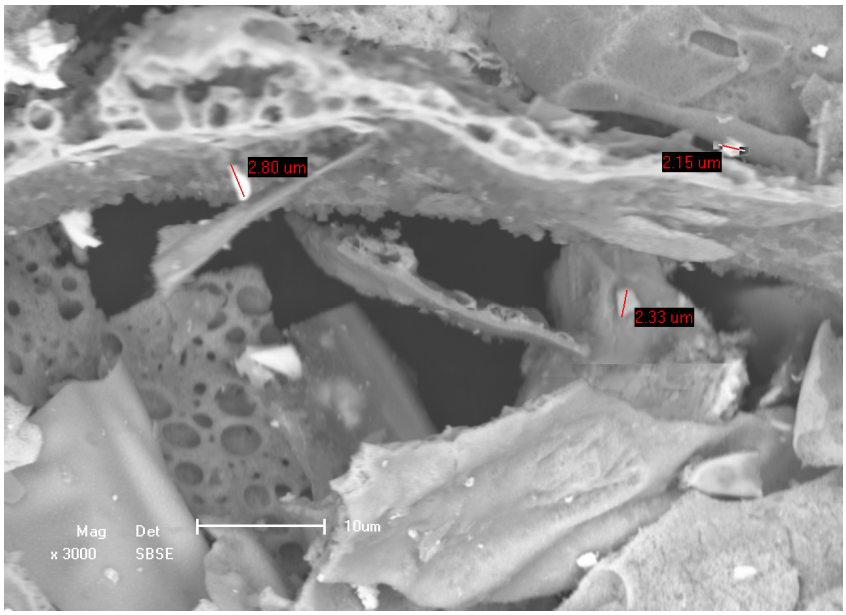

Figure 8.2.b: SEM morphology at higher resolution for $Ba_{0.97}Al_2O_4:Eu^{2+}_{0.01},Dy^{3+}_{0.02}$ prepared at 500^{o}C.

The SEM image obtained at a higher resolution is shown in figure 8.2(b). The morphology shows the pores and small particles within the grains that formed during the combustion process due to the high pressure of gases escaping in the heating process. The microstructure of $Ba_{0.97}Al_2O_4:Eu^{2+}_{0.01},Dy^{3+}_{0.02}$ particles reflects the inherent nature of the combustion process.

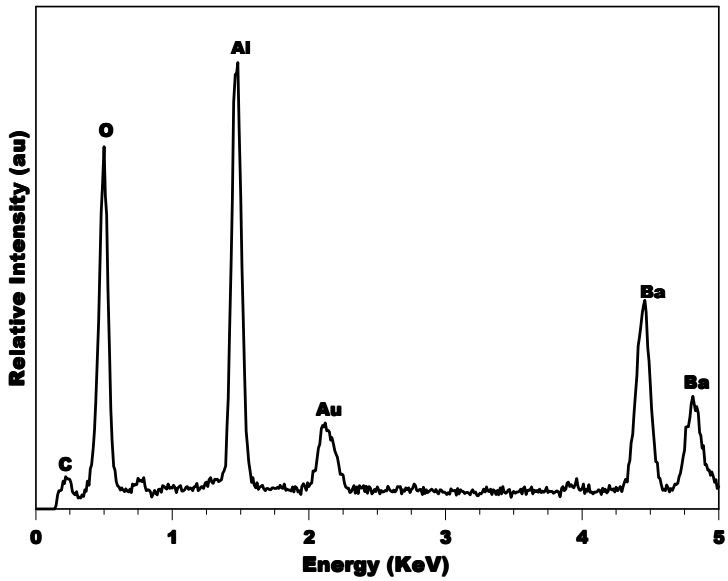

Figure 8.3: EDS spectrum of the $Ba_{0.97}Al_2O_4:Eu^{2+}_{0.01},Dy^{3+}_{0.02}$ phosphor prepared at 500^{0}C.

All the elements incorporated in the $Ba_{0.97}Al_2O_4:Eu^{2+}{}_{0.01}$,$Dy^{3+}{}_{0.02}$ phosphor prepared at the initiating temperature of 500 ^{0}C, are present as shown in the EDS spectrum in figure 8.3. All the phosphor powders were coated with gold to reduce the electron beam induced surface charging. The Dy^{3+} and Eu^{2+} concentrations were too low to be detected by EDS.

The emission spectra of $Ba_{0.97}Al_2O_4:Eu^{2+}{}_{0.01},Dy^{3+}{}_{0.02}$ prepared at different initiating combustion temperature are shown in Figure 8.4(a). The broad blue - green emission spectra can be attributed to the $4f^65d^1$ - $4f^7$ transition of Eu^{2+} ions in the host matrix [5]. All the samples were excited with the 325 nm He-Cd laser. The phosphor sample prepared at the initiating temperature of 500 ^{0}C showed much higher intensity compared to other samples. The broad emission spectra in all the samples range from 350 to 650 nm. As shown in figure 8.4(a) there is a peak at 450 nm with a shoulder at 500 nm for some samples. The 450 nm peak tends to decrease as the initiating temperature increases and vanishes completely for the sample prepared at 800 ^{0}C. Yu *et al*. [3] prepared $SrAl_2O_4:Eu^{2+}$ using the combustion method with initiating temperatures of 400-1000 ^{0}C, and the optimum PL intensity was observed at 600 ^{0}C.

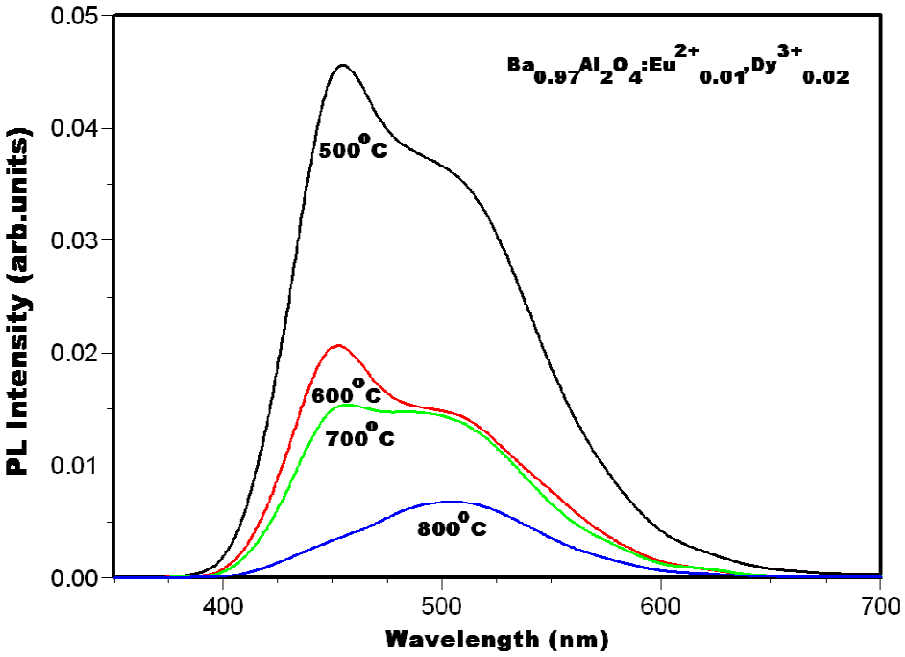

Figure 8.4.a: PL emission spectra of $Ba_{0.97}Al_2O_4:Eu^{2+}{}_{0.01},Dy^{3+}{}_{0.02}$ phosphors powder samples prepared at different initiating combustion temperatures.

The shift to lower energy of the emission spectra as the temperature increases as shown in figure 8.4(a), may be attributed to changes in the crystal field around Eu^{2+} ions [6]. Aiziwa *et al.* [7] proposed that the PL peak shift towards the lower energy side of the spectrum with an increase in temperature is attributed to an increase of the crystal field strength surrounding the Eu^{2+} centers in $BaAl_2O_4$. Ravichandran *et al.* [5] accounted for different emission spectra observed in $BaAl_2O_4$ by assuming that there is a different distribution of Eu^{2+} over the two cations sites. The wavelength and intensity variations observed on these samples may be attributed to crystal field effects on the 5d electrons states of Eu^{2+} ions due to the variation of parameters such as composition, preparation temperature, etc [8]. Suli *et al.* [9] reported that different phase compositions can lead to changes in crystal field of the Eu^{2+} ion and this has been observed in different excitation and emission spectra.

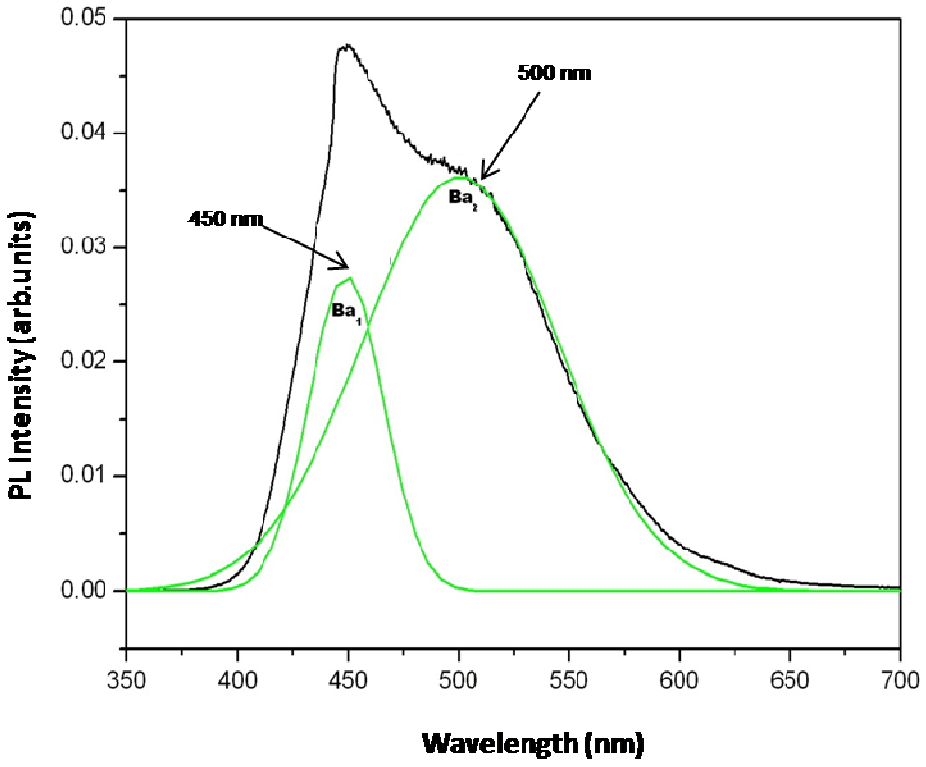

Figure 8.4.b: A Gaussian fit of the emission spectrum of $Ba_{0.97}Al_2O_4:Eu^{2+}_{0.01},Dy^{3+}_{0.02}$ phosphors prepared at an initiating temperature of 500 ^{0}C.

Peng *et al.* [10] reported that the structure of $BaAl_2O_4$ compound has two different barium sites Ba (1) and Ba (2) positioned on 6c and 2a and coordinated by nine oxygen ions with average Ba-O distances of 2.97 Å for Ba(1) and 2.89 Å for Ba(2), respectively [10]. Figure 8.4(b) shows the Gaussian fit performed on a sample with the maximum PL intensity, in order to account for different Ba sites that can be occupied by the Eu^{2+} in the matrix. The data of the fitted emission spectra are shown in table 8.1.

Table 8.1 Fitting parameters of PL emission spectrum of $Ba_{0.97}Al_2O_4:Eu^{2+}_{0.01},Dy^{3+}_{0.02}$ phosphors

Peak	Area	Center	Width	Height
1	1.16	450	0.03	0.028
2	4.0034	500	28.08	0.036

The observed emission peaks that are symmetric at 450 and 500 nm are ascribed to the Ba (1) and Ba (2) sites in the matrix when occupied by Eu^{2+} ions, respectively. The 500 nm emission peak which is more intense and broader compared to the 450 nm peak may be attributed to the energy transfer from the 450 nm to the 500 nm emission peak [11]. The 500 nm emission peak in the present work is more intense and much broader than the peak at 450 nm and this is in contrast with the results obtained by Peng *et al*. [10] where the peak related to the Ba (1) site was broader and more intense. Suriyamurthy *et al*. [12] reported that the bond length difference of Ba-O at Ba (1) and Ba (2) sites may cause the crystal field strength at one site to be stronger than at the other site will result in the difference in emission intensities. Sakai *et al*. [8] reported the main emission peak at 500 nm for $BaAl_2O_4:Eu^{2+},Dy^{3+}$ prepared by the floating zone technique.

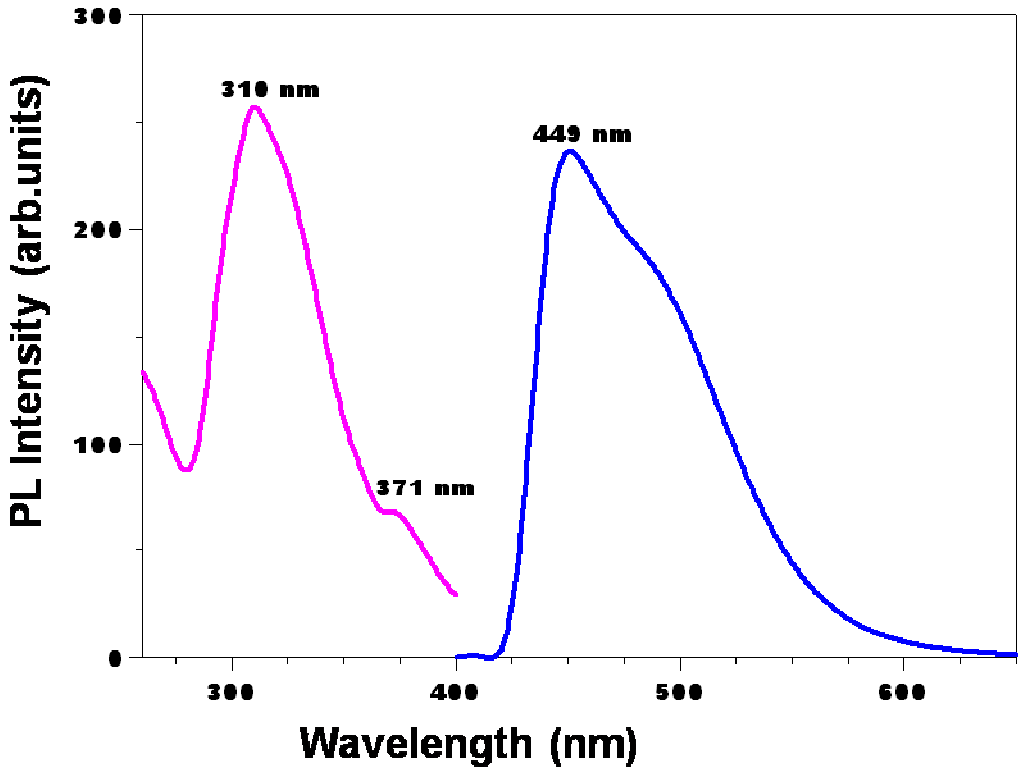

Figure 8.5: The PL excitation and emission spectra of $Ba_{0.97}Al_2O_4:Eu^{2+}_{0.01},Dy^{3+}_{0.02}$ phosphor powder prepared at an initiating combustion temperature of 500^0C.

Figure 8.5 presents the PL excitation and emission spectra of the $Ba_{0.97}Al_2O_4:Eu^{2+}_{0.01},Dy^{3+}_{0.02}$ phosphor prepared at an initiating temperature of 500 ^{0}C. The spectra were recorded using the Cary eclipse fluorescence spectrophotometer. The broad band excitation spectrum of $Ba_{0.97}Al_2O_4:Eu^{2+}_{0.01},Dy^{3+}_{0.02}$ with a maximum peak at 310 nm is due to the crystal field splitting of the Eu^{2+} in the d orbital [13], The emission spectrum is similar to the results in figure 8.4(a), where the samples were excited with a 325 nm excitation source.

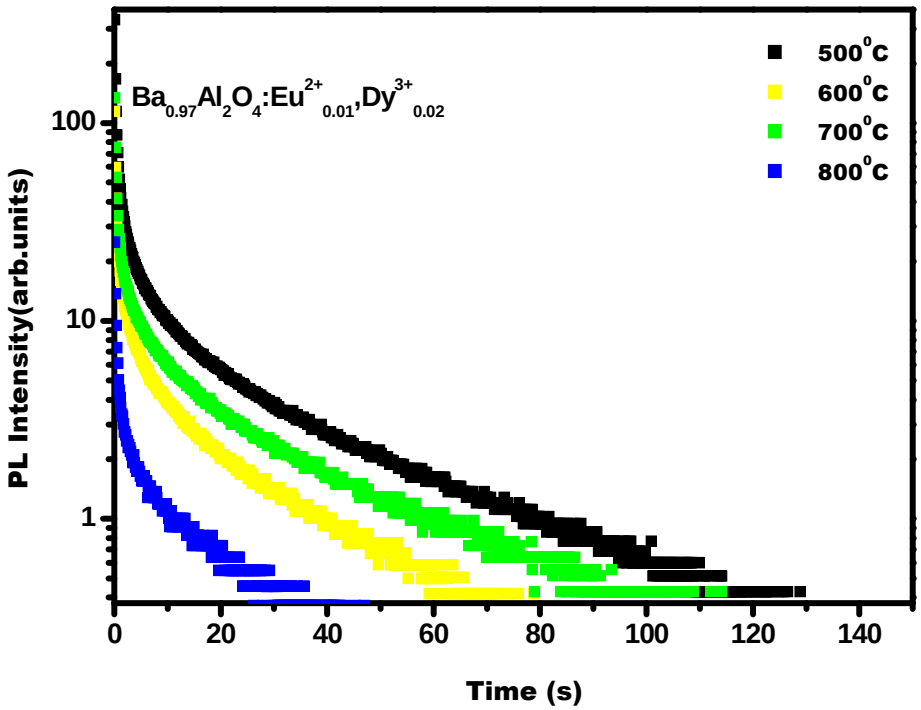

Figure 8.6: Decay curves of $Ba_{0.97}Al_2O_4:Eu^{2+}_{0.01},Dy^{3+}_{0.02}$ phosphors prepared at different initiating combustion temperatures.

The phosphorescence decay curves were obtained by irradiating the samples with a monochromatized xenon lamp at an excitation wavelength of 320 nm. Figure 8.6 shows the phosphorescence spectra of the phosphors prepared at different initiating temperatures. The sample prepared at the initiating temperature 500 ^{0}C shows a higher initial compared to the other samples. The decay parameters for the fitting data are listed in table 8.2.

The different decay times observed for these phosphors may be attributed to the different initiating combustion temperatures. The afterglow decay times as shown in table 8.2 are described as follows: Initial rapid decay, intermediate transitional and then long lasting phosphorescence [15,16]. The initial rapid decay is due to the short survival time of an electron in Eu^{2+}, the intermediate transitional decay might be the capture of Eu^{2+} by a shallow trap energy centre and the very long-lasting decay could be attributed to the deep trap energy centre of Dy^{3+} [16].

Table 8.2: Decay parameters of curves of $Ba_{0.97}Al_2O_4:Eu^{2+}_{0.01},Dy^{3+}_{0.02}$ phosphors prepared at different initiating combustion temperatures.

Phosphors	τ_1 *(sec)*	τ_2 **(sec)**	τ_3 *(sec)*
$Ba_{0.97}Al_2O_4:Eu^{2+}_{0.01},Dy^{3+}_{0.02}$ (500 ^{0}C)	**0.2**	**11.0**	**44.3**
$Ba_{0.97}Al_2O_4:Eu^{2+}_{0.01},Dy^{3+}_{0.02}$ (600 ^{0}C)	**0.21**	**2.2**	**20.7**
$Ba_{0.97}Al_2O_4:Eu^{2+}_{0.01},Dy^{3+}_{0.02}$ (700 ^{0}C)	**0.21**	**10.3**	**40.3**
$Ba_{0.97}Al_2O_4:Eu^{2+}_{0.01},Dy^{3+}_{0.02}$ (800 ^{0}C)	**0.2**	**1.78**	**26.4**

8.4. CONCLUSION

$Ba_{0.97}Al_2O_4:Eu^{2+}_{0.01},Dy^{3+}_{0.02}$ phosphors were successfully prepared at different initiating temperatures using the combustion method. The XRD were performed and the results suggest that phosphors with better crystallinity can be produced even at a low initiating combustion temperature. The blue-green emission attributed to the Eu^{2+} ion when it occupies one of the two available sites of Ba in $Ba_{0.97}Al_2O_4:Eu^{2+}_{0.01},Dy^{3+}_{0.02}$ phosphors was observed. From a Gaussian fit of the PL two peaks at 449 nm and 500 nm that are attributed to Eu^{2+} ions occupying the Ba (1) and Ba (2) sites, respectively were identified.

REFERENCES

1. P.J. Saines, M. M. Elcombe, B. J. Kennedy, Journal of Solid State Chemistry **179** (2006) 613 -632
2. D. Jia , X. Wang, E. van der Kolk, W.M. Yen , Optics Communications **204** (2002) 247-251
3. L.. Haiyen, S. Gengshen, J. Jaiyue, J. Rare earths **25** (2007) 19-22
4. V. Singh, T.K. Gundu Rao, J. Solid State Chem. **181** (2008) 1387– 139
5. D. Ravichandran, Shikik T. Johnson, S. Erdei, Rustum Roy, William B. White, Displays **19** (1999) 197–203
6. R. Zhang, G. Han, L. Zhang, B Yang, Material Chemistry and Physics, **111** (2009) (255-259)
7. H. Aizawa, S. Komuro, T. Katsumata, S. Sato, T. Morikawa, Thin Solid Films **496** (2006) 179 – 182
8. R. Sakai , T. Katsumata, S. Komuro, T. Morikawa, J.Lumin. **85** (1999) 149-154
9. W. Suli, S. Zhang,B. Yang, Materials Chem. and Phys. **102** (2007) 80-85
10. M. Peng, G. Hong, J.Lumin. **127** (2007) 735-740
11. C. Zhao, D. Chen, Y. Yuan, Ming Wu, Materials Science and Engineering B **133** (2006) 200–204
12. N. Suriyamurthy,B.S Panigrahi, J.Lumin. **127** (2007) 483 – 488
13. H. Ryu, B.K. Singh, K.S. Bartwal, Physica B **403** (2008) 126–130
14. V Singh , V. Natarajan, J. Zhu, Optical Materials **29** (2007) 1447–1451
15. H. Song, D. Chen, W. Tang, Y. Peng, Displays **29** (2008) 41-44
16. H. Zhong, X. Zeng, S. Afr. J. Chem., **61** (2008) 22–25

CHAPTER 9

THE EFFECT OF THE CONCENTRATION OF Eu^{2+} and Dy^{3+} in $Sr_{1-x}Al_2O_4:Eu^{2+}_x$, $Sr_{1-z}Al_2O_4:Eu^{2+}_{0.04},Dy^{3+}_z$ and$Sr_{1-y}Al_2O_4:Eu^{2+}_y,Dy^{3+}_{0.04}$ PHOSPHORS PREPARED BY COMBUSTION METHOD

9.1. INTRODUCTION

In this chapter the main objective is to investigate the effects of the concentration of Eu^{2+} and Dy^{3+} ions in the host matrix. The combustion synthesis of $Sr_{1-x}Al_2O_4:Eu^{2+}_x$,$Sr_{1-z}Al_2O_4:Eu^{2+}_{0.04}$,$Dy^{3+}_z$ and $Sr_{1-y}Al_2O_4:Eu^{2+}_y$,$Dy^{3+}_{0.04}$ was carried out by varying the concentrations of the dopant and the co-dopant. The preparation procedures for these phosphors were illustrated using a flow diagram in chapter 5. The photoluminescent and phosphorescent properties of the phosphor were investigated using a 325 nm He-Cd laser (fitted with a SPEX 1870 0.5 m spectrometer and a photomultiplier detector) and a Cary Eclipse UV-Vis spectrophotometer equipped with a monochromatized xenon lamp (325 nm excitation wavelength).The PL data was collected in air at room temperature.

9.2. RESULTS AND DISCUSSIONS

To study the effect of concentration of the luminescent ions (Eu^{2+}) and the co – activator ions (Dy^{3+}) it is essential that the preparation conditions such as the temperature and the preparation time should be kept same. The PL excitation spectrum, recorded with a monochromatized xenon lamp, is shown in figure 9.1. The typical absorption spectrum is attributed to the transition from the $4f^7$ ground state to the excited state $4f^65d^1$ of the Eu^{2+} ion [1]. The spectrum consists of two excitation bands at 340 and 375 nm.

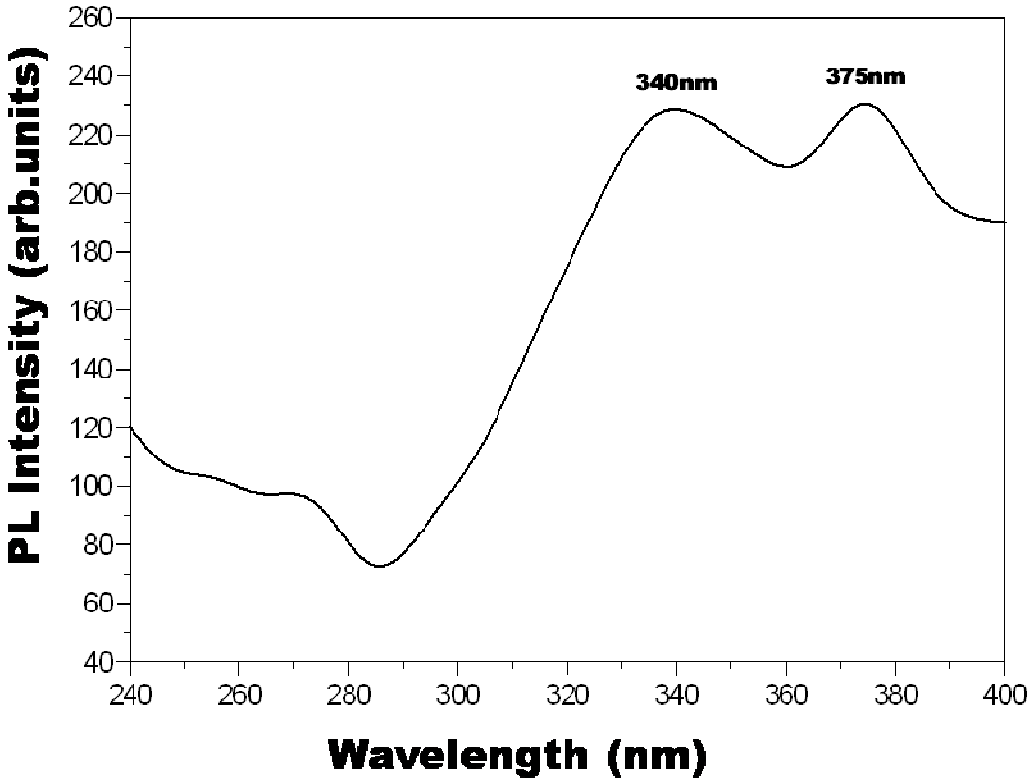

Figure 9.1: PL excitation spectrum recorded using monochromatized light from xenon lamp.

Figure 9.2 shows the PL emission spectra of $Sr_{1-x}Al_2O_4:Eu^{2+}{}_x$ (x = 0.015, 0.02, 0.03, 0.04 and 0.45). The PL intensity increased with concentration from 1.5 - 3 mol % of Eu^{2+} and drops at 4 – 4.5 mol % of Eu^{2+}. The drop in the PL intensity at 4 mol% of Eu^{2+} can be attributed to concentration quenching effects. The critical quenching concentration of Eu^{2+} in $SrO_6Al_2O_3:Eu^{2+}$ was observed at 3.6 mol % by Wang *et al.* [2]. The highest PL intensity was observed for the $Sr_{0.97}Al_2O_4:Eu^{2+}{}_{0.03}$ (i.e. Eu^{2+} = 3 mol %) spectrum, with the dominant emission band at ~520 nm and minor emissions lines at 615 and 690 nm. The emission at 520 nm can be attributed to $4f^65d \rightarrow 4f^7(^8S_{7/2})$ transition of Eu^{2+} and the line emissions are associated with radiative $^5D_0$-^7F_j (j

= 1,0,3,4) transitions arising from residual Eu^{3+} ions which have been reported to be always present in trace amounts [3,4] in the host matrix. It should be noted that the green emission from the Eu^{2+} singly doped $SrAl_2O_4$ was fluorescent, i.e. emission stopped immediately when the UV excitation was cut off.

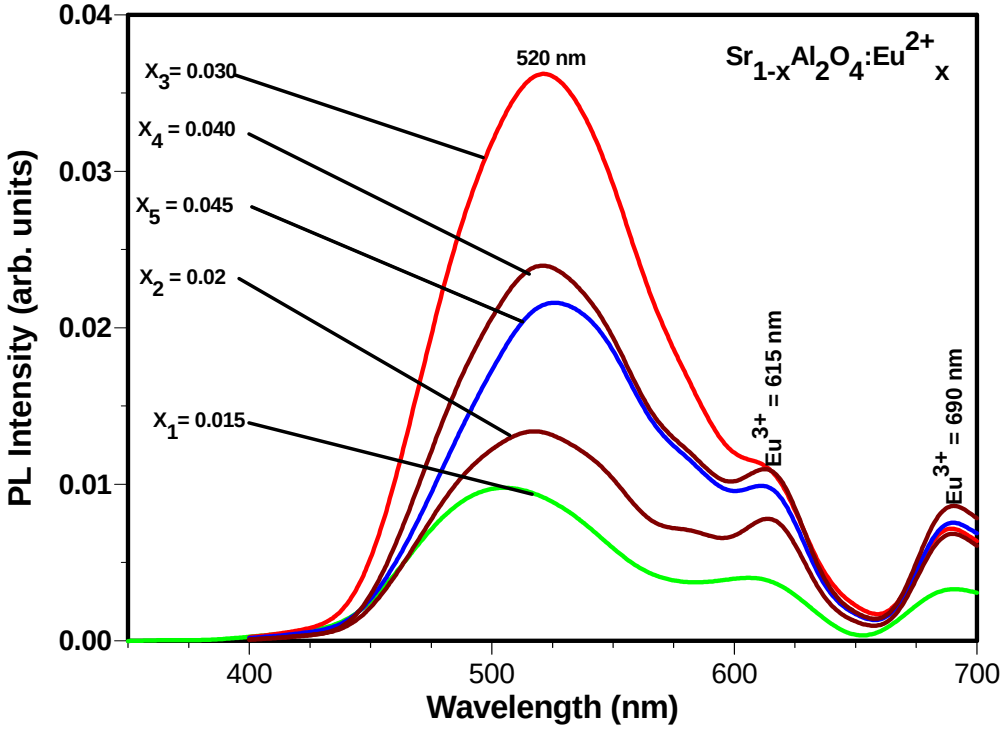

Figure 9.2: PL emission spectra of $Sr_{1-x}Al_2O_4:Eu^{2+}_x$ with different concentrations of Eu^{2+}.

Figure 9.3 shows the emission spectra of $Sr_{1-z}Al_2O_4:Eu^{2+}_{0.04}$, Dy^{3+} with the concentration of Eu^{2+} being kept constant at 4 mol% while varying the concentration of Dy^{3+} from 1 to 4 mol%. The optimum PL intensity was observed when the concentration of Dy^{3+} was 1.5 mol%, with a broad emission spectrum peaking at 525 nm. The minimum intensity was observed at 4 mol% of Dy^{3+} and similar results were reported [3].

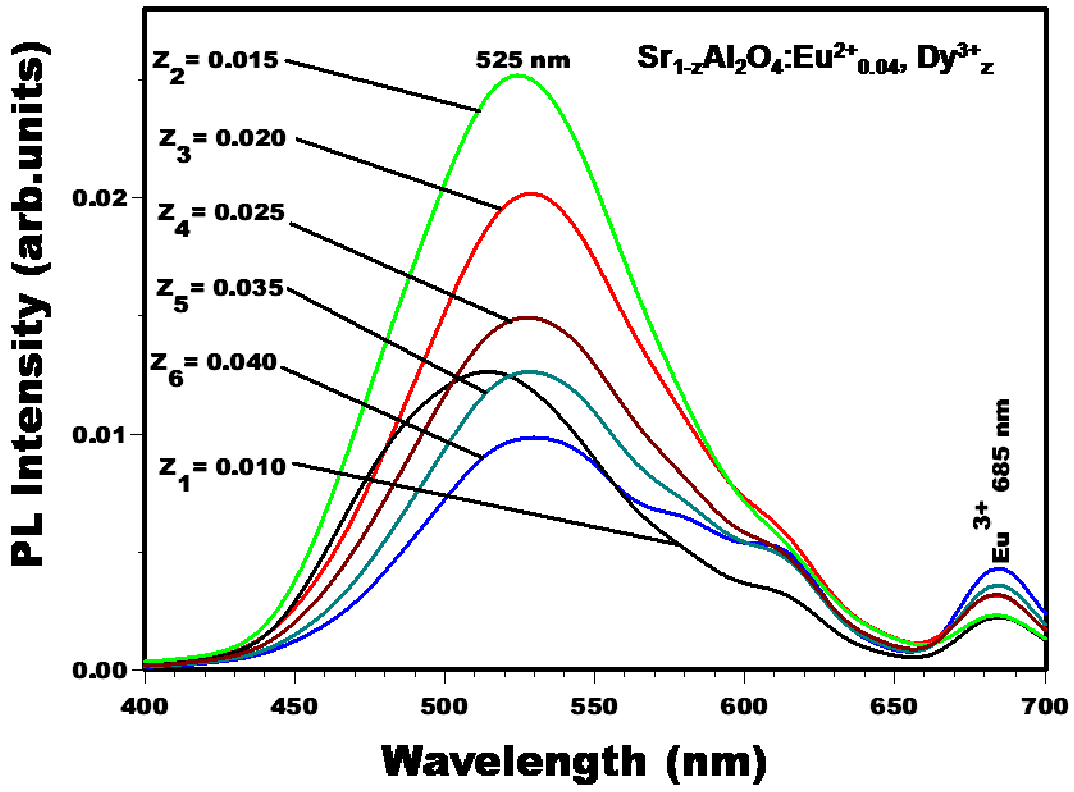

Figure 9.3: PL emission spectra of $Sr_{1-z}Al_2O_4:Eu^{2+}_{0.04}, Dy^{3+}_z$ (z = 0.01, 0.02, 0.03 and 0.04)

Figure 9.4 shows the PL spectra of $SrAl_2O_4$ co-doped with Eu^{2+} and Dy^{3+} ions. The concentration of Eu^{2+} was varied from 1– 4 mol% and that of Dy^{3+} was maintained at 4 mol%. An intense stable green phosphorescence attributed to the $4f^65d^1 \rightarrow 4f^7(^8S_{7/2})$ transition of Eu^{2+} was observed at ~528 nm from all the powders. Minor emission lines from residual Eu^{3+} were present at 590, 615 and 685 nm. The highest PL intensity with prolonged phosphorescence was observed from the powder co-doped with 2 mol% of Eu^{2+} and 4 mol% of Dy^{3+} (i.e. $Sr_{0.94}Al_2O_4:Eu^{2+}_{0.02},Dy^{3+}_{0.04}$), and the lowest intensity, probably due to concentration quenching, was observed from the powder co-doped with equal concentrations of Eu^{2+} and Dy^{3+}, i.e. 4mol% each ($Sr_{0.92}Al_2O_4:Eu^{2+}_{0.04},Dy^{3+}_{0.04}$).

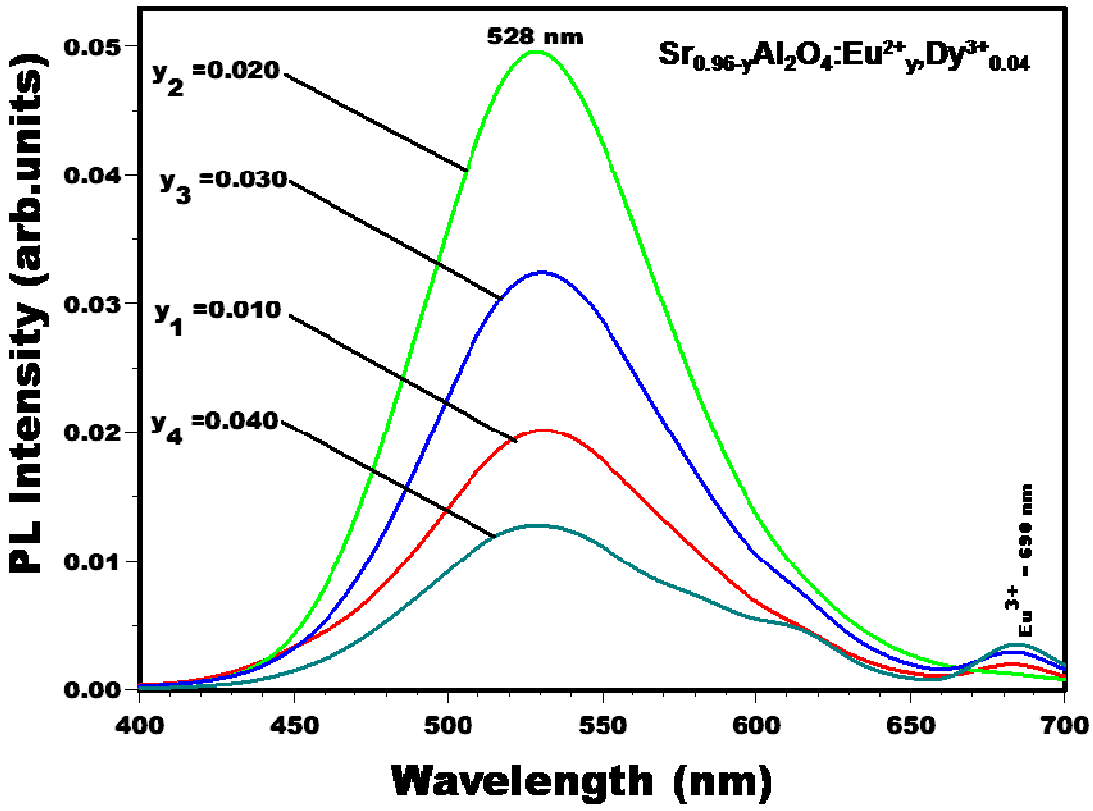

Figure 9.4: PL emission spectra of $Sr_{0.96-y}Al_2O_4:Eu^{2+}_y,Dy^{3+}_{0.04}$ (y = 0.01, 0.02, 0.03 and 0.04)

A snapshot of the $Sr_{0.94}Al_2O_4:Eu^{2+}_{0.02},Dy^{3+}_{0.04}$ powder, with prolonged green phosphorescence, taken after the UV excitation was removed, is shown in figure 9.5. The phosphorescence lasted for several minutes. It is obvious from the PL data that Dy^{3+} ions play an important role in prolonging and increasing the green phosphorescence of $SrAl_2O_4:Eu^{2+}$ phosphors.

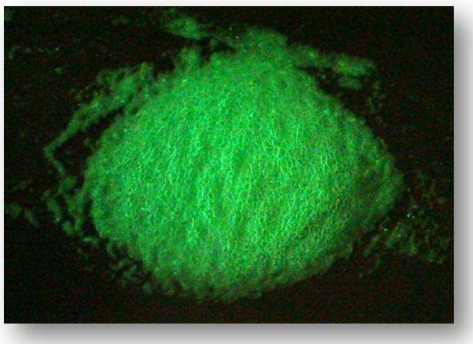

Figure .9.5: A snapshot of $Sr_{0.94}Al_2O_4:Eu^{2+}_{0.02},Dy^{3+}_{0.04}$ showing persistent green phosphorescence.

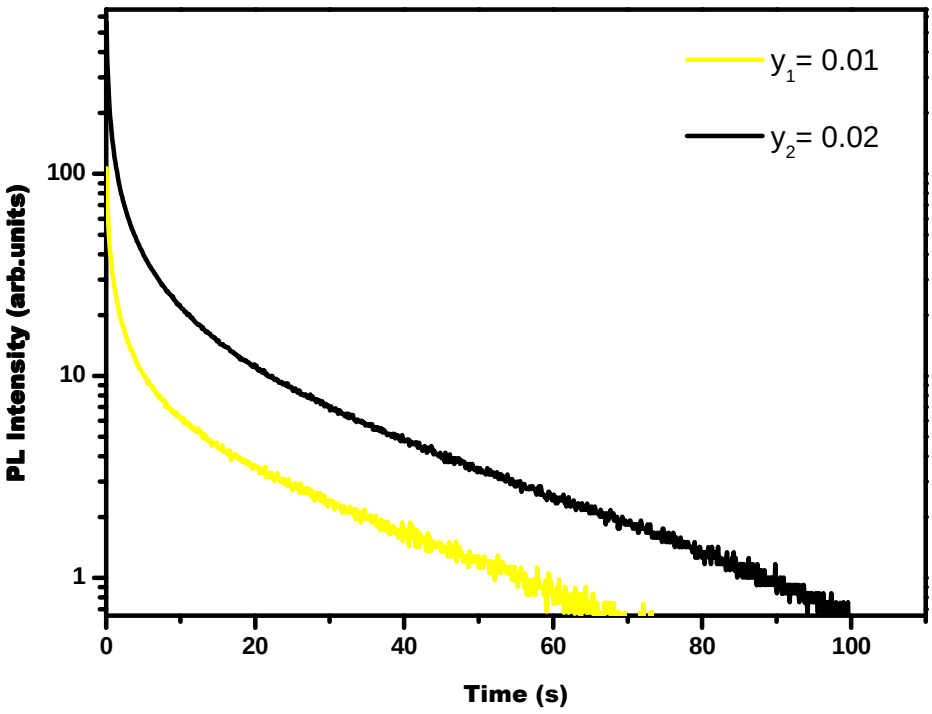

Figure 9.6: Decay curves of combustion synthesized $Sr_{0.96-y}Al_2O_4:Eu^{2+}_{y}$, $Dy^{3+}_{0.04}$ (y = 0.01 and 0.02) phosphors.

The decay characteristics of $Sr_{0.96-y}Al_2O_4:Eu^{2+}_y$, $Dy^{3+}_{0.04}$ (y = 0.01 and 0.02) phosphors are shown in figure 9.6. The data were collected using a monochromatized xenon lamp. The decay curves of both phosphors are characterized by an initial rapid decay followed by long lasting phosphorescence in the same as reported in refs [6,7]. The decay parameters for the fitting data are listed in table 9.1. The decay times of the $Sr_{0.94}Al_2O_4:Eu^{2+}_{0.02},Dy^{3+}_{0.04}$ were slightly longer than $Sr_{0.95}Al_2O_4:Eu^{2+}_{0.01},Dy^{3+}_{0.04}$.

Table: 9.1: Decay parameters of the phosphors

Phosphors	τ_1 *(sec)*	τ_2 **(sec)**	τ_3 *(sec)*
$\mathbf{Sr_{0.95}Al_2O_4:Eu^{2+}_{0.01},Dy^{3+}_{0.04}}$	**0.3**	**2.6**	**23**
$\mathbf{Sr_{0.96}Al_2O_4:Eu^{2+}_{0.02},Dy^{3+}_{0.04}}$	**0.6**	**5.1**	**30**

9.3. CONCLUSION

$Sr_{1-x}Al_2O_4:Eu^{2+}_x$, $Sr_{0.96-z}Al_2O_4:Eu^{2+}_{0.04},Dy^{3+}_z$ and $Sr_{0.96-y}Al_2O_4:Eu^{2+}_y,Dy^{3+}_{0.04}$ phosphor powders with different concentrations of Eu^{2+} and Dy^{3+} were successfully synthesized using the combustion method. The $Sr_{1-y}Al_2O_4:Eu^{2+}_y,Dy^{3+}_{0.04}$ and $Sr_{1-z}Al_2O_4:Eu^{2+}_{0.04},Dy^{3+}_z$ phosphors showed persistent phosphorescence at 525 nm and 528 nm respectively. In the case of $SrAl_2O_4:Eu^{2+}$, an intense green fluorescence was observed at 520 nm for 3 mol% Eu^{2+} doping.. All the emissions observed at 520 nm ($Sr_{1-x}Al_2O_4:Eu^{2+}_x$), 528 nm ($Sr_{0.96-y}Al_2O_4:Eu^{2+}_y,Dy^{3+}_{0.04}$) and 525 nm ($Sr_{0.96-z}Al_2O_4:Eu^{2+}_{0.04},Dy^{3+}_z$) were attributed to transitions of Eu^{2+} ion from the $4f^65d^1$ exited state to the $4f^7$ ($^8S_{7/2}$) ground state. The co-dopant Dy^{3+} in the host material is responsible for deep traps in the energy band gap. These traps are in a form of hole – trapping levels and when the excitation source is removed, the relaxation of these secondary ions from the deep traps is very slow and this process is responsible for the long persistence of these phosphors.

REFERENCES

1. Z. C Wu, J. X Shi, J. Wang, M.L Gong, Materials Letters **60** (2006) 3499 – 3501
2. D. Wang, Q. Yin, Y. Li, *J. Mater. Sci.* **37** (2002) 381
3. H. Song, D. Chen, W. Tang, Y Peng, Displays **29** (2008) 41
4. Z. Qiu, Y. Zhou, A. Zhang, Q. Ma, Acta Materialia, **55** (2007) 2615
5. B. Faridnia, M.M.K Motlagh, A. Maghsoudipour, Pigment and Resin Technology, **36** (2007) 216 -223
6. J. Geng, Z. Wu, *J. Mater. Synthesis and Processing* **10(5)** (2002) 245
7. T. Peng, L. Huajun, H Yang, C Yan, *Mater. Chem. Phys.* **85** (2004) 68
8. Z. Tang, F. Zhang. Z Zhang, Q. Huang, Y Lin, Journal of the European Ceramic Society **20** (2000) 2129 – 2132

CHAPTER 10

RED-EMMITTING $SrAl_2O_4:Eu^{3+}$ PHOSPHORS PREPARED BY A SOL-GEL PROCESS

10.1. INTRODUCTION

Recent studies have shown that aluminates (MAl_2O_4, M = Sr, Ca or Ba) are getting more recognition as promising host matrices for rare-earth activators to prepare long afterglow phosphors that could be used in a variety of applications in the lighting industry. Because of their chemical stability, high quantum efficiency and long afterglow luminescence, rare-earths activated aluminate phosphors are seen as possible future replacement for traditional sulphide-based phosphors [1] in the lighting industry. Green and blue $SrAl_2O_4:Eu^{2+},Dy^{3+}$ [1-8] and $CaAl_2O_4:Eu^{2+},Dy^{3+}$[2,9] long afterglow phosphors respectively have been synthesized using a variety of methods including solid state reaction [5,8], combustion [4,10], floating zone [2,7] and sol-gel [5,6,9]. In both phosphors, emission is attributed to a 5d→4f transition in Eu^{2+} while Dy^{3+} is an auxiliary - activator that acts as a trap for charge carriers (holes) and this process accounts for the long-afterglow characteristics of the phosphors. Since these phosphors are not radioactive, they can be used in luminous paints, watches and clocks [2,4,6]. In this study, an intense orange-to-red emission was observed from Eu^{3+} in a singly activated $SrAl_2O_4$ matrix prepared by a sol process. Although this emission was sufficiently intense to be detected in normal laboratory lighting, it did not show long afterglow and it is possible that co-activation with Dy^{3+} or other rare-earth activators can lead to much brighter orange-red emission and persistent afterglow, and the study to this effect is in progress. Since $SrAl_2O_4$ like other already studied oxide-based host matrices for Eu^{3+} such as yttrium oxide (Y_2O_3) and gadolinium oxide [Gd_2O_3] is reported to be chemically stable, its potential as a red emitting phosphor is demonstrated in this study.

10.2. EXPERIMENTAL

$SrAl_2O_4:Eu^{3+}$ was prepared by dissolving 2g of strontium acetate hydrate ($Sr(CH_3CO_2)_2 \cdot \frac{1}{2} H_2O$) and 2 g of aluminium isopropoxide ($Al(i\text{-}OC_3H_7)_3$ in 50 mL of distilled water and 50 mL of mono-glycol ethyl-ether ($C_4H_{10}O_2$) and the two mixtures were vigorously stirring at 25 and 90^oC respectively. X g of europium oxide or Eu_2O_3 (where X = mass of Eu_2O_3 weighed for 0.5, 1 or 1.5 mol% Eu^{3+} doping) dissolved in 10 mL of 0.6 M nitric acid (HNO_3) was added to the strontium acetate solution and the mixture was stirred for 30 minutes. The solution of aluminium isopropoxide was then added drop wise to the Sr:Eu solution and the mixture was stirred for 1 hour at room temperature. To prevent undesirable precipitation of $Al(OH)_3$, 10 ml of glycerol ($C_3H_8O_3$) was added drop wise to the solution while stirring. The solution was dried in an oven at 60 – 75 ^0C for 14 hours to remove unwanted volatile ions and also to convert the resulting sol to a gel. The gel was further dried in the oven at 200 ^0C for 24 hours. The dried gel was ground to get a fine powder which was later annealed in air at 1000^oC for 4 hours. The schematic flow diagram for the synthesis of $SrAl_2O_4:Eu^{3+}$ phosphors by sol-gel method is shown in figure 10.1

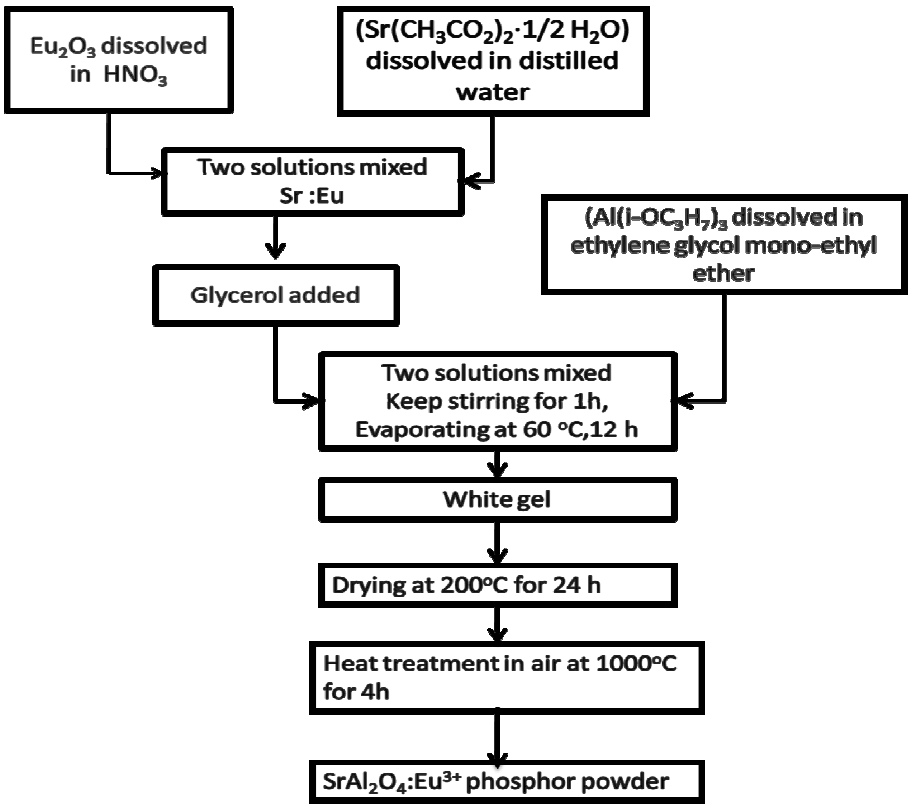

Figure 10.1: Flow diagram of the synthesis of $SrAl_2O_4:Eu^{3+}$ phosphors by sol-gel method.

10.2.1. CHARACTERIZATION

The crystalline structure, particle morphology and chemical composition of the powder were analyzed using a Siemens X-ray Diffractometer (model D5000) with Cu K_α at λ = 1.5418 Å and a Shimadzu Superscan SSX-550 system for scanning electron microscopy (SEM) coupled with energy dispersive X-ray spectroscopy (EDS). A 325 nm He-Cd laser fitted with a SPEX 1870 0.5 m spectrometer and a photomultiplier detector was used to collect photoluminescence emission data in air at room temperature.

10.3 RESULTS AND DISSCUSIONS

Figure 10.1 shows the X-ray diffraction (XRD) patterns of Eu^{3+} doped $SrAl_2O_4$ powder. The structure compares very well with a monoclinic phase of $SrAl_2O_4$ (JPCDS file no. 34-0379) and

is similar to structures reported in the literature [5,6,8,10]. Two phases have been reported for $SrAl_2O_4$, namely a high temperature hexagonal phase (β-phase) and a low temperature monoclinic phase (α-phase). The transition from the low temperature monoclinic to hexagonal phase occurs at ≥650^oC [4,11,12].

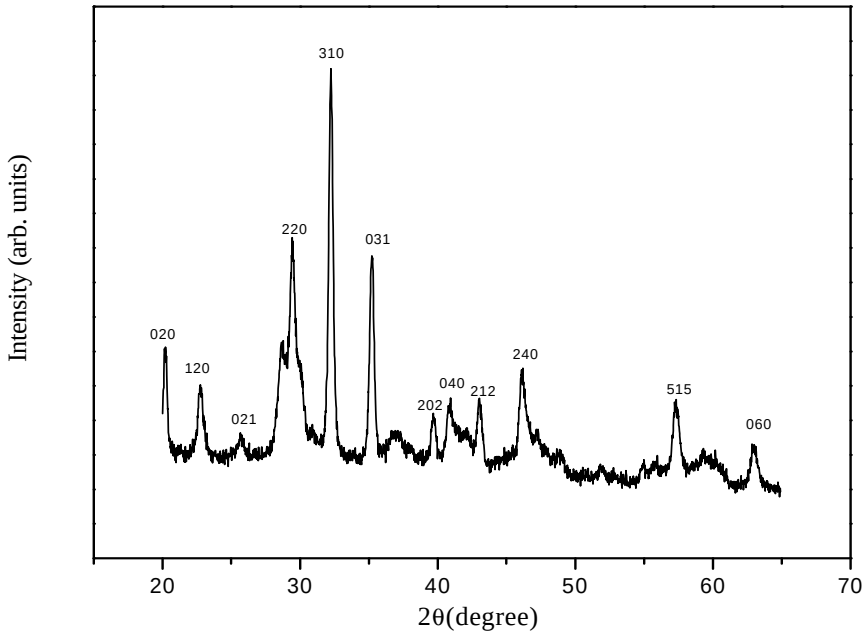

Figure 10.2 XRD spectrum of $SrAl_2O_4:Eu^{3+}$ powder calcined at 1000^{o}C.

A hexagonal $SrAl_2O_4$ phase was observed in samples prepared at 800 – 1500^oC [10,11]. In this study, $SrAl_2O_4:Eu^{3+}$ samples were prepared and dried at relatively low temperatures but were annealed at a high temperature of 1000^oC for four hours. Peng *et al.* [6] have used the combustion method to prepared $SrAl_2O_4:Eu^{2+}$, Dy^{3+} at 500^oC and annealed some of the samples at 1100^oC for 2 hours and they observed stable α-phase (monoclinic) from both annealed and as prepared samples.

Figure 10.3 shows the SEM image of $SrAl_2O_4:Eu^{3+}$ powder annealed at 1000^oC. The powder consists of highly agglomerated nano-sized rods with an average edge thickness of 27 nm. The

EDS data in figure10.3 confirms the presence of all the elements (Al, O and Sr) together with the adventitious carbon. Eu^{3+} ions were not detected probably due to their relatively low concentration (0.5 -1.5 mol%) in the $SrAl_2O_4$ matrix.

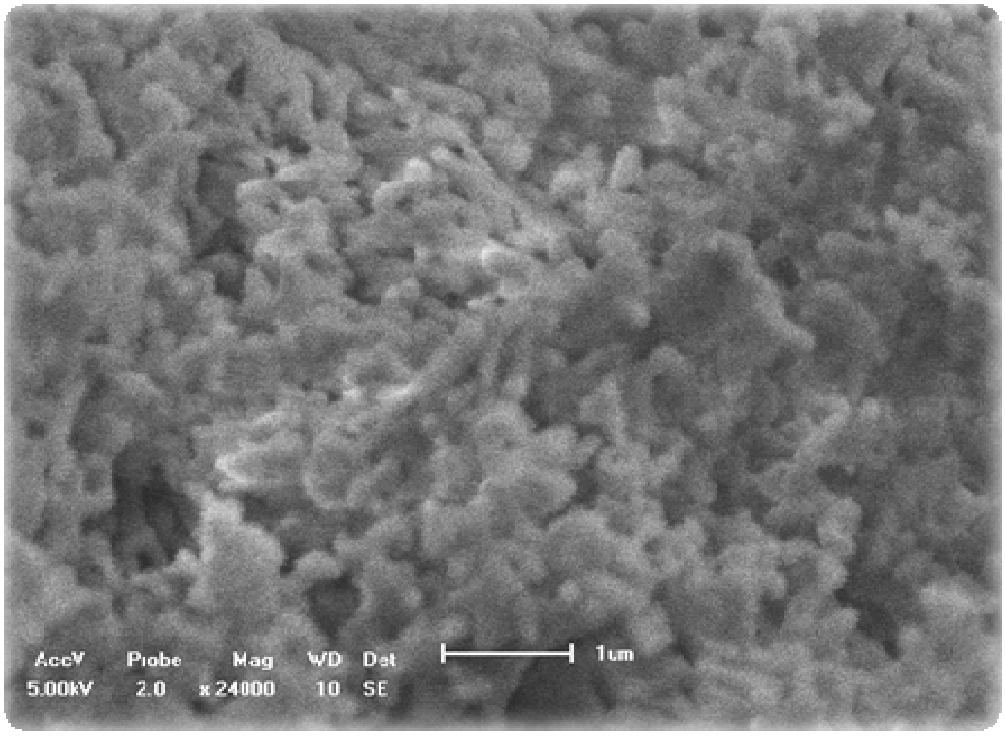

Figure 10.4: SEM image of $SrAl_2O_4:Eu^{3+}$ powder calcined at 1000^oC

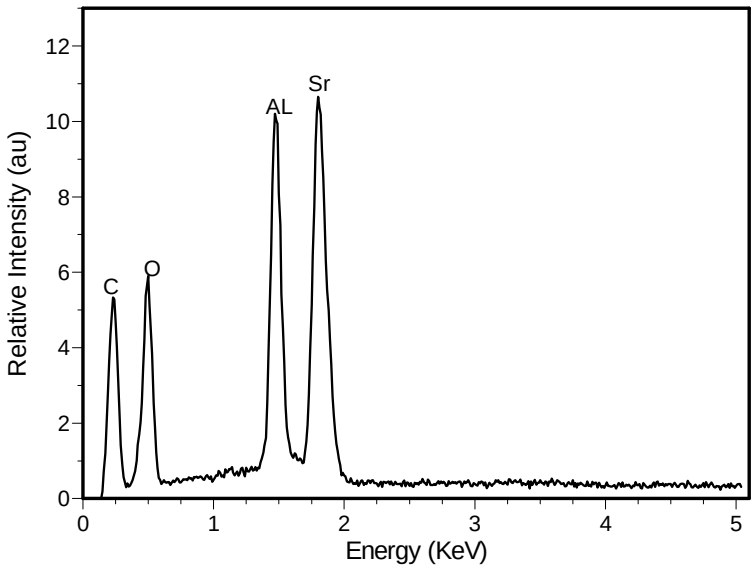

Figure 10.4: EDS spectrum of $SrAl_2O_4:Eu^{3+}$ powder calcined at 1000 ^{0}C.

Figure 10.5 (a) shows PL emission spectra for different molar concentrations of Eu^{3+} in $SrAl_2O_4$. The intensity was high for 1.5 mol% Eu^{3+} doping. It is known that the characteristic emission lines in Eu^{3+} ion involve transitions from the singly degenerate excited $^5D_0$ level to the crystal-field-split ^7F_J (J = 0,1,2,3,4,5,6) sublevels of the $4f^6$ electronic configuration [13,14]. Although the Eu^{3+} optical transitions were not determined in this study, the emission lines observed in figure 10.4 can be assigned to $^5D_0 \rightarrow {}^7F_1$, $^5D_0 \rightarrow {}^7F_2$, $^5D_0 \rightarrow {}^7F_3$ and $^5D_0 \rightarrow {}^7F_4$ transitions based on the literature [15-18]. Prominent emission lines resulting from the $^5D_0 \rightarrow {}^7F_{2,4}$ transitions are at 620 nm and 700 nm respectively. Figure 10.5(b) shows a simplified energy level diagram for these transitions. The Eu^{3+} transitions observed in $SrAl_2O_4$ are similar to those observed in other host_matrices such as Y_2O_3 and Gd_2O_3 as reported in the literature [15-19]. This observation is in agreement with the reported practical insensitivity of the absorption and emission spectra of the Eu^{3+} ion to different host crystals [14]. It should however be noted that the emission lines and intensities are sensitive to crystallographic environment of the sites in which Eu^{3+} ion is

accommodated [15]. Because of this, the Eu^{3+} ion can be used to probe crystallographic symmetries of host lattices. For example, monoclinic Gd_2O_3 provides three different C_s sites whereas cubic Gd_2O_3 provides two sites (S_6 and C_2) for Eu^{3+} occupation [20]. Thus, Eu^{3+} ions show different emission lines and intensities in the two different Gd_2O_3 crystal structures. Actually, differences in the PL emission lines and intensities for cubic versus monoclinic crystal lattices have been reported for fiber single crystals [15], thin films [20] and nanocrystallites [16]. The Eu^{3+} transitions for monoclinic $SrAl_2O_4$ host lattice observed in figure 4 resemble those observed from monoclinic Gd_2O_3 [15-18]. Prominent emission lines for $^5D_0 \rightarrow ^7F_{2,4}$ transitions were observed in monoclinic Gd_2O_3 and it has been reported that they originate from forced electric dipole transitions of the Eu^{3+} ion occupying C_2 sites where there is a lack of inversion symmetry [18]. Similar effects are most likely responsible for the prominent emission lines of Eu^{3+} at 620 nm and 700 nm in monoclinic $SrAl_2O_4$, where Eu^{3+} is expected to readily occupy Sr^{2+} as is the case in other reported Sr-containing systems [21]. Although the emission peak at 700 nm ($^5D_0 \rightarrow ^7F_4$) is lower in intensity than that at 620 nm ($^5D_0 \rightarrow ^7F_2$) for 1.5 mol% Eu^{3+} doping, it appears to be at a comparatively higher intensity than other similar and widely reported peaks observed in Y_2O_3 and/or Gd_2O_3 hosts. This observation further confirms the sensitivity of the Eu^{3+} ion to different crystallographic symmetries. For practical application, red emission resulting from the $^5D_0 \rightarrow ^7F_2$ hypersensitive forced electric-dipole transition is used. The PL data for 1.5 mol% Eu^{3+} in $SrAl_2O_4$ suggest a need for more studies to elucidate on how to improve the weakly forced electric dipole $^5D_0 \rightarrow ^7F_4$ transition for future consideration in lighting industry.

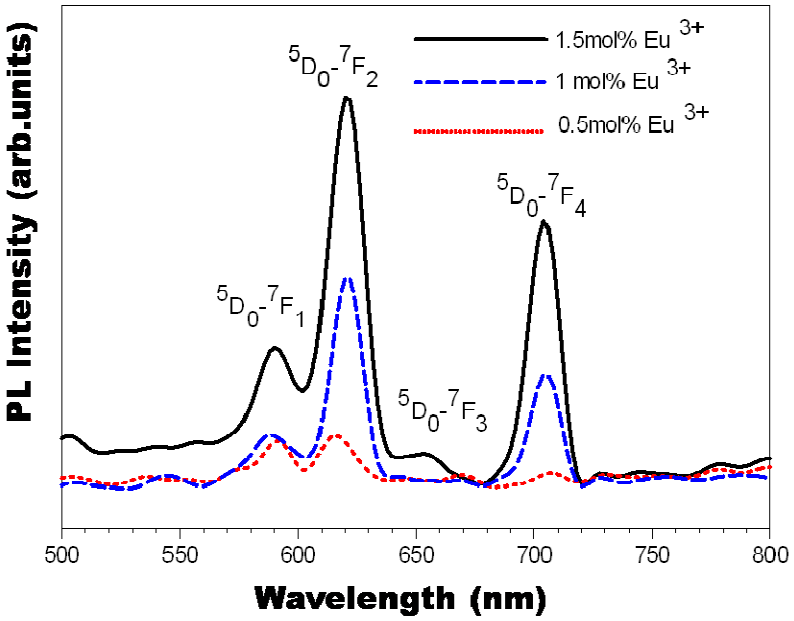

Fig 10.5.a: PL emission spectra for different concentrations of Eu^{3+} in $SrAl_2O_4$

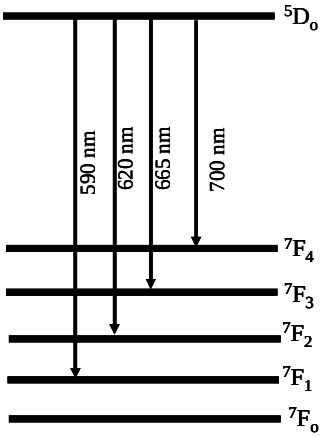

Fig 10.5.b: simplified energy level showing possible transitions in Eu^{3+}.

10.4. CONCLUSION

Red emitting $SrAl_2O_4:Eu^{3+}$ (Eu^{3+} = 0.5, 1 or 1.5 mol %) phosphors were synthesized using a sol-gel process. The structure, morphology and photoluminescent properties were analyzed using scanning electron microscopy, x-ray diffraction and a 325 nm He-Cd laser respectively. $SrAl_2O_4$ was shown to grow as agglomerated nanorod-like particles with an average edge thickness of ~27 nm. The $SrAl_2O_4$ nanorods were found to crystallize as a metastable monoclinic phase when annealed at a temperature of 1000^oC for four hours. Prominent red photoluminescence emission peaks from Eu^{3+} ion at 620 nm and 700 nm due to a hypersensitive forced electric dipole $^5D_0 \rightarrow {}^7F_2$ and a weak forced electric dipole $^5D_0 \rightarrow {}^7F_4$ transition respectively ,were reported.

REFERENCES

1. L. Xingdong and S. Wagen, Rare Met. **26**(4) (2007), p. 305
2. T. Katsumata, T. Nabae, K. Sasjima and T. Matsuzawa, J. Crys. Growth **183** (1998), 361.
3. T. Matsuzawa, Y. Aoki, N. Takeuchi and Y. Murayama, J. Electrochem. Soc. **143**(8) (1996), p. 2670.
4. H. Song, D. Chen, W. Tang and Y. Peng, Displays **29** (2008) p. 41.
5. Z. Tang, F. Zhang, C. Huang and Y. Lin, J. Euro. Ceram. Soc. **20** (2000), p.2129.
6. T. Peng, L. Huajun, H. Yang, C. Yan, Mater. Chem. Phys. **85** (2004), p. 68.
7. T. Kutsamata, K. Sasajima, T. Nabae, S. Komuro and T. Morikawa, J. Am. Ceram. Soc. **81**(2) (1998), p.413.
8. S. Han, K. Singh, T-Y. Cho, H-S. Lee, D. Jakhar, J.P. Hulume, C-H. Han, J-D. Kim, Il-S. Chun and J. Gwak, J. Lumin. **128** (2008) 301 – 305.
9. T Aitasalo, J Hölsa, H Junger, M. Lastusaari and J. Niittykoski, J. Alloys Comp. **341** (2002) 76.
10. T. Peng, H. Yang, X. Pu, B. Hu, Z. Jiang, C. Yan, Mater. Lett. **58** (2004) 352.
11. K Fukuda, K Fukushima, J. Sol. State Chem. **178** (2005) 2709-2714.
12. X. Yu, C. Zhou, X. He, Z. Peng, S-P. Yang, Mater. Lett. **58** (2004) 1087.
13. G. Blasse, B.C. Grabmaier, Luminescent Materials, Springer Verlag, Berlin Heidelberg, Germany 1994.
14. J.G. Solé, L.E. Bausá, D. Jaque, An Introduction to Optical Spectroscopy of Inorganic Solids, John Wiley and Sons Ltd., Chichester-England, 2005.

15. L. Sun, C. Liao, C. Yan, Sol. State Chem. **171** (2003) 304

16. C. Louis, K. Lebbou, M.A. Flores-Gonzalez, R. Bazzi, H. Hautefeuille, B. Mercier, S Roux, P Perriat, C. Olagnon, O. Tillement, J. Cryst. Growth **265** (2004) 459.

17. S.H. Shin, J.H. Kang, D.Y. Jeon, D.S. Zang, J. Lumin. **144** (2005) 275

18. H. Yang, H. Lee, PH Holloway, Nanotechnology **16** (2005), p. 2794.

19. C. Zhu, Y. Yang, G. Chen, S. Baccaro, A. Cecilia, M. Falconieri, J. Phys. Chem. Sol. **68** (2007), p. 1721.

20. S.Y. Seo, S. Lee, H.D. Park, N. Shin, K-S. Sohn, J. Appl. Phys. **92** (2002), p. 5249.

21. N. Cockcroft, S.H. Lee, J.C. Wright, Phys. Rev. **9** (1991), p. 4117.

Chapter 11

SUMMARY AND CONCLUSION

CONCLUSIONS

In this study the luminescent and structural properties of the alkaline earth aluminate phosphors prepared by solid state reaction, combustion and sol-gel methods are discussed. The Solid state and Sol-gel methods require much longer time (3-9 hours) for preparation of the phosphors. The annealing processes in both methods are performed at very high temperatures (1000 - 1300 ^{0}C) and require a lot of energy. Furthermore in order to reduce Eu^{3+} to Eu^{2+} toxic gases such as N_2 and H_2 must be introduced during the annealing process.

The combustion method is more efficient because the phosphors of high efficiency were obtained at low temperatures (500 – 600 ^{0}C) in a very short period of time (5 min). The Eu^{2+} was obtained by adding a small amount of urea to the mixture during synthesis.

In this study the following were investigated:

The Optical properties of $SrAl_2O_4:Eu^{2+},Dy^{3+}$ phosphors prepared by solid state reaction method (1), the effect of crystal field changes and distortion of the host matrix prepared at an initiating combustion temperature of 500 ^{0}C (2), the effects of the initiating combustion temperatures (500 - 800 ^{0}C) in $CaAl_2O_4:Eu^{2+},Dy^{3+}$, $BaAl_2O_4:Eu^{2+},Dy^{3+}$and $SrAl_2O_4:Eu^{2+},Dy^{3+}$ phosphors (3), $SrAl_2O_4$ doped with different concentrations of Dy^{3+} and Eu^{2+} ions (4) and $SrAl_2O_4:Eu^{3+}$ (Eu^{3+} = 0.5, 1 or 1.5 mol%) annealed in air at 1000 ^{0}C (5). The luminescent properties of the phosphors were determined by a 325 nm He-Cd laser and a Cary Eclipse fluorescence spectrophotometer.

$SrAl_2O_4:Eu^{2+},Dy^{3+}$ phosphors were successfully synthesized by the solid state reaction method at different annealing temperatures (1000 — 1200 ^{0}C) in a reducing atmosphere of N_2 and 25% of H_2. The broad emission bands at 497 nm confirm that the reducing atmosphere was sufficient to reduce the Eu^{3+} ions to Eu^{2+} ions. The long afterglow displayed by the $SrAl_2O_4:Eu^{2+},Dy^{3+}$

phosphors, may be attributed to the Dy^{3+} ions acting as the hole trap levels, which play an important role in prolonging the lifetime of luminescence. The main diffraction peaks of the monoclinic structure of $SrAl_2O_4$ were observed in all the samples.

The effect of the crystal field changes and distortion in different hosts were investigated. The $CaAl_2O_4:Eu^{2+},Dy^{3+}$, $BaAl_2O_4:Eu^{2+},Dy^{3+}$ and $SrAl_2O_4:Eu^{2+},Dy^{3+}$ phosphors were synthesized at an initiating combustion temperature of 500 ^{0}C. The low temperature monoclinic structure for both $CaAl_2O_4$ and $SrAl_2O_4$ and the hexagonal structure of $BaAl_2O_4$ were observed. The broad band emission spectra observed at 449 nm, (450nm – with a shoulder peak at 500nm) and 528 nm for $CaAl_2O_4:Eu^{2+},Dy^{3+}$, $BaAl_2O_4:Eu^{2+},Dy^{3+}$and $SrAl_2O_4:Eu^{2+},Dy^{3+}$ respectively, are attributed to the distortions experienced in the host lattice when Eu^{2+} ions substitute the sites of the cations. The monoclinic crystal structures of both $CaAl_2O_4$ and $SrAl_2O_4$ are more appropriate in creating the traps, and this is directly related to the long afterglow phenomena. However the hexagonal structure of $BaAl_2O_4$ can only produce shallow traps.

The luminescent properties of $Sr_{0.97}Al_2O_4:Eu^{2+}{}_{0.01},Dy^{3+}{}_{0.02}$, $Ca_{(0.97)}Al_2O_4:Eu^{2+}{}_{0.01},Dy^{3+}{}_{0.02}$ and $Ba_{(0.97)}Al_2O_4:Eu^{2+}{}_{0.01},Dy^{3+}{}_{0.02}$ phosphors prepared at different initiating combustion temperatures (500 – 800 ^{0}C) were investigated.. The optimum PL intensity were observed at an initiating combustion temperature of 500^{0}C for both $Sr_{0.97}Al_2O_4:Eu^{2+}{}_{0.01},Dy^{3+}{}_{0.02}$ and $Ba_{(0.97)}Al_2O_4:Eu^{2+}{}_{0.01},Dy^{3+}{}_{0.02.}$ For $Ca_{(0.97)}Al_2O_4:Eu^{2+}{}_{0.01},Dy^{3+}{}_{0.02}$ the optimum intensity illustrated by a sample prepared at an imitating combustion temperature of 600 ^{0}C. The broad emission spectra for these phosphors can be attributed to the transition of the Eu^{2+} ions from the excited state $4f^65d^1$ to the ground state $4f^7$. The long afterglow observed in all the samples was attributed to deep electron traps due to the Dy^{3+} ions incorporated in the host matrix.

$Sr_{1-x}Al_2O_4:Eu^{2+}{}_x$, $Sr_{1-z}Al_2O_4:Eu^{2+}{}_{0.04},Dy^{3+}{}_z$ and $Sr_{1-y}Al_2O_4:Eu^{2+}{}_y,Dy^{3+}{}_{0.04}$ phosphors powders doped with different concentrations of Eu^{2+} and Dy^{3+} were prepared by the combustion method. In the case of $SrAl_2O_4:Eu^{2+}$ (x = 1.5- 4.5 mol% of Eu^{2+}), an intense green fluorescence was observed from 3 mol% Eu^{2+} doping concentration at 520 nm. The $Sr_{1-y}Al_2O_4:Eu^{2+}{}_y,Dy^{3+}{}_{0.04}$ and $Sr_{1-z}Al_2O_4:Eu^{2+}{}_{0.04},Dy^{3+}{}_z$ phosphors showed the broad emission spectra at 525 nm and 528 nm

respectively. The maximum PL intensity for $Sr_{1-y}Al_2O_4:Eu^{2+}{}_y,Dy^{3+}{}_{0.04}$ (y = 1- 4 mol % was illustrated by a phosphor doped with 2 mol % of Eu^{2+} and in the case of $Sr_{1-z}Al_2O_4:Eu^{2+}{}_{0.04},Dy^{3+}{}_z$ (z = 1- 4 mol%) the optimum intensity was observed at 1.5 mol% of Dy^{3+} concentration.

Red emitting $SrAl_2O_4:Eu^{3+}$ (Eu^{3+} = 0.5, 1 or 1.5 mol %) phosphors were synthesized using a sol-gel process. The structure, morphology and photoluminescence properties were analyzed using scanning electron microscopy, x-ray diffraction and a 325 nm He-Cd laser respectively. $SrAl_2O_4$ was shown to grow as agglomerated nanorod-like particles with an average edge thickness of ~27 nm. The $SrAl_2O_4$ nanorods were found to crystallize as a metastable monoclinic phase when annealed at a temperature of 1000 ^oC for four hours. Prominent red photoluminescence emission peaks from Eu^{3+} ion at 620 nm and 700 nm due to a hypersensitive forced electric dipole $^5D_0 \rightarrow {}^7F_2$ and a weak forced electric dipole $^5D_0 \rightarrow {}^7F_4$ transition, respectively were observed. The maximum PL intensity was shown by a sample with 1.5 mol % doping concentration of the Eu^{3+} ions.

FUTURE PROSPECTS

The alkaline earth aluminate ($MAl_2O_4:Eu^{2+}$, Dy^{3+}) (M= Ca, Sr, Ba) phosphors are well known luminescent materials emitting in the visible region when doped with suitable activators. Many researchers have proposed different phosphorescence mechanisms for the alkaline earth aluminate phosphors and the discrepancy on the mechanisms still require further investigations. To further investigate the effects concentration of the RE^{3+} (Dy^{3+}) ions on the emission peak and the traps leading to phosphorescence.

The TEM analysis on the phosphors prepared at different initiating combustion temperatures must be done in order to determine the particles sizes and the diffraction patterns in order to compare them with the XRD results obtained. It was found that XRD structure of $SrAl_2O_4$ show some impurity phase, therefore it is important to improve the synthesis technique. In addition PL emission spectra of $SrAl_2O_4:Eu^{2+},Dy^{3+}$ prepared at different temperatures showed some emission lines that are related Eu^{3+}, therefore it is important to establish the proper amount of urea, that will create a reducing atmosphere in order to reduce Eu^{3+} completely.

To further investigate the phase transition of $SrAl_2O_4$ from the low temperature structure (monoclinic) to the higher temperature structure (hexagonal), and its influence on the optical properties of the phosphors.

PUBLICATIONS

H.C. Swart, **B.M. Mothudi**, S. Nieuwoudt, J.J. Terblans, E. Coetsee, O.M.Ntwaeaborwa, Luminescent properties and degradation of SrAlxOy:Eu^{2+},Dy^{3+}, phosphors, Proceedings - 14th International Workshop on Inorganic and Organic Electroluminescence & 2008 International Conference on the Science and Technology of Emissive Displays and Lighting, 367-370.

O.M. Ntwaeaborwa, M.S.Dhlamini, J.J. Terblans, **B.M. Mothudi**, P.D. Nsimama, H.C. Swart, Phonon-mediated energy transfer from ZnO nanoparticles to SiO2:PbS, Proceedings - 14th International Workshop on Inorganic and Organic Electroluminescence & 2008 International Conference on the Science and Technology of Emissive Displays and Lighting, 177-179.

H.C. Swart, J.J. Terblans, O.M. Ntwaeaborwa, E Coetsee, **B.M. Mothudi** and M.S.Dhlamini, Photon emission mechanisms of different phosphors, Nucl. Instr. and Meth.B, accepted November 2008

B.M Mothudi, O.M. Ntwaeaborwa, J.R Botha and H.C. Swart, Photoluminescence and phosphorescence properties of MAl2O4:Eu2+,Dy3+ (M = Ca, Ba, Sr) phosphors prepared at an initiating combustion temperature of 500 ^{0}C, Physica B, submitted March 2009.

INTERNATIONAL CONFERENCES

Conference on Photonic Materials, Mabula Game Reserve, South Africa, 23 to 27 March 2009.
Photoluminescence and phosphorescence properties of MAl_2O_4:Eu^{2+},Dy^{3+} (M = Ca, Ba, Sr) phosphors prepared at an initiating combustion temperature of 500 ^{0}C,
B.M Mothudi, O.M. Ntwaeaborwa, J.R Botha and H.C. Swart

2nd International Symposium on Luminescence, Port Elizabeth, South Africa, 30 June – 4 July 2008.

Phosphorescence Mechanism of $SrAl_2O_4:Eu^{2+},Dy^{3+}$ phosphors prepared by combustion method.

B.M Mothudi, O.M. Ntwaeaborwa, J.R Botha and H.C. Swart

NATIONAL CONFERENCES

53 nd Conference of South African Institute of Physics – Limpopo (RSA) – July 2008.

Characterization of $SrAl_2O_4:Ce^{3+}$ and $SrAl_2O_4:Eu^{2+},Dy^{3+}$ phosphors prepared via the combustion method. SAIP, Limpopo (2008).

B.M. Mothudi, O.M. Ntwaeaborwa and H.C. Swart,

53 nd Conference of South African Institute of Physics – Limpopo (RSA) – July 2008.

Characterization of $SrAl_2O_4:Eu^{3+}$ and $SrAl_2O_4:Eu^{2+},Dy^{3+}$ phosphors prepared via the combustion method. SAIP, Limpopo (2008).

B.M. Mothudi, O.M. Ntwaeaborwa and H.C. Swart

52 nd Conference of South African Institute of Physics – Johannesburg (RSA) – July 2007.

Synthesis and characterization of $SrAl_2O_4:Eu^{3+},Dy^{3+}$ Phosphors prepared by Sol-Gel method

BM Mothudi, O M Ntwaeaborwa, B F Dejene and HC Swart,

SAIP, Johannesburg (2007)

49 th Conference of South African Institute of Physics – Bloemfontein (RSA) – July 2004.

The Health Impact of the Emissions of Cr, Ni, Pb and Co particulate Matter from the Rustenburg Mines

B. M. Mothudi, A.G.K. Perera, N. Kgabi